SYNTHESIS, STRUCTURAL CHARACTERIZATION AND DFT CALCULATIONS OF *meta*-BENZIPORPHODIMETHENES AND THEIR METAL COMPLEXES

Thesis Submitted to the Delhi Technological University
for the award of the degree of

DOCTOR OF PHILOSOPHY
IN
CHEMISTRY

By

SHIKHA RANA
(2k17/Ph.D/AC/04)

Under the supervision of:

Prof. (Dr.) ANIL KUMAR

DEPARTMENT OF APPLIED CHEMISTRY
DELHI TECHNOLOGICAL UNIVERSITY
Delhi-110042 (INDIA)

2023

©DELHI TECHNOLOGICAL UNIVERSITY-2023

ALL RIGHTS RESERVED

Dedication

To my grandmother
Maa

To my Parents

To my Brother
Ankit

and

To my Husband
Priyavart

Thanks for your endless sacrifices, love, support and prayers

DEPARTMENT OF APPLIED CHEMISTRY
DELHI TECHNOLOGICAL UNIVERSITY
Delhi-110042 (INDIA)

DECLARATION

I declare that the research work reported in the thesis entitled "**Synthesis, structural characterization and DFT calculations of *meta*-benziporphodimethenes and their metal complexes**" for the award of degree of ***Doctoral of Philosophy*** in Chemistry has been carried out by me under the supervision of **Prof. (Dr.) Anil Kumar**, Department of Applied Chemistry, Delhi Technological University, India.

The research work embodied in this thesis, except where otherwise indicate, is my original research. This thesis has not been submitted by me in part or full to any other University for the award of any degree or diploma. This thesis does not contain other person's data, graphs or other information, unless specifically acknowledged.

Shikha Rana
Candidate
2k17/Ph.D/AC/04

Prof. (Dr.) Anil Kumar
Supervisor

Prof. (Dr.) Anil Kumar
Head of Department
Applied Chemistry, DTU

DEPARTMENT OF APPLIED CHEMISTRY
DELHI TECHNOLOGICAL UNIVERSITY
Delhi-110042 (INDIA)

CERTIFICATE

This is to certify that the Ph.D. thesis entitled "**Synthesis, structural characterization and DFT calculations of *meta*-benziporphodimethenes and their metal complexes**" submitted to Delhi Technological University, Delhi, for the award of Doctoral of Philosophy in Chemistry, is based on original research work carried out by me, under the supervision of Prof. Anil Kumar, Department of Applied Chemistry, Delhi Technological University, Delhi, India. It is further certified that the work embodied in this thesis has neither partially or fully submitted to any other university or institution for the award of any degree or diploma.

Shikha Rana
Candidate
2k17/Ph.D/AC/04

This is to certify that the above statement made by the candidate is correct to the best of our knowledge.

Prof. (Dr.) Anil Kumar
Supervisor

Prof. (Dr.) Anil Kumar
Head of Department
Applied Chemistry, DTU

ACKNOWLEDGEMENTS

This thesis is the compilation of my hard work and dedication. The support of numerous people has led me here today. It gives me immense pleasure to present my gratitude to all of them. Firstly, I would like to acknowledge my supervisor, Prof. Anil Kumar for his proficient guidance and motivation.

I would also like to present my gratitude to the former Vice Chancellor of DTU, Prof. Yogesh Singh, and the current Vice-Chancellor Prof. J. P. Saini.

I would also like to thank Prof. Archna Rani, former Head of Department, Department of Applied Chemistry; Prof. S. G. Warkar, former Head of Department, Department of Applied Chemistry and Prof. Anil Kumar current Head of Department, Department of Applied Chemistry

I would also like to thank Dr. Manish Jain, Prof. Ram Singh, Dr. Poonam, Dr. Raminder Kaur and other faculty and staff members of Department of Applied Chemistry, DTU, for their important contributions during my doctoral journey.

I am sincerely thankful to my SRC committee members: Prof. Mahendra Nath, University of Delhi, Prof. Sharif Ahamd, Jamia Millia Islamia, Delhi, Prof. S. G. Warkar and Dr. Vivek Aggarwal from DTU, for their meaning suggestions.

I would like to thank the administrative staff and other members of Chemistry Department. I am extremely thankful particularly to Mr. Raju for being available when needed.

I am thankful to Dr. Milind M. Deshmukh from Dr. Harisingh Gour University, Madhya Pradesh, for helping me in Molecular Tailoring Approach. I would like to present my gratitude to him for all his lessons.

I am thankful to Natalia Fridman, Schulich Faculty of Chemistry, Technion-Israel Institute of Technology, Haifa, Israel for helping me in Crystallography.

I gratefully acknowledge the financial assistance provided by Delhi Technological University in the form of DTU Fellowship.

I specially thank my labmate Deepali, Jyoti and Sachin for being a great support here at DTU. I wish to thank all my fellow Ph.D. scholars at the Department of Applied Chemistry, particularly Priya Bansal, Ram Mangyan, Ravi Kumar Sharma, Usha Raju ma'am, Saurav, Ritika and others.

I would like to thank my best friends Neha and Gazal. Thank you for holding me tight and strong wherever I seek support. I am fortunate to have friends like them in my life.

I pay my sincere gratitude to my late daadi (maa) who believed in me when no one did.

Last but not the least I would like to thank my parents for their immense sacrifices, love and prayers. I owe my existence to them. They've made numerous sacrifices for me. It is their blessings that has made me who I am today and what I may become tomorrow.

Thank you, God, for being so kind. I am grateful for everything.

(**Shikha Rana**)

LIST OF CONTENTS

Title	*Page No.*
Declaration	*i*
Certificate	*ii*
Acknowledgements	*iii*
List of Contents	*v*
List of Tables	*viii*
List of Schemes	*ix*
List of Figures	*x*
List of Charts	*xii*
Abstract	*xiii*
CHAPTER 1: INTRODUCTION	**1-22**
1.1. General Introduction	1
1.1.1. Modifications in Porphyrin	2
1.2. Benziporphyrin: A class of Carbaporphyrinoids	4
1.3. *meta*-benziporphodimethene	4
1.3.1. Synthetic Route for *meta*-Benziporphodimethene Analogues	5
1.3.2. UV-Vis Spectroscopy	7
1.3.3. Structural Analysis	10
1.3.4. Electronic structure Studies	12
1.3.5. NMR shifts in *meta*-Benziporphodimethenes	13
1.4. Properties of Metalated *meta*-Benziporphodimethene Complexes	15
1.4.1. Weak Metal-Arene Interactions	15
1.4.2. Fluorescence Enhancement	15
1.4.3. Fluorescence Phenomena: Structure co-relation	16
1.4.4. Cell-Imaging Applications	16
1.5. Conclusion	18
References	19
CHAPTER 2: SCOPE OF THE WORK	**23-26**

Title *Page No.*

CHAPTER 3: SYNTHESIS AND CHARACTERIZATIONS OF *meta*-BENZIPORPHODIMETHENE ANALOGUES AND ITS METAL COMPLEXES 27-39

3.1. Introduction 27
3.2. Experimental Section 27
3.2.1. Reagents 27
3.2.2. General Information 28
3.2.3. Synthetic Procedure 28
3.3. Results and Discussion 34
3.3.1. Spectroscopy 34
3.3.2. Single Crystal X-Ray Crystallography 35
References 38

CHAPTER 4: DFT CALCULATIONS OF *meta*-BENZIPORPHODIMETHENE AND ITS N-CONFUSED ISOMERS 40-80

4.1. Introduction 40
4.2. Density Functional Theory (DFT) 42
4.2.1. Basics of Density Functional Theory 42
4.2.2. Principle of Density Functional Theory 42
4.2.3. Theorems of Density Functional Theory 42
4.3. Computational Methods 43
4.4. Results and Discussion 43
4.4.1. The Relative Energy of 1 and its Inverted Isomers 44
4.4.2. The Relative Energy of Oxa and Thia analogues of 1 48
4.4.3. The Relative Energy of O-up Isomers of 2 53
4.4.4. The Relative Energy of Lactam Ring Containing Isomers Presented in Chart 4.5 and Chart 4.6 56
4.4.5. The Relative Energy of O-down Isomers of 3 Presented in Chart 4.7 and Chart 4.8 59
4.4.6. The Structural Features of the Isomers 64
4.4.7. The Structural Features of oxa- and thia- Analogues 67
4.4.8. The Intramolecular Hydrogen Bond Energy 68
4.5. DFT of Metalated *meta*-Benziporphodimethene Complexes 71
References 73

Title *Page No.*

CHAPTER 5: CONCLUSION AND FUTURE PROSPECTS 81-82

5.1. Conclusion 81

5.2. Future Scope 82

LIST OF PUBLICATIONS AND CONFERENCES 83

ABOUT THE AUTHOR 84

LIST OF TABLES

Table No.	*Descriptions*	*Page No.*
1.1	Consolidated UV data for Figure 1.7	9
1.2	Consolidated NMR data for Figure 1.7	14
4.1	Total Energy, Relative Energy of the Theoretically Optimized Structures of Chart 4.1 and 4.2	46
4.2	Non-bonded distance (Å) and Angle (degrees) for structures in Charts 4.1 to 4.8	50
4.3	Total Energy, Relative Energy the Theoretically Optimized Structures of Chart 4.3 to 4.6[a]	52
4.4	Total Energy, Relative Energy of the Theoretically Optimized Structures of Chart 4.7 and 4.8[a]	60
4.5	Intramolecular hydrogen bond (H-Bond) distances (Angstrom) and energy ($kcalmol^{-1}$). See Figure 4.1 for corresponding geometries of the molecules	70
4.6	Energies of frontier molecular orbitals in eV	72

LIST OF SCHEMES

Scheme No.	*Descriptions*	*Page No.*
1.1	Synthesis of *meta*-benziporphodimethenes	5
1.2	The O-Up and O-Down γ-lactam embedded N-confused isomers	6
1.3	Tetramethyl-*meta*-benziporphodimethene (**1**) molecule along with its O-Up (**2**) and O-Down (**3**) isomer, R= H, COOMe	10
3.1	Synthesis of free base 11, 16- Bis (2, 6-difluorobenzene)-6, 6, 21, 21-tetramethyl-*meta*-benzi-6, 21-porphodimethene	29
3.2	Synthesis of free base 11,16- Bis (2,3,4,5,6-pentafluorobenzene)-6,6,21,21-tetramethyl-*meta*-benzi-6,21-porphodimethene	30
3.3	Cd^{2+} complex of 11,16-Bis(2,6-difluorobenzene)-6,6,21,21-tetramethyl-*meta*-benzi-6,21-porphodimethene and 11,16-Bis(2,3,4,5,6-pentafluorobenzene)-6,6,21,21-tetramethyl-*meta*-benzi-6,21-porphodimethene	32
3.4	Hg^{2+} complex of 11,16-Bis(2,6-difluorobenzene)-6,6,21,21-tetramethyl-*meta*-benzi-6,21-porphodimethene and 11,16-Bis(2,3,4,5,6-pentafluorobenzene)-6,6,21,21-tetramethyl-*meta*-benzi-6,21-porphodimethene	33
4.1	Molecular tailoring based approach for estimation of intramolecular H-bond energies.	69

LIST OF FIGURES

Figure No.	*Descriptions*	*Page No.*
1.1	Natural pigments consisting of Porphyrin-like moieties	1
1.2	Possible pathways for the delocalization of π-electrons in porphyrins	2
1.3	Structure of porphyrin and the sites of modifications	3
1.4	Representation of modifications in the central core and the types of porphyrin analogues	3
1.5	Structure of free-base *meta*-benziporphodimethene	5
1.6	UV-Vis Spectra of *meta*-benziporphodimethene	6
1.7	*meso-substituted meta*-benziporphodimethene derivatives by Kumar *et. al.*	7
1.8	Colour change in *meta*-benziporphodimethene upon metalation using $ZnCl_2$ salt	8
1.9	UV-Vis Spectra for free-base *meta*-benziporphodimethene analogues	8
1.10	UV-Vis Spectra of *meta*-benziporphodimethene, 1-8 (Figure 1.7) zinc chloride complexes	9
1.11	Depiction of core geometry of porphyrin molecule, non-planar *meta*-benziporphodimethene molecule and its metal complex (M= Zn, Cd, Hg)	10
1.12	Molecular model of 11,16-Bis(phenyl)-6,6,21,21-tetramethyl-*m*-benzi-6,21-porphodimethene (**1)** along with its O-Up (**2)** and O-Down (**3)**isomers . Crystal structure coordinates were taken from ref. [20]	11
1.13	Molecular model of 11,16-Bis(3,4,5-trimethoxy-phenyl)-6,6,21,21-tetramethyl-*meta*-benziporphodimethene. Crystal structure coordinates were taken from [21]	12
1.14	Overview of TMBPDM analogues studied by Kumar *et. Al*	13
1.15	MDA-MB-468 cells incubated with different *meta*-benziporphodimethenes and Zn^{2+} ions for 30 min and respective bright field marked with A-D as well as fluorescence images (just down to its respective bright field image) were captured at 10X objective lens magnification[33]	17
3.1	Structure of free base *meta*-benziporphodimethene	27

Figure No.	*Descriptions*	*Page No.*
3.2	UV-Vis Spectra for free base *meta*-benziporphodimethene with 2,6-difluorobenzaldehyde at *meso* position and its Cd^{2+} and Hg^{2+} metal complexes	34
3.3	UV-Vis Spectra for free base *meta*-benziporphodimethene with penta-fluorobenzaldehyde at *meso* position and its Cd^{2+} and Hg^{2+} metal complexes	35
3.4	X-ray structure of free base *meta*-benziporphodimethene, 1	36
3.5	Polymorphs of free base *meta*-benziporphodimethene, 1	37
4.1	Structures of *meta*-benziporphodimethene (1) and N-confused *meta*-benziporphodimethene containing γ – lactam ring isomers (O-up, 2, and O-down, 3)	44
4.2	B3LYP/6-31g** optimized geometries of 1 and its inverted isomers	48
4.3	Optimized geometries of thia and oxa analogues of 1	50
4.4	Optimized geometries of O-up isomers with hydrogen on nitrogen	54
4.5	Optimized geometries of O-up isomers without hydrogen on nitrogen	55
4.6	Optimized geometries of isomers presented in Chart 4.5 oxidized at pyrrole ring opposite to the phenylene ring with hydrogen atom	57
4.7	Optimized geometries of isomers presented in Chart 4.6 oxidized at pyrrole ring opposite to the phenylene ring without hydrogen atom	58
4.8	Optimized geometries of O-down isomers presented in Chart 4.7 oxidized at pyrrole ring adjacent to the phenylene ring with hydrogen atom	62
4.9	Optimized geometries of O-down isomers presented in Chart 4.8 oxidized at pyrrole ring adjacent to the phenylene ring without hydrogen atom	63
4.10	Optimized geometries of (a) CdCl-BPDM and (b) HgCl-BPDM	71
4.11	Frontier molecular orbital of (a) CdCl-BPDM and (b)HgCl-BPDM. (Isosurface value= 0.02)	72

LIST OF CHARTS

Chart No.	*Descriptions*	*Page No.*
4.1	*meta*-Benziporphodimethene, 1 and its inverted tautomers, in parenthesis relative energy of 1b, 2a to 2i are given with respect to 1a and 2f, respectively in kcal/mol	47
4.2	Oxa- and thia- analogues of *meta*-benziporphodimethene, relative energy of 3b, 3b', 4b and 4b' are given with respect to 3a, 3a', 4a and 4a', respectively in parenthesis in kcal/mol	49
4.3	Reduced form of O-up, 2 isomers; their relative energy are given in parentheses with respect to 5b in kcal/mol	54
4.4	Oxidized form of O-up, 2 isomers; their relative energy are given in parentheses with respect to 6b in kcal/mol	55
4.5	Reduced form of isomers having oxidized pyrrole ring opposite to the phenylene ring; their relative energies are given in parentheses with respect to 7b in kcal/mol	57
4.6	Oxidized form of isomers having oxidized pyrrole ring opposite to the phenylene ring; their relative energies are given in parentheses with respect to 8b in kcal/mol	58
4.7	Reduced form of O-down, 3 isomers, and their relative energy are given in parentheses with respect to 9e in kcal/mol	62
4.8	Oxidized form of O-down, 3 isomers, their relative energy are given in parentheses with respect to 10b in kcal/mol	63

ABSTRACT

Thorough review of *meta*-benziporphodimethene analogues and their metal complexes is presented in this thesis. Foundation of research gap was laid through exhaustive literature review. The focus of the research was then directed to identifying the factors that could improve the stability of the free base *meta*-benziporphodimethene analogues. Synthesis of sterically hindered analogues of *meta*-benziporphodimethene and its cadmium and mercury complexes have been discussed in Chapter 3 of this thesis. UV-Vis, ^{1}H-NMR and mass spectrometry was used to confirm the synthesis of different analogues. Then we moved to determine the structural features that lead to thermodynamically stable moieties, various tautomer have been analysed computationally, which were obtained either by shuffling N-confused pyrrole subunits, oxygenated pyrrole subunit (both O-up and O-down), position of hydrogen on inner nitrogen atom of pyrrole or replacing pyrrolic nitrogen with a heteroatom. Further, the intramolecular hydrogen bond energies have been determined using a Molecular Tailoring approach (MTA), *viz.* Chapter 4 of this thesis. The X-ray solid state structures affirmed the presence of two conformers of *meta*-benziporphodimethene *viz. syn* and *anti*.

Chapter 1

Introduction

CHAPTER 1

INTRODUCTION

1.1 General Introduction

Porphyrin often referred as “pigments of life” is an important molecule of macrocyclic systems whose different aspects have been investigated and has undergone vast research over a period of time making it one of the important molecules in various biological systems. Porphyrin being very stable, aromatic, and tetra-pyrrolic moiety has variety of biological functions. Porphyrin has a well-known tendency to bind with numerous transition metal ions. Metal complexes of porphyrin moieties play important role in the molecular sensing [1], artificial photosynthesis [2], medicine [3] – [5], and electro-optics [6].Because of its potential application in fields including molecular devices, dye-sensitizing solar cells, and photodynamic therapy, the chemistry of porphyrin derivatives has drawn considerable attention over time. The porphyrin-like moieties are universally found in natural pigments including heme, chlorophyll, bacteriochlorophyll, vitamin B12, and cytochromes (**Figure 1.1**) [7].

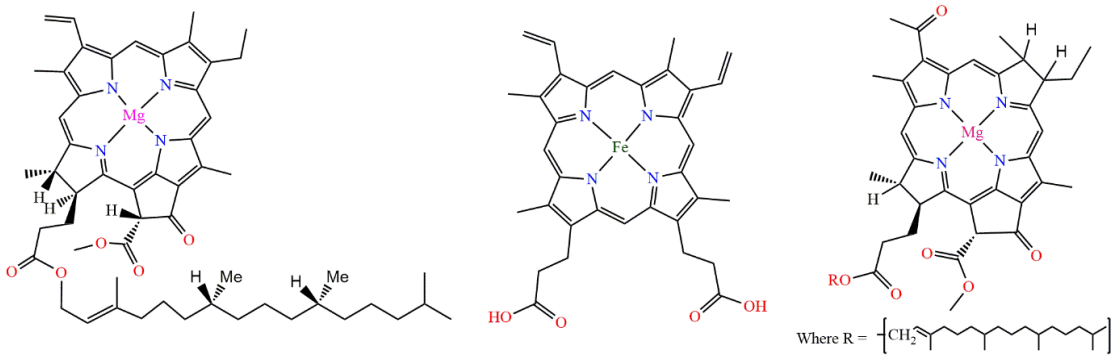

Chlorophyll a Heme Bacteriochlorophyll- a

Figure 1.1. Natural pigments consisting of Porphyrin-like moieties.

The porphyrin molecule, which is highly aromatic in nature, has 22 π -electrons, out of which only 18 π -electrons participate in complete conjugation, resulting in numerous delocalization pathways as depicted in **Figure 1.2**[8]**.**

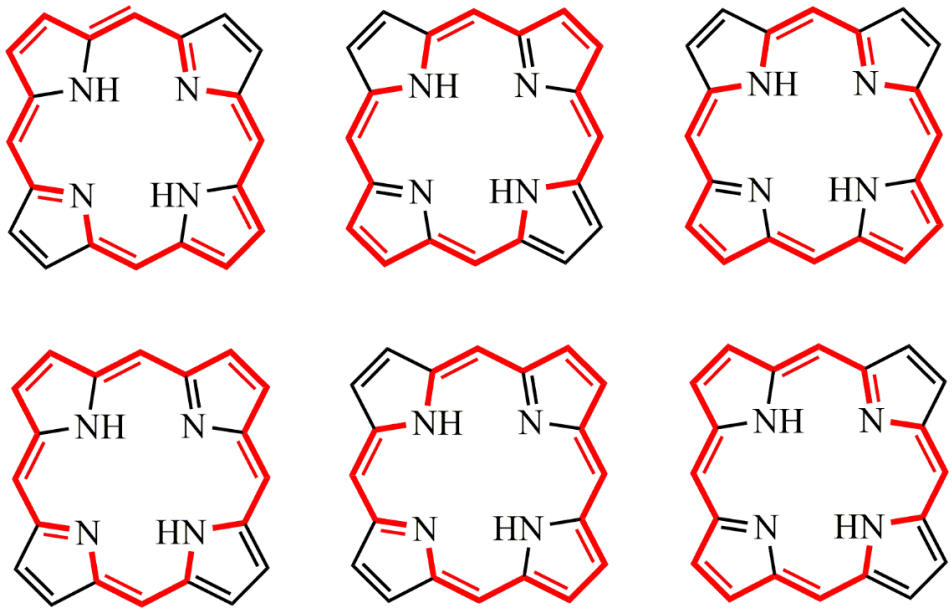

Figure 1.2. Possible pathways for the delocalisation of π-electrons in porphyrins**.**[5]

Designing a novel framework for the porphyrin core and examining its properties is one of the major aspects for future research in porphyrin derivatives. In the recent past, researchers have employed several modifications at various sites of this prosthetic molecule (**Figure 1.3**). Finding applications that are similar to natural porphyrins to mimic natural events in vitro is the main goal of demonstrating such great interest in porphyrin research. Four pyrrolic nitrogens surround the porphyrin's NNNN core, or central region of the moiety (**Figure 1.3**).

1.1.1. Modifications in Porphyrin

Porphyrin moiety can be modified at different sites such as modifications in inner core, at *meso* positions, and at β positions as depicted in **Figure 1.3**[9]– [13]. The new synthetic moieties which are classified according to their electronic current possessed by them and

their structure, and are usually referred to as modified class of porphyrins[14].Modified porphyrin system can be generalized as Core modified porphyrins, Contracted porphyrins, Isomeric porphyrins, Periphery modified porphyrins, Inverted porphyrins or N-confused porphyrins and Expanded porphyrins (**Figure 1.4**).

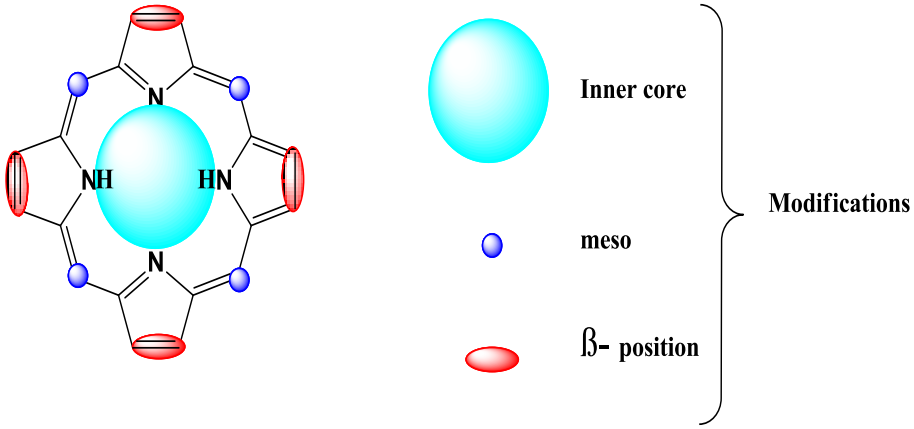

Figure 1.3. Structure of porphyrin and the sites of modifications.

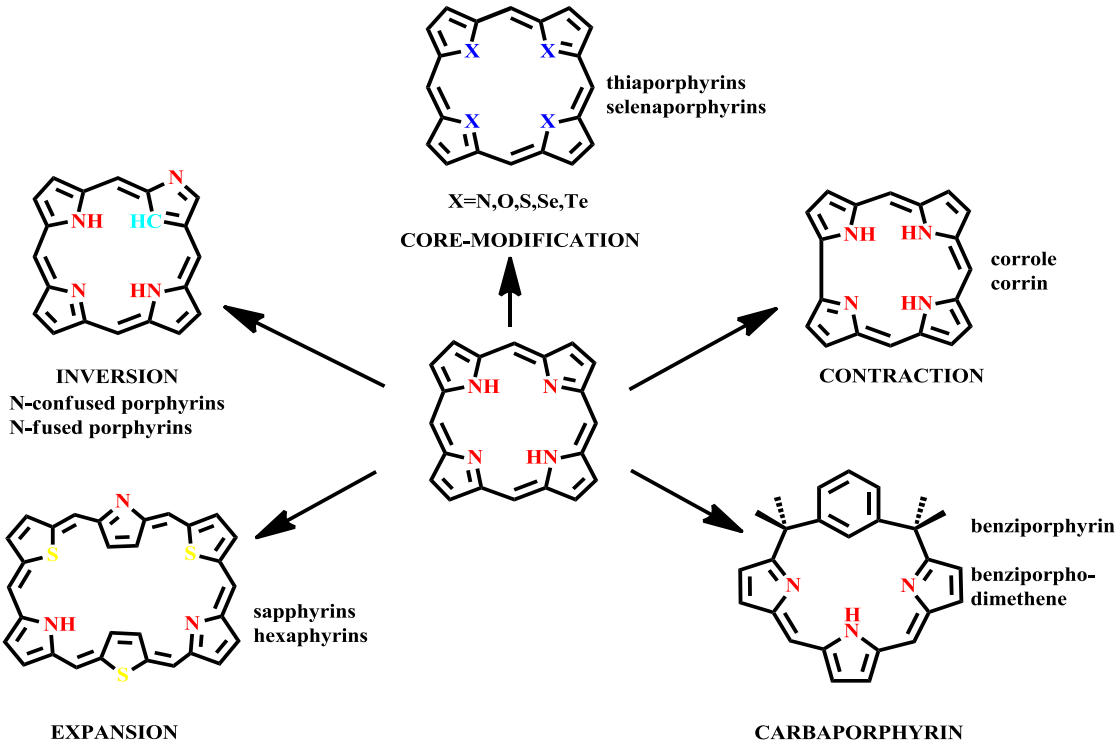

Figure 1.4. Representation of modifications in the central core and the types of porphyrin analogues.

1.2 Benziporphyrin: A class of carbaporphyrinoids

In 1994, N-confused porphyrin was the first carbaporphyrin to be reported independently by Furuta and Latos-Grażyński. Carbaporphyrins are the core modified porphyrins which involve replacement of pyrrolic nitrogen by carbon. Due to the presence of C-H moiety in the inner core, the π-electrons delocalization is deeply affected and, in some cases, it ceases completely in case of carbaporphyrinoids[7]. NMR spectroscopy is used to detect the loss of electronic current [15]. Benziporphyrins are a subclass of porphyrins formed when one of the pyrrole rings in the porphyrin macrocycle is replaced by the phenylene ring. *meta*-benziporphyrin, where a *meta*-phenylene ring replaces a pyrrolic moiety of porphyrin macrocycle, is a significant moiety in the class of benziporphyrin. Berlin and Breitmaier were the first to synthesise *meta*-benziporphyrinin 1994[16]. *meta*-Benziporphyrin was reported to be unstable in solution and therefore it was found to be difficult to obtain a pure sample of *meta*-benziporphyrin. Martin Stepien and Latos-Grazynski synthesized synthetic analogues of *meso* substituted benziporphyrins in order to obtain a pure sample of *meta*-Benziporphyrin [17].

1.3 *meta*-benziporphodimethene

Martin Stępień while working on his Ph.D. thesis was the first one to synthesize *meta*-Benziporphodimethene (**Figure 1.5)** [18]. Those benziporphodimethene which were synthesized by Martin Stępień were alkoxy and hydroxy analogues which were obtained by oxidation of *meta*-benziporphyrins. *meta*-BPDM are *meta*-benziporphyrins with two tetrahedral *meso* carbon atoms at 6- and 21- positions[19].

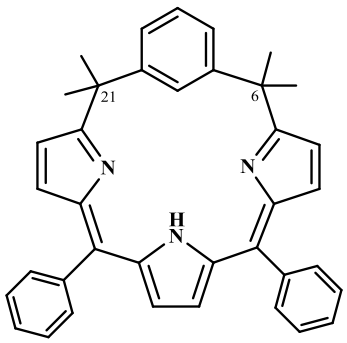

Figure 1.5. Structure of free-base *meta*-benziporphodimethene.

1.3.1. Synthetic Route of meta-benziporphodimethene analogues

Latos Grażyński and Martin Stępień synthesized *meta*-benziporphodimethenes by carrying out condensation reaction between α,α'–dihydroxy–1, 3–diisopropylbenzene; pyrrole and an aromatic aldehyde; the reaction was catalyzed by using Lewis acid i.e., boron-trifluoride etherate [19] which was followed by oxidation reaction using DDQ. A good yield of around 14% was produced from this reaction (**Scheme 1.1.)** [18].

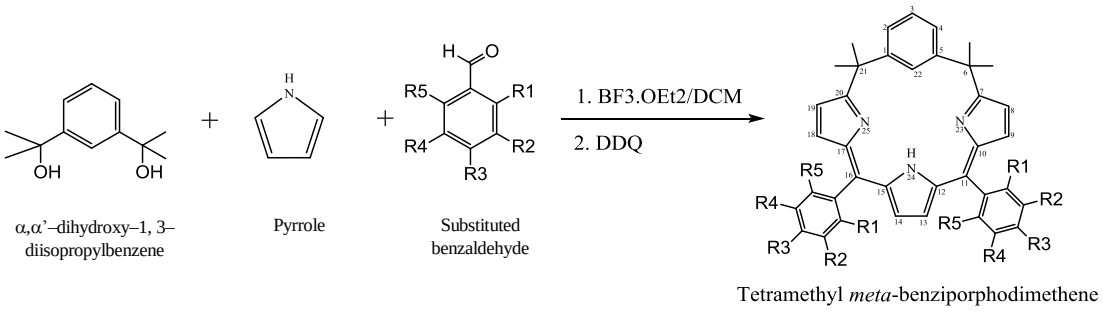

Scheme 1.1. Synthesis of *meta*-benziporphodimethene.

meta-benziporphodimethenes show broad UV-Visible spectrum because of presence of discrete conjugated system and are generally red coloured compounds. A high energy Soret band and a lower energy Q band are both observed in the UV-visible spectrum of *meta*-benziporphodimethenes at about 350 nm and 510 and 550 nm, respectively.

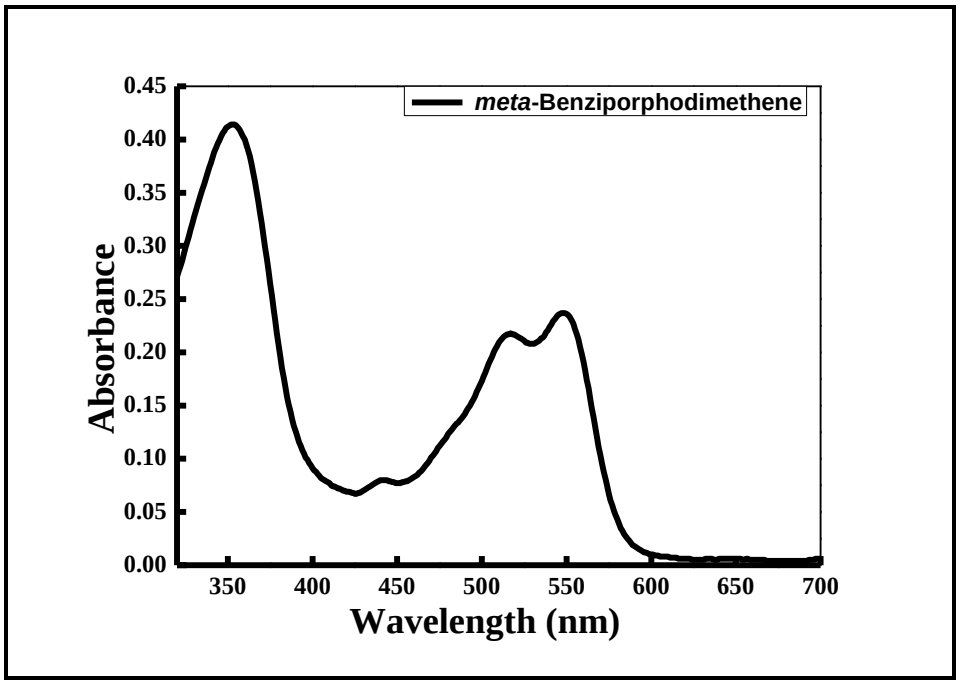

Figure 1.6. UV-Vis Spectra of *meta*-benziporphodimethene

Synthetic pathway mentioned above for the synthesis of *meta*-benziporphodimethene also leads to synthesis of isomeric α, β-unsaturated γ-Lactam embedded N-Confused-tetra-methyl *meta*-benziporphodimethenes[20].

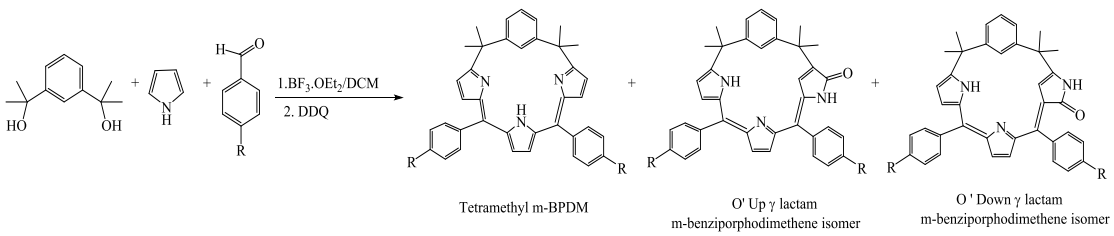

Scheme 1.2. The O-Up and O-Down γ-lactam embedded N-confused isomers.

meta-benziporphodimethenes are found to be more distorted than the other two isomers as shown by X-ray analysis. Computational studies using Density Functional Theorem calculation on porphyrin analogues can provide important information to understand how modifications play role in amending the physical properties of the analogues [20].

Various research groups attempted different modifications at *meso* carbon atoms of *meta*-benziporphodimethene using same synthetic pathway and various applications of *meta*-benziporphodimethene were explored. In 2016, Kumar *et. al.* reported different analogues of *meta*-benziporphodimethene with 15-17% yield. The research group utilized UV-Vis, NMR, mass spectroscopy, and X-ray crystallographic studies to confirm the synthesized product. Quantum yield, fluorescence studies, and bio-cell imaging applications have also been explored.

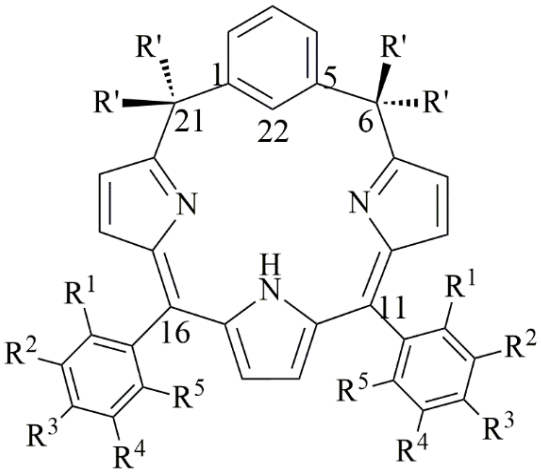

where, R'=CH_3
(1) R^1=R^2=R^4=R^5=H, R^3=Cl
(2) R^1=R^2=R^4=R^5=H. R^3=Br
(3) R^1=R^5=Cl, R^2=R^3=R^4=H
(4) R^1=R^5=F, R^2=R^3=R^4=H
(5) R^1=R^2=R^3=R^4=R^5=F
(6) R^1=R^2=R^4=R^5=H, R^3=CF_3
(7) R^1=R^2=R^4=R^5=H, R^3=OCH_3
(8) R^1=R^5=H, R^2=R^3=R^4=OCH_3

Figure 1.7. *meso*-substituted *meta*-benziporphodimethene derivatives by Kumar *et. al.*[21]

Kumar *et. al.* attempted various modifications at *meso* carbon atoms of *meta*-benziporphodimethene (**Figure 1.7**) using the same synthetic pathway (**Scheme 1.1**) and explored various advancements in applications of this novel molecule[21].

Spectroscopic Analysis

1.3.2. UV-Vis Spectroscopy

Broad UV-Visible spectrum is observed for the *meta*-Benziporphodimethene analogues owing to the discrete conjugated system of the analogues[22]. Free-base form of *meta*-Benziporphodimethene analogues is non-fluorescent but the fluorescence is switched on

upon metalation i.e., addition of zinc chloride metal salt, and an instant colour change from pink to greenish blue was observed (**Figure 1.8**) [21].

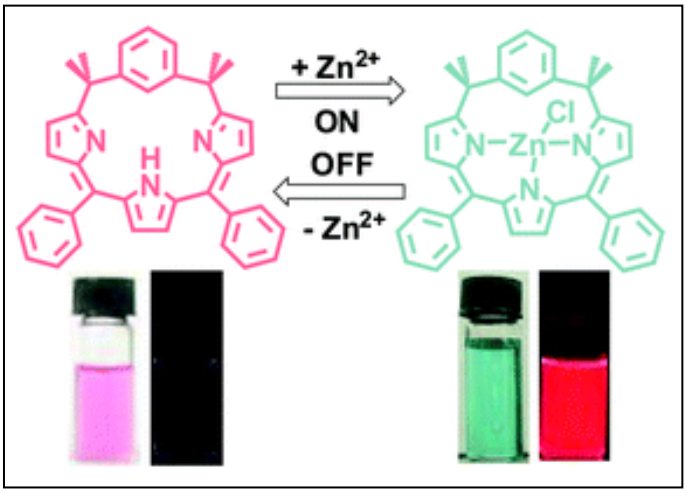

Figure 1.8. Colour change in *meta*-benziporphodimethene upon metalation using $ZnCl_2$ salt[22].

Broad UV-Vis spectra observed in *meta*-Benziporphodimethene analogues due to the presence of sp^2-sp^3 mixed *meso* carbon atoms. Kumar et. al. (**Figure 1.9**) presented that, for *para* and *ortho*- substituted *meso*-phenyl groups of free-base *meta*-benziporphodimethenes the Soret like high energy band was observed at around 342-378 nm, **1-8** in **Figure 1.7** (**Table 1.1**).

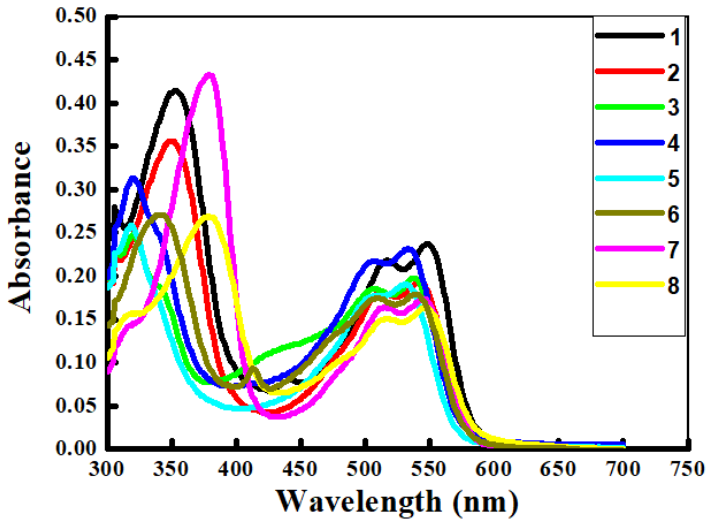

Figure 1.9. UV-Vis Spectra for free-base *meta*-benziporphodimethene analogues[21]

Table 1.1. Consolidated UV data for **Figure 1.7**[21].

Compound	Wavelength (λ_{max}) in nm			
	Freebase TMBPDM		Zn^{2+} TMBPDM complex	
	Soret Band	Q-Band	Soret Band	Q-Band
1	353	517-548	351	594-639
2	351	513-542	350	594-638
3	321	508-538	348	602-649
4	320	507-533	346	598-642
5	319	508-531	346	600-642
6	342	509-539	347	594-641
7	378	513-545	343	592-643
8	376	513-546	346	598-642

Due to the strong interactions of d-orbital of zinc ions with the macrocycle in the ground state absorption spectra of metal complexes of these novel analogues with respect to their free-base forms, a significant red shift is observed upon metalation of free-base *meta*-benziporphodimethene analogues.

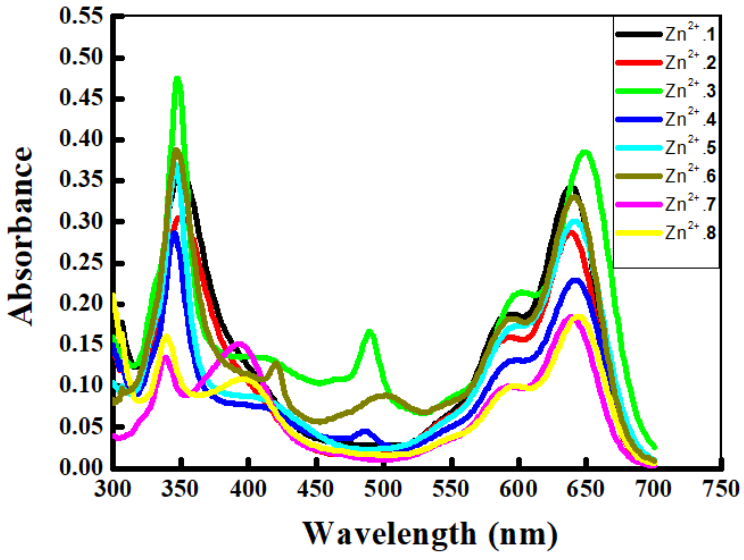

Figure 1.10. UV-Vis Spectra of *meta*-benziporphodimethene, **1-8** (**Figure 1.7**) zinc chloride complexes[21].

1.3.3. Structural Analysis

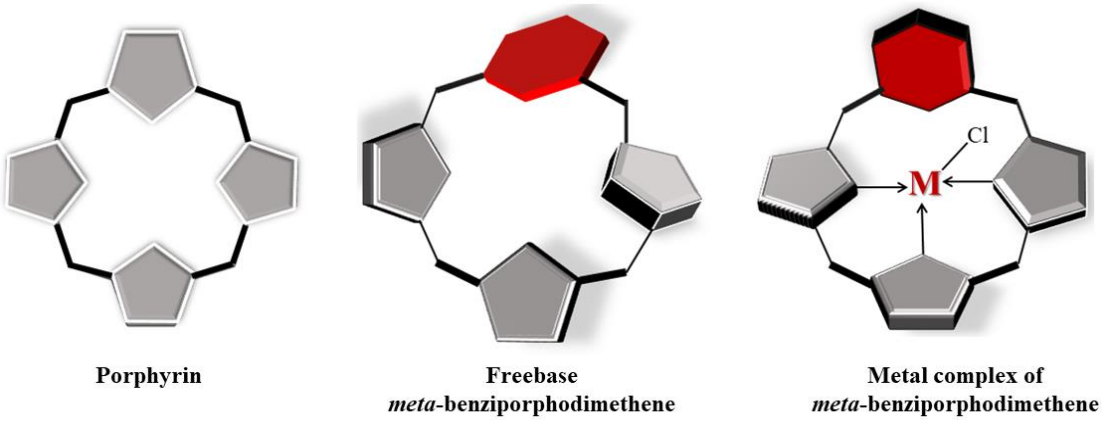

Figure 1.11. Depiction of core geometry of porphyrin molecule, non-planar *meta*-benziporphodimethene molecule and its metal complex (M= Zn, Cd, Hg)

In 2008, Hung *et. al.* reported crystal structure of *meta*-benziporphodimethene zinc complex for the first time. Coordination of zinc ion with *meta*-benziporphodimethene through the three nitrogen or pyrrole rings and an axial chloride was confirmed after analysis[22].

Later on, the same group came up with the crystal structures of TMBPDM (free-base tetramethyl-*meta*-benziporphodimethene) along with its two isomers (**Scheme 1.3**).

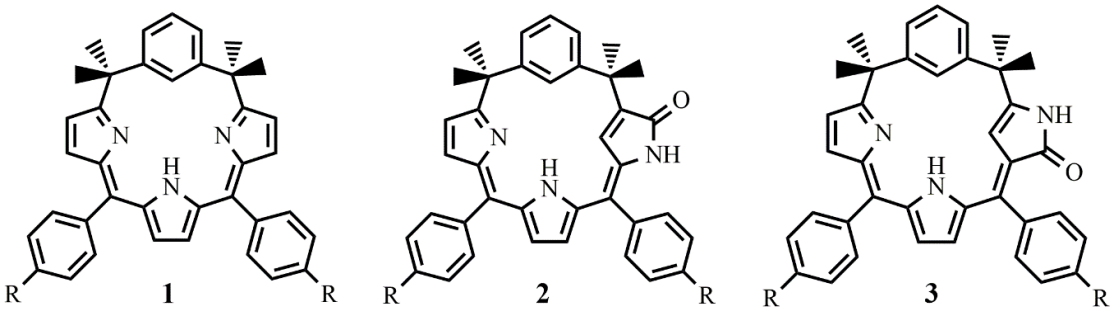

Scheme 1.3. Tetramethyl-*meta*-benziporphodimethene (**1**) molecule along with its O-Up isomer (**2**) and O-Down (**3**) isomer, R= H, COOMe.

TMBPDM was found to be more distorted than its O-Up isomer and O-down isomer after X-ray analysis. The average deviation for **1** (TMBPDM) of 25 atoms on the

macrocycle from a mean tripyrrin plane (plane through 17 atoms i.e., atoms of 3 pyrrole rings and 2 sp^2 hybridised *meso*-carbon atoms) is 1.044 Å while the values for O-Up Isomer (**2**) is found to be 0.680 Å and for O-Down Isomer (**3**) is 0.630 Å. The angle between the CNNN inner-core plane and the macrocyclic phenylene plane is 70.35° for O-Up Isomer and angle between the CNNN inner-core plane and the macrocyclic phenylene plane is69.76° for O-Down Isomer. However, in case of TMBPDM the angle between phenylene plane and three pyrrolic nitrogen plane is only 52.39°. These data are consistent with the fact that O-Up Isomer (**2**) and O-Down Isomer (**3**) are found to be less puckered than TMBPDM (**1**) with phenylene rings oriented vertical to the mean plane of the macrocycle (**Figure 1.12**)[20].

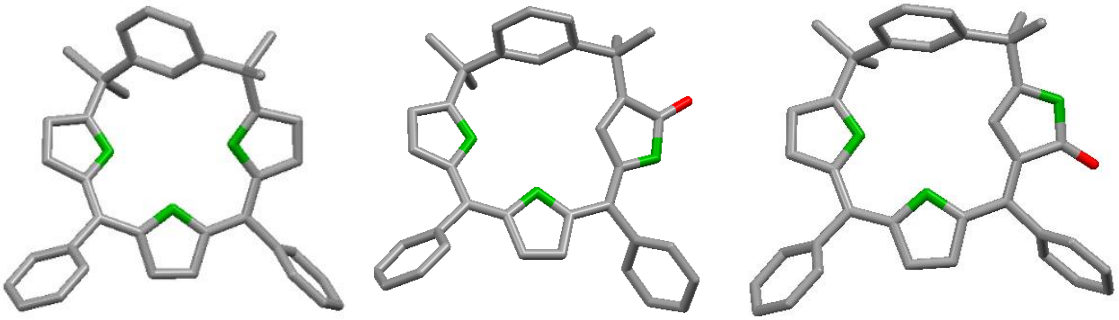

Figure 1.12. Molecular model of TMBPDM (**1**) along with its O-Up (**2)** and O-Down (**3)** isomers. Crystal structure coordinates were taken from ref.[20]

Later, the crystal structure of free base 11,16-Bis (3,4,5-trimethoxy-phenyl)-6,6,21,21-tetramethyl-*meta*-benziporphodimethene was determined by Kumar *et. al.* and its geometry were found lesser distorted than earlier reported structures of *meta*-benziporphodimethenes (**Figure 1.13**).

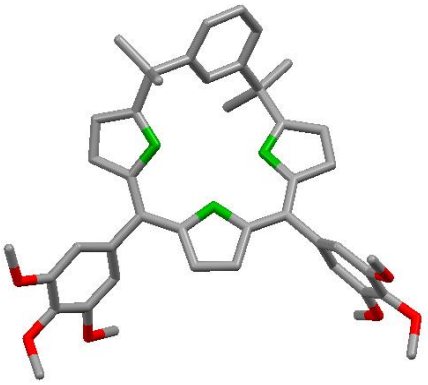

Figure 1.13. Molecular model of 11,16-Bis(3,4,5-trimethoxy-phenyl)-6,6,21,21-tetramethyl-*meta*-benziporphodimethene. Crystal structure coordinates were taken from[21].

1.3.4. Electronic structural studies of sterically hindered meta-benziporphodimethenes

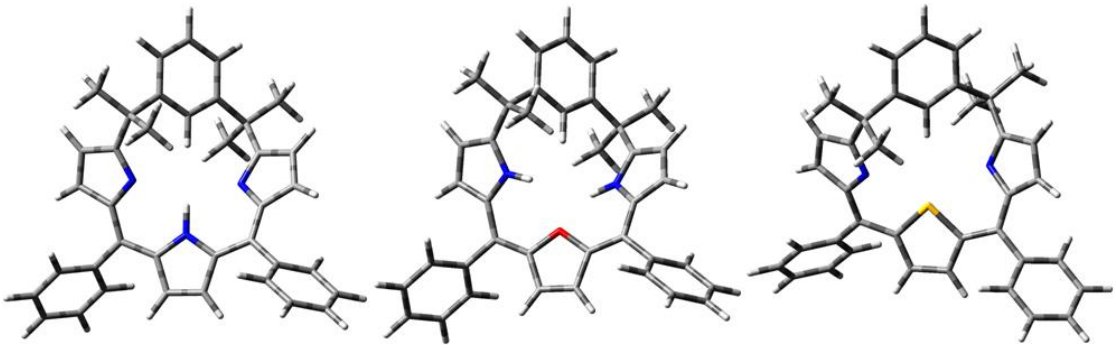

The structures and relative energies of 11,16-bis(phenyl)-6,6,21,21-tetramethyl-*meta*-benzi-6,21-porphodimethene (**1**) and its N-confused akin containing a γ–lactam ring (**2** and **3**) have been calculated using density functional theory (DFT) method (**Scheme 1.3)**. The DFT calculation was also carried out on thia- and oxa- analogue of **1**. The optimized structure reveals that thia-*meta*-benziporphodimethene has a more symmetrical conformation than the oxa- and aza- analogue. The tautomerisms in these compounds were investigated. The γ–lactam ring close to the adjacent sp^3 hybridized carbon was found to be more stable[23]. The energy difference between the *meta*-benziporphodimethene and inverted isomers range from 4-10 Kcal/mol. Higher energy difference was calculated between the isomers with or without γ-lactam ring.

The energy difference between O-up isomers containing γ-lactam ring is relatively low in comparison to those which have oxidized pyrrole and inverted pyrrole ring at different positions. But the energy difference between those isomers having oxidized pyrrole and inverted pyrrole ring at different positions is comparable. It has been found that O-up isomers are more favourable than O-down isomers. In contrast, in case of inverted isomers of **1**, the inverted pyrrole having nitrogen towards down side is more stable. The structure of thia- analogue without inner hydrogen atom is more symmetrical in comparison to their oxa- and aza- analogues[23].

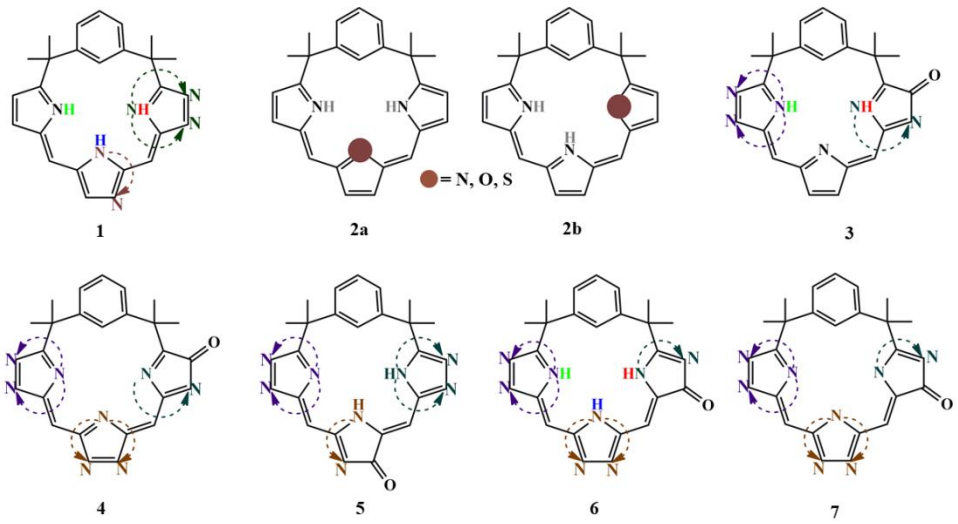

Figure 1.14. Overview of TMBPDM analogues studied by Kumar *et. al.*[23]

The effect on the geometries and relative energies of *meta*-benziporphodimethene was studied by varying the positions of N-confused ring and oxygenation at one of the pyrrole rings (**Figure 1.14**)[23].

1.3.5. NMR shifts in meta-benziporphodimethenes

The two N-confused isomers exist as dimer and the dimerization was confirmed by taking the concentration dependent NMR spectra in $CDCl_3$. The ring current in *meta*-

benziporphodimethenes is attenuated due to presence of tetrahedral *meso*-carbon atoms hence *meta*-benziporphodimethenes are non-aromatic[22]. NMR spectra of *meta*-benziporphodimethenes also confirms this character as the chemical shift of inner N-H proton appears at δ ~12.0, which signifies the absence of internal shielding by ring current. At ~1.7 ppm methyl peaks of tetrahedral group are observed[21].

Table 1.2. Consolidated NMR data for **Figure 1.7**[21].

Compound	N-H (H27, Py_o)	Ar-H (H26)	Ar-H (C2, C3, C4, C11, C16)	β-Py_1, Py_2-H (C8, C9, C18, C19)	β-Py_o-H (C13, C14)	OCH_3 (R^2, R^3, R^4)	sp^3-CH_3 (C6, C21)
1	12.32 (br, s)	7.93(s)	7.24-7.39 (m)	6.81 (ab quartet)	6.15 (s)	---	1.72 (s)
2	12.32 (br, s)	7.94(s)	7.31-7.57 (m)	6.83 (ab quartet)	6.16 (s)	---	1.74 (s)
3	12.16 (br, s)	8.06(s)	7.28-7.41 (m)	6.59 (d) -6.82 (d)	5.86 (s)	---	1.81 (s)
4	12.18 (br, s)	7.97(s)	6.91-7.45 (m)	6.70 (d) -6.83 (d)	6.00 (s)	---	1.79 (s)
5	12.08 (br, s)	7.89(s)	7.25-7.34 (m)	6.65 (d) -6.90 (d)	5.98 (s)	---	1.78 (s)
6	12.00 (br, s)	7.92(s)	7.68 (d,4H-ArH), 7.56 (d,4H-ArH), 7.29 (m,3H-ArH)	6.75 (d) -6.85 (d)	6.07 (s)	---	1.75 (s)
7	12.38 (br, s)	7.93(s)	7.44 (d, 4Ar-H), 7.27-7.32 (m, 3H,2,3,4 Ar-H), 6.95 (d, 4Ar-H)	6.77 (d) -6.88 (d)	6.30 (s)	3.87 (s)	1.69 (s)
8	12.33 (br, s)	7.92(s)	7.30(q, 3H 2,3,4 Ar-H) + 6.74 (s, 4Ar-H)	6.80 (d) -6.95 (d)	6.35 (s)	3.92 (s,6H, *para* OMe) + 3.83 (s,12H, *meta* OMe)	1.70 (s)

1.4 Properties of metalated *meta*- benziporphodimethene complexes

1.4.1. Weak Metal-Arene Interaction

Presence of metal-arene interactions in metal complexes of tetramethyl-*meta*-benziporphodimethene analogues is one their most important properties. C-H bond of *meta* phenylene ring is activated in the vicinity of transition metal atoms in *meta*-Benziporphodimethenes which becomes a new horizon to explore. The weak metal–arene interactions in nickel and cadmium complexes of *meta*-benziporphyrin have been confirmed by X-ray structure analysis. The strength of the metal-arene interaction is highly dependent on the conformation of the arene moiety [19], [24].

1.4.2. Fluorescence enhancement

Free-base forms of *meta*-benziporphodimethene analogues are non-fluorescent but fluorescence is turned on upon metalation with no background emission[21], [22]. The fact that *meta*-benziporphodimethenes act as a specific zinc ion sensor is the most significant aspect of this finding[21]. However, in case of cadmium and mercury metal complexes very less fluorescence is observed comparatively. This type of fluorescence comes under the category of "chelation enhanced fluorescence"(CHEF) since the fluorescence "turns on" upon zinc metalation. The majority of CHEF sensors are based on fluorophores that emits at wavelengths less than 600 nm, like fluorescein, dansyl, and anthracene[25],[26]. Light-induced tissue damage is minimized by sensors functioning above 600 nm, where background emission is minimal. These sensors also penetrate and scatter light less in sample with optical diffraction problems. Hung and coworkers demonstrated that these kinds of moieties do not form complexes with alkali, alkaline earth and other some transition metals

which are important physiologically and further provided that the stability constant for zinc complexation with *meta*-benziporphodimethene is greater than the cadmium and mercury metal ions[22].

1.4.3. Fluorescence phenomena: Structure co-relation

meta-benziporphodimethene is found to be a selective zinc ion sensor and fluorescence intensity was found to be higher than that in cadmium or mercury metal complexes. The reason for this phenomenon is planarity of the macrocycle in the bind state. The tripyrrin moiety exists as highly distorted non-planar molecule, but upon metalation the free-base macrocycle becomes planar. The average deviation of the three pyrrolic nitrogens reduces from 0.27 Å to 0.10 Å upon metalation. It has also been observed that the zinc has the minimum apical deviation of 0.48-0.50 Å from the tripyrrine plane of the molecule as compared to that of 0.70-0.71 Å for mercury and 0.62-0.67 Å for cadmium, and the orientation of *meta*-phenylene ring in metal-*meta*-benziporphodimethene changed from 81.4° in Zn-*meta*-benziporphodimethene to 89.3° for Cadmium and 92.1° for Mercury. The data depicts a better resonance tendency for zinc as the binding metal ion and is very consistent with the effective transfer of electron density from ligand to metal[24].

1.4.4. Cell-Imaging Applications

Numerous biological activities in the human body include zinc ions. As a structural cofactor and regulator of gene expression, zinc is found in the human body in bound state to protein. The vesicles of neurons may potentially produce a labile zinc ion pool. Patients with malignancies and inflammatory disorders also have abnormally

high levels of zinc in their tissues. Zn^{2+} detection may aid in elucidating its physiological and pathological functions because both vital roles and harmful effects of Zn^{2+} are frequently reported. In order to identify Zn^{2+} in liquid medium in real time and without the need of indicators, a small-sized semiconductor optoelectronic device is therefore needed[27]– [32].

For real-time and indicator-free detection of zinc ions in the solution, Hung and co-workers designed an organic hydrogel film with micron-sized pillar array by introducing 11,16-bis(phenyl)-6,6,21,21-tetramethyl-*m*-benzi-6,21-porphodimethene as a fluorescent indicator in a hydrogel host poly (2-hydroxyethyl methacrylate).

Kumar and his coworkers explored the cellular imaging properties of *meta*-benziporphodimethenes in MDA-MB-468 breast carcinoma cells and found that these molecules are lesser cytotoxic for longer time and can internalize successfully and further concluded that electron releasing and withdrawing group does not impact on internalization (**Figure 1.15.**).

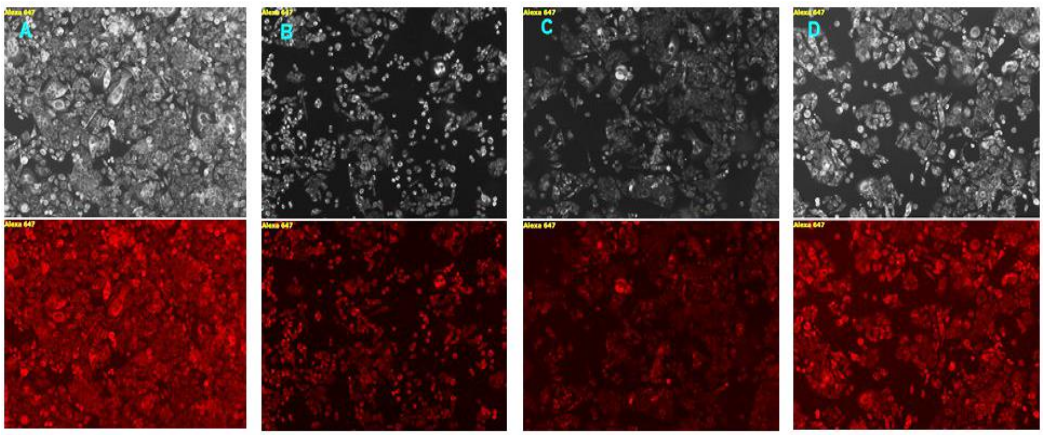

Figure 1.15. MDA-MB-468 cells incubated with different *meta*-benziporphodimethenes and Zn^{2+} ions for 30 min and respective bright field marked with A-D as well as fluorescence images (just down to its respective bright field image) were captured at 10X objective lens magnification[33].

1.5 Conclusion and Outlook

One of the potential synthetic porphyrin analogues is carbaporphyrinoids, which also includes corroles, benziporphyrins, and *meta*-benziporphodimethenes. In both in-vitro and in-vivo analysis, the use of *meta*-benziporphodimethenes analogues has significant potential for estimation and detection of spectroscopically silent Zn^{2+} ions. In these molecules fluorescence occurs at high wavelength in visible region leading to lesser photo damage and further has an advantage of low background emission. *meso*-phenyl substituents have a significant effect in zinc metal complexation of *meta*-benziporphodimethenes. Advancements in this area of research is forwarded by electronic structure properties of these molecules. Accurate zinc ion estimation inside the cells can be explored further. It is also noteworthy that so far only aromatic aldehydes have been used for synthesis of *meta*-benziporphodimethene analogs. So far, no research groups have reported the synthesis via condensation reaction of a typical aliphatic aldehyde with diol and pyrrole. The probable notion that the oxidation potential of the electron-donating aliphatic substituents is too low to allow the product to survive can be used to support the notion that the macrocycle is inherently electron-rich.

References

[1] S. D. Starnes *et al.*, "Anion sensors based on β,β′-disubstituted porphyrin derivatives," *Tetrahedron Letters,* vol. 43, pp. 7785-7788, 2002.

[2] S. D. Straight *et al.*, "Self-regulation of photoinduced electron transfer by a molecular nonlinear transducer," *Nature Nanotechnol*ogy vol. 3, no. 5, pp. 280–283, 2008.

[3] J. Králová *et al.*, "Porphyrin - Cyclodextrin conjugates as a nanosystem for versatile drug delivery and multimodal cancer therapy," *J Med Chem*, vol. 53, no. 1, pp. 128–138, 2010.

[4] T. Ozawa *et al.*, "In vivo evaluation of the boronated porphyrin TABP-1 in U-87 MG intracerebral human glioblastoma xenografts.," *Mol Pharm*, vol. 1, no. 5, pp. 368–374, 2004.

[5] G. Jori *et al.*, "Photodynamic therapy in the treatment of microbial infections: Basic principles and perspective applications," *Lasers in Surgery and Medicine*, vol. 38, no. 5, pp. 468–481, 2006.

[6] V. S. Lin *et al*., "Highly Conjugated, Acetylenyl Bridged Porphyrins: New Models for Light Harvesting Antenna Systems," *Science*, vol. 264, pp. 1105-1111, 1994.

[7] K. M. Kadish *et al*., "The Porphyrin Handbook," *Academic Press*: San Diego, CA, 2000.

[8] M. Yedukondalu *et al*., "Core-modified porphyrin-based assemblies," *Coordination Chemistry Reviews*, vol. 255, no. 5–6. pp. 547–573, 2011.

[9] T. Ishizuka *et al*., "Inverted N-confused porphyrin dimer," *Angew. Chem. - International Edition*, vol. 43, no. 38, pp. 5077–5081, 2004.

[10] T. Ishizuka *et al.*, "Substitution, dimerization, metalation, and ring-opening reactions of N-fused porphyrins," *Tetrahedron*, vol. 64, no. 18, pp. 4037–4050, 2008.

[11] M. Siczek *et al*., "Synthesis, Characterization, and Chirality of Dimeric N-Confused Porphyrin–Zinc Complexes: Toward the Enantioselective Synthesis of Bis(porphyrinoid) Systems," *Angew. Chem.*, vol. 119, no. 39, pp. 7576–7580, 2007.

[12] P. J. Chmielewski, "Synthesis and Characterization of a Cyclic Bis-silver(I) Assembly of Four 2-Aza-21-carbaporphyrinatosilver (III) Subunits," *Angew. Chem.*, vol. 117, no. 39, pp. 6575–6578, 2005.

[13] P. J. Chmielewski, "Synthesis and Characterization of a Directly Linked N-Confused Porphyrin Dimer," *Angew. Chem.* vol. 116, no. 42, pp. 5773–5776, 2004.

[14] P. J. Chmielewski e*t al*., "Nickel Complexes of 21-Oxaporphyrin and 21,23-Dioxaporphyrin," *Chemistry- A European Journal*, vol. 3, pp. 268-278, 1997.

[15] M. Stepien *et al*., "Benziporphyrins: Exploring Arene Chemistry in a Macrocyclic Environment," *Acc. Chem. Res.*, vol. 38, pp. 88-98, 2005.

[16] K. Berlin *et al*., "Benziporphyrin, a Benzene-Containing, Nonaromatic Porphyrin Analogue," *Angew. Chem. Int. Ed. Engl.*, vol. 33, no. 12, 1994.

[17] M. Stepien *et al.*, "Tetraphenylbenziporphyrin-A Ligand for Organometallic Chemistry," *Chem. Eur. J.*, vol. 7, no. 23, 2001.

[18] M. Stępień *et al*., "Tetraphenyl-*p*-benziporphyrin: A carbaporphyrinoid with two linked carbon atoms in the coordination core," *J Am Chem Soc*, vol. 124, no. 15, pp. 3838–3839, 2002.

[19] M. Stępien *et al*., "Cadmium (II) and Nickel (II) Complexes of Benziporphyrins. A Study of Weak Intramolecular Metal-Arene Interactions," *J Am Chem Soc*, vol. 126, no. 14, pp. 4566–4580, 2004.

[20] G. F. Chang *et al*., "Tetramethyl-*m*-benziporphodimethene and isomeric α, β-unsaturated γ-lactam embedded N-confused tetramethyl-*m*-benziporphodimethenes," *Chem Asian J*, vol. 4, no. 1, pp. 164–173, 2009.

[21] R. K. Sharma *et al*., "Synthesis, characterization and fluorescence turn-on behavior of new porphyrin analogue: *meta*-benziporphodimethenes," *Spectrochem Acta A Mol Biomol Spectroscopy*, vol. 169, pp. 58–65, 2016.

[22] C. H. Hung *et al.*, "*m*-Benziporphodimethene: A new porphyrin analogue fluorescence zinc (II) sensor," *Chemical Communications*, no. 8, pp. 978–980, 2008.

[23] A. Kumar *et al*., "Study on the structure, stability and tautomerisms of *meta*-benziporphodimethene and N-Confused isomers containing γ–lactam ring," *J Mol Struct*, vol. 1187, pp. 138–150, 2019.

[24] G. F. Chang *et al.*, "Factors that regulate the conformation of *m*-benziporphodimethene complexes: Agostic metal-arene interaction, hydrogen bonding, and η^2, π coordination," *Chemistry - A European Journal*, vol. 17, no. 40, pp. 11332–11343, 2011.

[25] W. Breuer *et al*., "Transport of iron and other transition metals into cells as revealed by a fluorescent probe," *American Journal of Physiology – Cell Physiology*, 1995.

[26] E. H. Cox *et al*., "Zinc-dependent protein folding," *Current Opinion in Chemical Biology*, pp. 162-165, 2000.

[27] M. P. Cuajungco *et al*., "Zinc and Alzheimer's disease: is there a direct link?" *Brain Research Reviews*, vol 23, pp. 219-236, 1997.

[28] G. A. Qureshi *et al.*, "Impact of selenium, iron, copper and zinc in on / off Parkinson's patients on L-dopa therapy," *Journal of Neural Transmission*, pp. 229-236, 2006.

[29] D. T. Dexter *et al.*, "Alterations in the levels of iron, ferritin and other trace metals in parkinson's disease and other neurodegenerative diseases affecting the basal ganglia," *Brain,* vol. 114, pp. 1953-1975, 1991.

[30] G. K. Andrews, "Cellular zinc sensors: MTF-1 regulation of gene expression," *BioMetals,* pp. 223-237, 2001.

[31] C. Devirgiliis *et al.*, "Zinc fluxes and zinc transporter genes in chronic diseases," *Mutation Research - Fundamental and Molecular Mechanisms of Mutagenesis,* vol. 622, no. 1–2, pp. 84–93, 2007.

[32] A. Q. Truong-Tran *et al.,* "The role of zinc in caspase activation and apoptotic cell death,"*BioMetals,* vol. 14, pp. 223-237, 2001.

[33] R. K. Sharma *et al.*, "*meta*-Benziporphodimethenes: New Cell-Imaging Porphyrin Analogue Molecules," *ChemistrySelect*, vol. 1, no. 13, pp. 3502–3509,2016.

Chapter 2

Scope of the Work

CHAPTER 2

SCOPE OF THE WORK

There has been a plethora of studies on the porphyrinoid macrocyclic ring system leading to extensive expansion of porphyrinoid family over the years. Several modifications on the porphyrin molecule leading to formation of new compounds were also being discovered alongside. Corrole, first reported by Johnson and Kay in the year 1965, is a contracted porphyrin system. The chemistry of corrole has been vastly investigated since then. Although, in terms of computational studies, corroles are less diverse than porphyrins. Not only corroles, the expanded, hetero-atom substituted and various other analogues of porphyrins have been intensely investigated over time. Computational chemistry acts as a bridge between the experimental and theoretical studies of any system. This bridging has been done for porphyrins and corroles majorly. Other analogues of porphyrinoid family still have a great scope for being investigated using various computational methods.

The new carbaporphyrinoid system *meta*-benziporphodimethene was introduced 18 years ago. The recent advancements in *meta*-benziporphodimethenes (*meta*-BPDM) have proved that the compound must gather great importance owing to its wide range of applications as a chemosensor [1]– [7]. After a thorough literature review, it was found that despite the outstanding properties exhibited by *meta*-BPDM, the compound reached out only to a small audience [8], [9]. This means, owing to the less yield and tendency for rapid oxidation the molecule fails to be meticulously investigated. For this reason, the current work focuses on finding out the possible factors that could enhance the stability and yield of this unique class of carbaporphyrinoid systems.

Sometimes, experimental methods are not sufficient to answer many crucial steps resulting in a number of chemical and biological processes. Also, computational chemistry is said to be a great tool to study the insights of a reaction even before one performs it in a laboratory. The advancements in technology have opened doors for theoretical chemists to analyse the systems under study, computationally and check the feasibility of the reactions beforehand.

Our work is the attempt to club the computational chemistry with the experimental procedures *meta*-benziporphodimethene analogues and its metal complexes. Herein, we intend to investigate the possible aspects that may or that may not participate in intensifying the yield or stability of *meta*-benziporphodimethene, theoretically. Fascinating results that were obtained through the theoretical analysis opens up a wide pathway for the research groups to overcome the low yield barrier and further study the applications of these prosthetic molecules.

The objectives of the present dissertation are as follows:

1. Synthesis of tetramethyl-substituted analogues of free base *m*-BPDM and its Cd (II) and Hg (II) complexes.
2. Detailed DFT studies of N-confused isomers of *m*-BPDM analogues involving γ-lactam ring.
3. DFT studies of metal complexes of *m*-BPDM analogues.

References

[1] M. Stępień *et al*., "Cadmium (II) and Nickel (II) Complexes of Benziporphyrins. A Study of Weak Intramolecular Metal-Arene Interactions," *J. Am. Chem. Soc.*, vol. 126, no. 14, pp. 4566–4580, 2004.

[2] C. H. Hung *et al.*, "*meta*-Benziporphodimethene: A new porphyrin analogue fluorescence zinc (II) sensor," *Chemical Communications*, no. 8, pp. 978–980, 2008.

[3] R. K. Sharma *et al*., "Synthesis, characterization and fluorescence turn-on behavior of new porphyrin analogue: *meta*-benziporphodimethenes," *Spectrochimica Acta- Part A: Mol. and Biomol. Spectroscopy*, vol. 169, pp. 58–65, 2016.

[4] R. K. Sharma *et al*., "*meta*-Benziporphodimethenes: New Cell-Imaging Porphyrin Analogue Molecules," *ChemistrySelect*, vol. 1, no. 13, pp. 3502–3509, 2016.

[5] D. Chauhan *et al.*, "Synthesis, characterization and metal ions sensing applications of *meta*-benziporphodimethene-embedded polyacrylamide/ carboxymethyl guargum polymeric hydrogels in water," *Environmental Technology (United Kingdom)*, vol. 43, no. 7, pp. 991–1002, 2022.

[6] D. Chauhan *et al*., "An efficient adsorbent for the removal of Zn^{2+} Cd^{2+} and Hg^{2+} from the real industrial effluents," *International Journal of Environmental Science and Technology*, vol. 19, no. 3, pp. 1483–1494, 2022.

[7] D. Chauhan *et al.*, "Modified polymeric hydrogels for the detection of Zn^{2+} in E. coli bacterial cells and Zn^{2+}, Cd^{2+} and Hg^{2+} in industrial effluents," *Environmental Technology (United Kingdom)*, vol. 43, no. 23, pp. 3600–3607, 2022.

[8] A. Kumar *et al*., "Study on the structure, stability and tautomerisms of *meta*-benziporphodimethene and N-Confused isomers containing γ–lactam ring," *J Mol Struct*, vol. 1187, pp. 138–150, 2019.

[9] D. Ahluwalia *et al.*, "Recent developments in *meta*-benziporphodimethene: A new porphyrin analogue," *J Mol Struct*, vol. 1228, 2021.

Chapter 3

Synthesis and Characterizations of meta- Benziporphodimethene Analogues and its Metal Complexes

CHAPTER 3

SYNTHESIS AND CHARACTERIZATIONS OF *meta*-BENZIPORPHODIMETHENE ANALOGUES AND ITS METAL COMPLEXES

3.1 Introduction

meta-Benziporphodimethenes (*m*-BPDM) are modified *meta*-benziporphyrins having two tetrahedral *meso* carbon atoms at positions 6 and 21. Martin Stępień was the first to synthesize alkoxy and hydroxy analoguesof *meta*-Benziporphodimethenes (*m*-BPDM) in the course of his works of Ph.D thesis. Herein, we present the free base 11,16-Bis(2,6-difluorobenzene)-6,6,21,21-tetramethyl-*meta*-benzi-6,21-porphodimethene and 11,16-Bis (2,3,4,5,6-pentafluorobenzene)-6,6,21,21-tetramethyl-*meta*-benzi-6,21-porphodimethene and their Cd (II) and Hg (II) metal complexes.

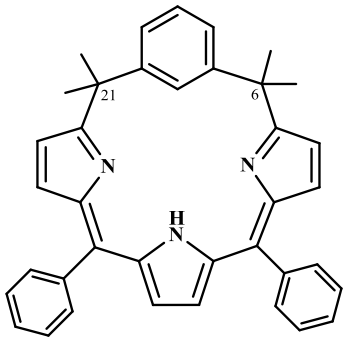

Figure 3.1. Structure of free base *meta*-benziporphodimethene

3.2 Experimental section

3.2.1. Reagents

Reagents used for the synthesis and characterization of the synthesized compounds are 2, 6-difluorobenzaldehyde, penta-fluorobenzaldehyde, $BF_3 \cdot OEt_2$ (Boron trifluoride etherate) from Sigma Aldrich, Pyrrole which was distilled before use, α, α'–

dihydroxy–1, 3–diisopropylbenzene from TCI, DDQ (2,3-dichloro-5,6-dicyano-p-benzoquinone), anhydrous mercuric chloride ($HgCl_2$), anhydrous cadmium chloride ($CdCl_2$) were obtained from Sigma-Aldrich. All other reagents and solvents were received from E. Merck Ltd. and were used as received.

3.2.2. General Information

Bruker Avance III 400 spectrometer was used to record 1H NMR Spectra; Chemical shifts are reported relative to residual hydrogen atoms in $CDCl_3$ in ppm. Bruker MaXis Impact mass spectrometer was used to perform mass spectra for the synthesized compounds. Agilent Cary 8454 UV-Visible spectrophotometer was used to record absorption spectra of the compounds. Merck silica gel 60 F254 precoated aluminium sheets were used to perform thin-layer chromatography.

Single crystal structure determination: Bruker diffractometer was used to collect intensity data at 273(2) K. Appropriate single crystals were mounted using paratone oil on top of a glass fibre and it was instantly transferred to diffractometer. Bruker SAINT program was used to perform data collection, analytical absorption corrections. SHELXL-97 was used to solve crystal structures using direct methods.

3.2.3. Synthetic Procedure

Synthesis of 11, 16-Bis(2,6-difluorobenzene)-6,6,21,21-tetramethyl-*meta*-benzi-6,21-porphodimethene (1)

11,16-Bis(2,6-difluorobenzene)-6,6,21,21-tetramethyl-*meta*-benzi-6,21-porphodimethene was synthesized by carrying out boron trifluoride etherate catalysed condensation reaction between pyrrole (1.51 mmol, 104μL); 2,6- difluorobenzaldehyde(1.01 mmol, 102μL) and

α,α'-dihydroxy-1,3-diisopropylbenzene (0.50 mmol, 98 mg) i.e., in ratio of 3:2:1 at room temperature i.e., 27°C for 2 hours which was followed by addition of DDQ into the reaction mixture and again the reaction mixture was stirred for 2 hours. Trimethylamine was used to quench the reaction and solvent was removed in vacuo. Silica gel column chromatography was used to purify the crude mixture by eluting it with mixture of n-hexane and dichloromethane to give 11,16-Bis(2,6-difluorobenzene)-6,6,21,21-tetramethyl-m-benzi-6,21-porphodimethene (17% yield) as red coloured powder(**Scheme 3.1**)[1]–[11].^{1}H NMR (300 MHz, $CDCl_3$, 298 K): 12.18 (br, 1H,NH), 7.97 (s, 1H, 22-ArH), 7.35–7.45 (m,3H, (2,3,4-ArH), 6.91–7.05 (m,6H, ArH), 6.83 (doublet ^{2}JH,H = 4.40 Hz, HH, 9.18-Pyrr H), 6.70 (doublet ^{2}JH,H = 4.22 Hz, HH, 8,19-Pyrr H), 6.00 (s,2H, 13,14- Pyrr H), 1.79 (s,12H, CH_3).

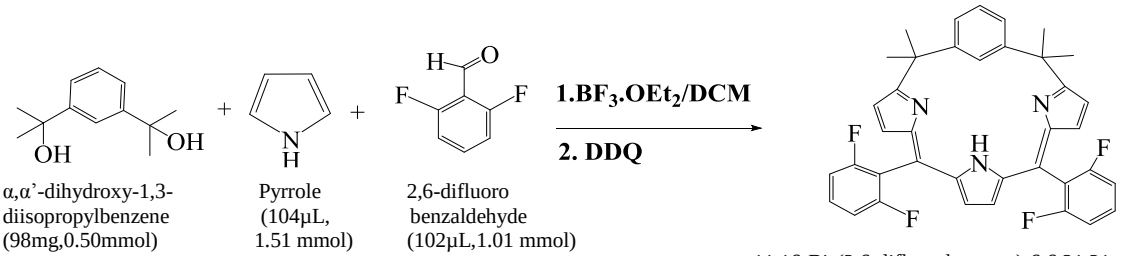

α,α'-dihydroxy-1,3-diisopropylbenzene (98mg,0.50mmol)

Pyrrole (104µL, 1.51 mmol)

2,6-difluoro benzaldehyde (102µL,1.01 mmol)

11,16-Bis(2,6-difluorobenzene)-6,6,21,21-tetramethyl-*meta*-benzi-6,21-porphodimethene

Scheme 3.1. Synthesis of free base11,16-Bis(2,6-difluorobenzene)-6,6,21,21-tetramethyl-*meta*-benzi-6,21-porphodimethene

Synthesis of 11,16-Bis(2,3,4,5,6-pentafluorobenzene)-6,6,21,21-tetramethyl-*meta*-benzi-6,21-porphodimethene (2)

11,16-Bis(2,3,4,5,6-pentafluorobenzene)-6,6,21,21-tetramethyl-*meta*-benzi-6,21-porphodimethene was synthesized by carrying out boron trifluoride etherate catalysed condensation reaction between pyrrole (1.51 mmol, 104µL); 2,3,4,5,6-pentafluorobenzene (1.01 mmol, 102µL) and α,α'-dihydroxy-1,3-diisopropylbenzene (0.50 mmol, 98 mg) i.e., in ratio of 3:2:1 at room temperature i.e., 27°C for 2 hours which was followed by

addition of DDQ into the reaction mixture and again the reaction mixture was stirred for 2 hours. Trimethylamine was used to quench the reaction and solvent was removed in vacuo. Silica gel column chromatography was used to purify the crude mixture by eluting it with mixture of n-hexane and dichloromethane to give 11,16-Bis(2,6-difluorobenzene)-6,6,21,21-tetramethyl-m-benzi-6,21-porphodimethene (17% yield) as red coloured powder(**Scheme 3.2**)[1]–[11].**^{1}H-NMR(400 MHz, $CDCl_3$, 25°C):** 12.08 (br,1H,NH), 7.89 (s, 1H, 22-ArH), 7.25–7.34 (m,3H, (2,3,4-ArH), 6.90 (doublet^{2}JH,H=4.58 Hz, HH, 9,18-Pyrr H), 6.65(doublet ^{2}JH,H=4.58 Hz,HH,8,19-Pyrr H), 5.98 (s,2H, 13,14-Pyrr H), 1.78 (s,12H, CH_3).

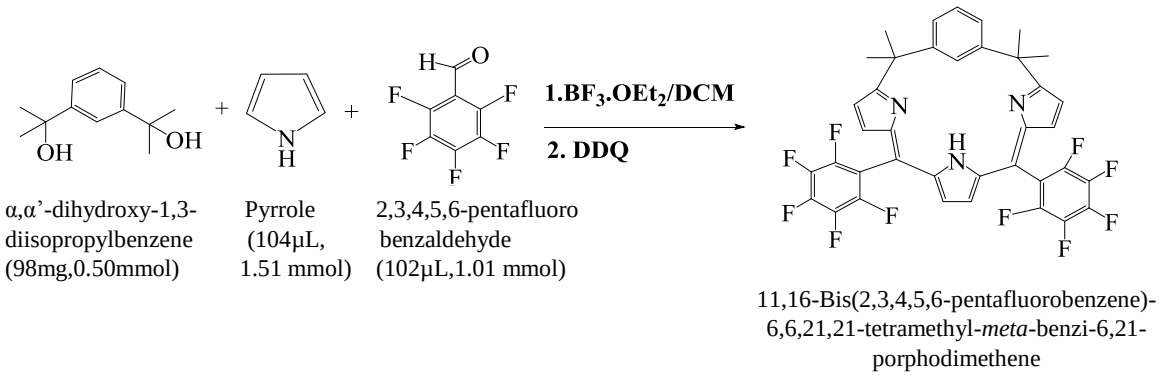

α,α'-dihydroxy-1,3-diisopropylbenzene (98mg,0.50mmol)

Pyrrole (104µL, 1.51 mmol)

2,3,4,5,6-pentafluoro benzaldehyde (102µL,1.01 mmol)

11,16-Bis(2,3,4,5,6-pentafluorobenzene)-6,6,21,21-tetramethyl-*meta*-benzi-6,21-porphodimethene

Scheme 3.2. Synthesis of free base11,16-Bis(2,3,4,5,6-pentafluorobenzene)-6,6,21,21-tetramethyl-*meta*-benzi-6,21-porphodimethene

Synthesis of metal complexes of *meta*-Benziporphodimethene using transition metals (Cd^{2+}, Hg^{2+})

Various metal complexes of *meta*-benziporphodimethenes have been prepared so far, which are quite stable also. The Ni, Zn, Cd, Hg and Ag complexes of *meta*-benziporphodimethes have been reported so far. The metal complexes of *meta*-benziporphodimethenes with zinc, cadmium, mercury and nickel were reported by Latos Grażyński and co-workers in 2004.

The general synthesis includes mixing of free-base *meta*-benziporphodimethenes with anhydrous metal salt in mixed solvents of acetonitrile with either dichloromethane or chloroform in presence of mild base 2, 6-lutidiine. The metal complex results in minutes after mixing at room temperature and is indicated by changing of colour of solution from red to greenish blue. Evaporation of solvent invacuo under reduced pressure yields the metal complex. The crystals can be obtained by crystallization of metal complexes in hexane.

Synthesis of Cd^{2+}.1

10mg of 11,16-Bis(2,6-difluorobenzene)-6,6,21,21-tetramethyl-*meta*-benzi-6,21-porphodimethene was dissolved in 25 ml solution of CH_3CN/CH_2Cl_2 in ratio of 2:1. Anhydrous cadmium chloride which was pre dissolved in very less amount of CH3CN was added to this mixture followed by addition of a drop of 2,6-lutidine to initiate the reaction. After stirring for 2 minutes, solvent was removed under reduced pressure. CH_2Cl_2 was used to dissolve the residue and excess amount of metal salt was extracted using distilled water. After collection of organic layer solvent was removed in vacuo and it was crystallized in n-hexane to obtain bluish green final product i.e., Cd^{2+} complex of 11,16-Bis(2,6-difluorobenzene)-6,6,21,21-tetramethyl-*meta*-benzi-6,21-porphodimethene (yield 98%); (Scheme 3.3)[1]– [11].

Synthesis of Cd^{2+}.2

10mg of 11,16-Bis(2,3,4,5,6-pentafluorobenzene)-6,6,21,21-tetramethyl-*meta*-benzi-6,21-porphodimethene was dissolved in 25 ml solution of CH_3CN/CH_2Cl_2 in ratio of 2:1. Anhydrous cadmium chloride which was pre dissolved in very less amount of CH3CN was added to this mixture followed by addition of a drop of 2,6-lutidine to

initiate the reaction. After stirring for 2 minutes, solvent was removed under reduced pressure. CH_2Cl_2 was used to dissolve the residue and excess amount of metal salt was extracted using distilled water. After collection of organic layer solvent was removed in vacuo and it was crystallized in n-hexane to obtain bluish green final product i.e., Cd^{2+} complex of 11,16-Bis(2,3,4,5,6-pentafluorobenzene)-6,6,21,21-tetramethyl-*meta*-benzi-6,21-porphodimethene (yield 98%); (Scheme 3.3).

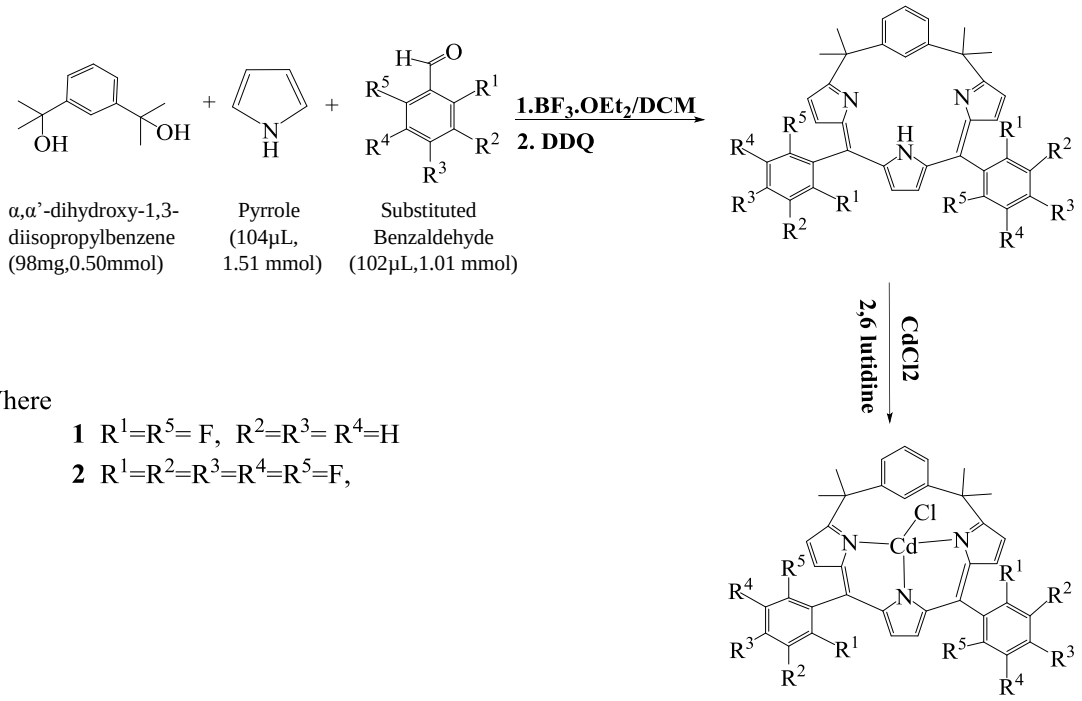

Where

1 $R^1=R^5=F$, $R^2=R^3=R^4=H$

2 $R^1=R^2=R^3=R^4=R^5=F$,

Scheme 3.3. Cd^{2+} complex of 11,16-Bis(2,6-difluorobenzene)-6,6,21,21-tetramethyl-*meta*-benzi-6,21-porphodimethene and 11,16-Bis(2,3,4,5,6-pentafluorobenzene)-6,6,21,21-tetramethyl-*meta*-benzi-6,21-porphodimethene.

Synthesis of Hg^{2+}.1

10mg of 11,16-Bis(2,6-difluorobenzene)-6,6,21,21-tetramethyl-*meta*-benzi-6,21-porphodimethene was dissolved in 25 ml solution of CH_3CN/CH_2Cl_2 in ratio of 2:1. Anhydrous mercuric chloride which was pre dissolved in very less amount of CH3CN was added to this mixture followed by addition of a drop of 2,6-lutidine to initiate the reaction. After stirring for 2 minutes, solvent was removed under reduced pressure.

CH_2Cl_2 was used to dissolve the residue and excess amount of metal salt was extracted using distilled water. After collection of organic layer solvent was removed in vacuo and it was crystallized in n-hexane to obtain bluish green final product i.e., Hg^{2+} complex of 11,16-Bis(2,6-difluorobenzene)-6,6,21,21-tetramethyl-*meta*-benzi-6,21-porphodimethene (yield 98%); (Scheme 3.4).

Synthesis of Hg^{2+}.2

10mg of 11,16-Bis(penta-fluorobenzene)-6,6,21,21-tetramethyl-*meta*-benzi-6,21-porphodimethene was dissolved in 25 ml solution of CH_3CN/CH_2Cl_2 in ratio of 2:1. Anhydrous mercuric chloride which was pre dissolved in very less amount of CH3CN was added to this mixture followed by addition of a drop of 2,6-lutidine to initiate the reaction. After stirring for 2 minutes, solvent was removed under reduced pressure. CH_2Cl_2 was used to dissolve the residue and excess amount of metal salt was extracted using distilled water.

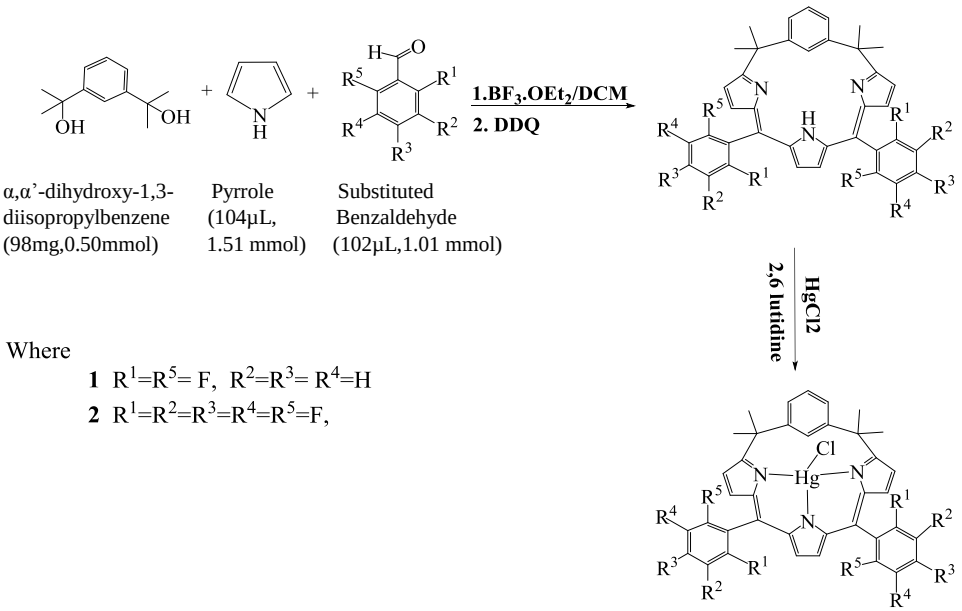

α,α'-dihydroxy-1,3-diisopropylbenzene (98mg,0.50mmol)

Pyrrole (104µL, 1.51 mmol)

Substituted Benzaldehyde (102µL,1.01 mmol)

Where

1 $R^1=R^5=F$, $R^2=R^3=R^4=H$

2 $R^1=R^2=R^3=R^4=R^5=F$,

Scheme 3.4. Hg^{2+} complex of 11,16-Bis(2,6-difluorobenzene)-6,6,21,21-tetramethyl-*meta*-benzi-6,21-porphodimethene and 11,16-Bis(2,3,4,5,6-pentafluorobenzene)-6,6,21,21-tetramethyl-*meta*-benzi-6,21-porphodimethene.

After collection of organic layer solvent was removed in vacuo and it was crystallized in n-hexane to obtain bluish green final product i.e., Hg^{2+} complex of 11,16-Bis(penta-fluorobenzene)-6,6,21,21-tetramethyl-*meta*-benzi-6,21-porphodimethene (yield 98%); (Scheme 3.4)[1]– [11].

3.3. Results and discussion

3.3.1. Spectroscopy

This sterically hindered free base *meta*-BPDM was then subjected to metalation at room temperature using metal (Cd (II) and Hg (II)) chloride metal salt in presence of 2,6-lutadine. The insertion of metal ion was validated by the change in color of the product *viz*., bluish-green. The UV–Vis spectra of free base *meta*-benziporphodimethenes and their metalated *meta*-benziporphodimethenes complexes was observed.

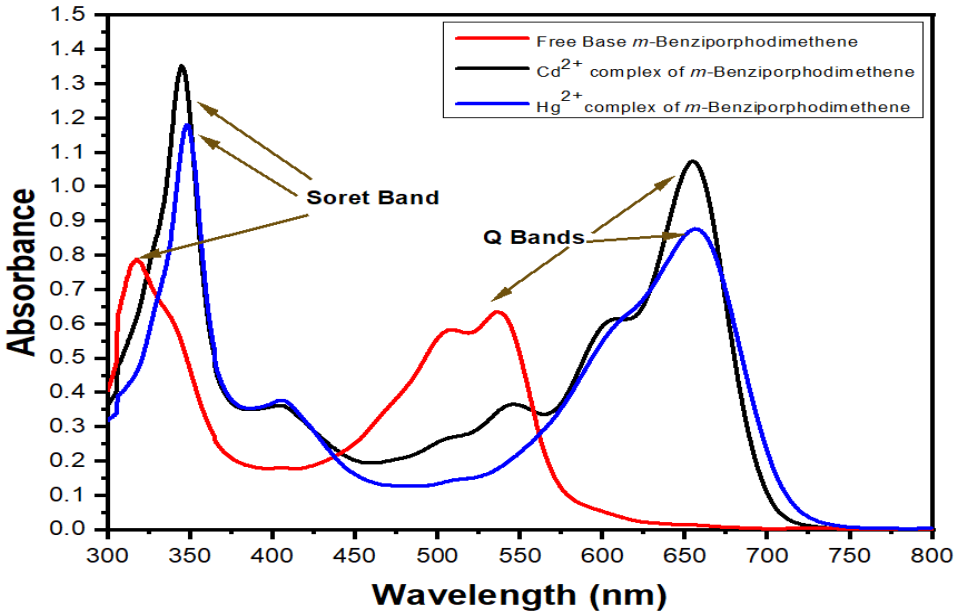

Figure 3.2. UV-Vis Spectra for free base *meta*-Benziporphodimethene with 2,6-difluorobenzaldehyde at *meso* position and its Cd^{2+} and Hg^{2+} metal complexes

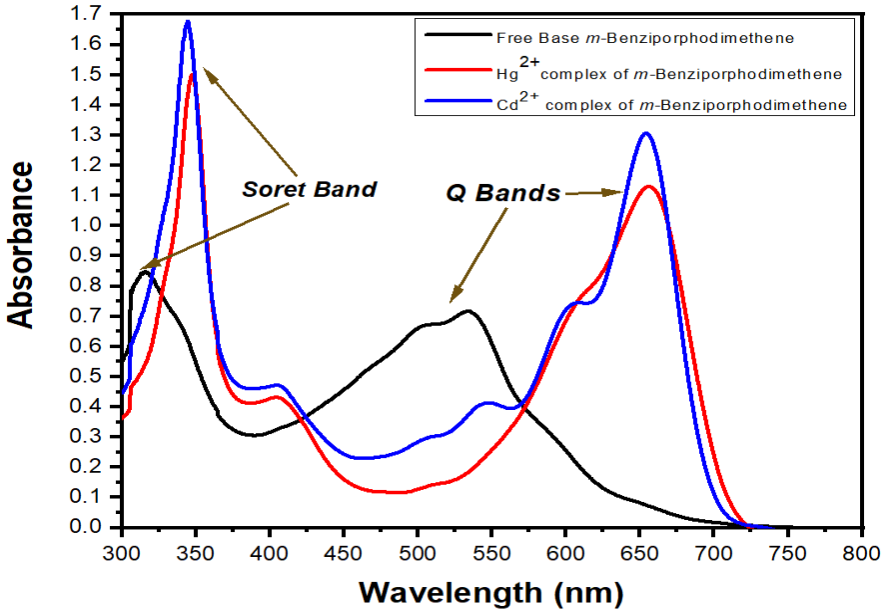

Figure 3.3. UV-Vis Spectra for free base *meta*-Benziporphodimethene with penta-fluorobenzaldehyde at *meso* position and its Cd^{2+} and Hg^{2+} metal complexes

3.3.2. Single Crystal X-ray crystallography

Single Crystal X-ray Diffraction studies of free base *meta*-Benziporphodimethene shows its ability to crystallize into different crystalline forms. These crystalline forms are called polymorphs. Structures **1a** and **1b** of **Fig. 3.5** are polymorphs.

The crystal **1a** was recrystallized from a mixture of n-heptane and DCM with the ratio (1:1). The crystal **1b** was recrystallized from the mixture of cyclohexane and ethylacetate with the ratio (1:1). The crystal **1a** belongs to the monoclinic space group C2/c and the crystal **1b** belongs to the triclinic space group P-1. Data collection was performed using monochromated MoKα radiation, λ = 0.71073 Å, using φ and ω scans to cover the Ewald sphere. Accurate cell parameters were obtained with the amount of indicated reflections. Using Olex2[12] the structure was solved with the olex2.solve[13] structure solution program using Charge Flipping and refined with the ShelXL [14] refinement package using Least Squares minimization. All nonhydrogen atoms were refined with anisotropic displacement parameters. The hydrogen atoms

were refined isotropically on calculated positions using a riding model with their U_{iso} values constrained to 1.5 times the U_{eq} of their pivot atoms for terminal sp^3 carbon atoms and 1.2 times for all other carbon atoms. Software used for molecular graphics: Mercury 2020.4.0.

3.3.2.1. Crystal data for compound 11,16-Bis(2,6-difluorobenzene)-6,6,21,21-tetramethyl-*meta*-benzi-6,21-porphodimethene

Crystal data for $C_{38}H_{30}F_4N_3$ (1a) empirical formula = $C_{38}H_{30}F_4N_3$; Space group = C2/c, wavelength = 0.71073, Z = 4, a = 43.134(3) Å, b = 12.3323(7) Å, c = 31.612(2) Å, α = 90°, β = 125.044°, γ = 90°, T = 200 K, V = 13767.2, D_{calcd}, g/cm3 = 1.289 μ, mm^{-1} = 0.166, R_1, % = 6.0, No. of reflections = 12,188. CCDC number: 2175543.

Crystal data for $C_{38}H_{30}F_4N_3$ (1b) empirical formula = $C_{38}H_{30}F_4N_3$; Wavelength = 0.71073, Z = 2, a = 12.100(3) Å, b = 14.313(3) Å, c = 20.276(5) Å, α = 89.614(5) °, β = 74.884(5) °, γ = 85.653(6) °, T = 200 K, Volume = 3380.0(14), Space group = P-1 D_{calcd}, g/cm3 = 1.294 μ, mm^{-1} = 0.091, R_1, %= 7.36, No. of reflections = 10,952. CCDC number: 2175544.

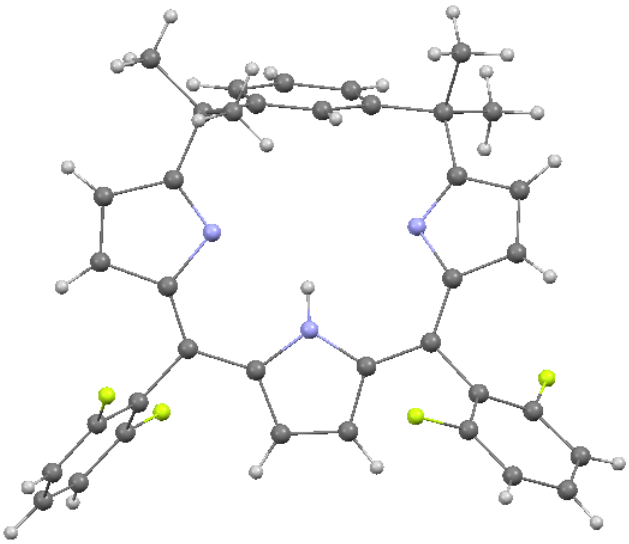

Figure 3.4. X-ray structure of free base *meta*-benziporphodimethene, **1.**

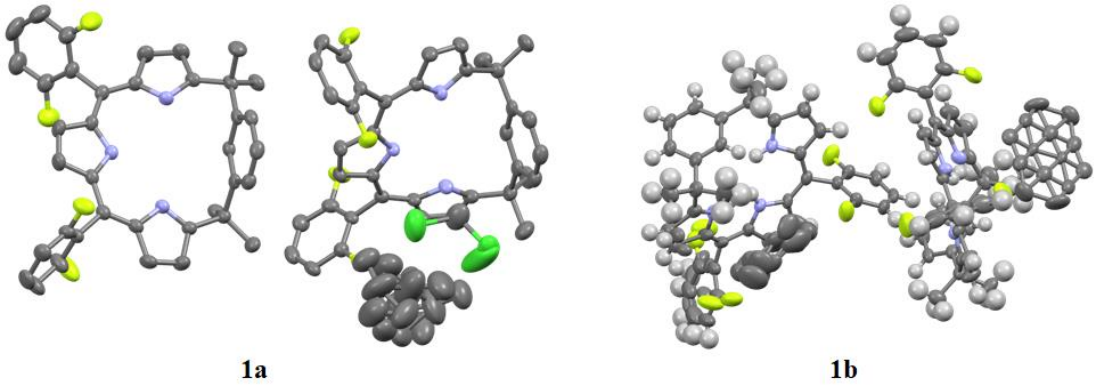

Figure 3.5. Polymorphs of free base *meta*-benziporphodimethene, **1.**

The single crystals of the *m*-BPDM complexes **1a** and **1b** were obtained and a comparative study of these crystal structures was performed. The important parameters of these crystal structures are tabulated in Table S1. The geometry is less puckered than the earlier reported structures of *meta*-BPDM. The average deviations of the macrocycle that constitute the macrocycle was 0.616 Å, which is less than other reported *meta*-BPDM structures[15].The angle between the tripyrrin plane created by 17 atoms and the vector across two sp^3*meso* carbons for **1a** and **1b** was 71.36° and 72.46°, respectively, which is also very high in comparison with earlier structures[14]– [16].The angle between the tripyrrin plane and phenylene ring plane formed 84.00° and 75.54°, respectively. Inside the moiety, the torsional angle achieved between all the *meso* carbon atoms was 23.99° and 22.49° for **1a** and **1b** complexes, respectively and the core moiety produced 4.89° and 1.07° for the **1a** and **1b** complexes, respectively. The angle formed by the three pyrrolic nitrogen (N3) and the phenylene ring plane of macrocycle for **1a** complex is 78.04° and 69.82° for complex **1b**. The ORTEP views of **1a** and **1b** are shown in **Figure 3.5**.

References

[1] D. Chauhan *et al*., "Synthesis, characterization and metal ions sensing applications of *meta*-benziporphodimethene-embedded polyacrylamide/ carboxymethyl guargum polymeric hydrogels in water," *Environmental Technology (United Kingdom)*, vol. 43, no. 7, pp. 991–1002, 2022.

[2] A. Kumar *et al*., "Study on the structure, stability and tautomerisms of *meta*-benziporphodimethene and N-Confused isomers containing γ–lactam ring," *J Mol Struct*, vol. 1187, pp. 138–150, 2019.

[3] K. P. Carter *et al*., "Fluorescent sensors for measuring metal ions in living systems," *Chemical Reviews*, vol. 114, no. 8. *American Chemical Society*, pp. 4564–4601, 2014.

[4] D. Chauhan *et al.*, "An efficient adsorbent for the removal of Zn^{2+} Cd^{2+} and Hg^{2+} from the real industrial effluents," *International Journal of Environmental Science and Technology*, vol. 19, no. 3, pp. 1483–1494, 2022.

[5] M. Stępień *et al.*, "Cadmium(II) and Nickel(II) Complexes of Benziporphyrins. A Study of Weak Intramolecular Metal-Arene Interactions," *J Am Chem Soc*, vol. 126, no. 14, pp. 4566–4580, 2004.

[6] D. Ahluwalia *et al.*, "Effect of substitutions on the geometry and intramolecular hydrogen bond strength in *meta*-benziporphodimethenes: A new porphyrin analogue," *J Mol Struct*, vol. 1220, 2020.

[7] D. Ahluwalia *et al.*, "Recent developments in *meta*-benziporphodimethene: A new porphyrin analogue," *J Mol Struct*, vol. 1228, 2021.

[8] R. K. Sharma *et al*., "Synthesis, characterization and fluorescence turn-on behavior of new porphyrin analogue: *meta*-benziporphodimethenes," *Spectrochim Acta Part A: Molecular and Biomolecular Spectroscopy*, vol. 169, pp. 58–65, 2016.

[9] R. K. Sharma *et al.*, "*meta*-Benziporphodimethenes: New Cell-Imaging Porphyrin Analogue Molecules," *ChemistrySelect*, vol. 1, no. 13, pp. 3502–3509, 2016.

[10] C. H. Hung *et al.*, "*m*-Benziporphodimethene: A new porphyrin analogue fluorescence zinc (II) sensor," *Chemical Communications*, no. 8, pp. 978–980, 2008.

[11] G. F. Chang *et al.*, "Factors that regulate the conformation of *meta*-benziporphodimethene complexes: Agostic metal-arene interaction, hydrogen bonding, and η^2, π coordination," *Chemistry - A European Journal*, vol. 17, no. 40, pp. 11332–11343, 2011.

[12] O.V. Dolomanov *et al.*, "OLEX2: A complete structure solution, refinement and analysis program," *Journal of Applied Crystallography*, vol. 42, no. 2, pp. 339–341, 2009.

[13] L. J. Bourhis *et al*., "The anatomy of a comprehensive constrained, restrained refinement program for the modern computing environment - Olex2 dissected," *Acta Crystallographica Section A Foundations and Advances*, vol. 71, no. 1, pp. 59–75, 2015.

[14] G. M. Sheldrick, "SHELXT - Integrated space-group and crystal-structure determination," *Acta Crystallographica Section A Foundations and Advances*, vol. 71, no. 1, pp. 3–8, 2015.

[15] W.Y. Lin *et al.*, "Effect of Metal Ions on the Fluorescence of Leucine Aminopeptidase and its Dansyl-Peptide Substrates," *Journal of Inorganic Biochemistry*, vol.32, pp. 21-38, 1988.

[16] C. H. Galka *et al.*, "Structural Patterns and Forms of Aggregation of Metallated Diamido Donor Ligands upon Going from Lithium to Thallium(I)," *Eur. J. Inorg. Chem*, pp. 2577-2583, 2000.

Chapter 4

DFT Calculations of meta-Benziporphodimethene and Its N-confused Isomers

CHAPTER 4

DFT CALCULATIONS OF *meta*-BENZIPORPHODIMETHENE AND ITS N-CONFUSED ISOMERS

4.1 Introduction

The chemistry of porphyrin derivatives has attracted significant attention because of its potential application in areas like molecular devices, dye-sensitizing solar cell, and photodynamic therapy [1]. One of the important research directions in porphyrin derivatives is designing a new framework of porphyrin core and studying the properties of the new framework [2]. Core modification in the skeleton leads to changes in the electronic structure and cavity size, and thereby altering the optical, electrochemical, photochemical properties, and chelating properties of modified systems [3]-[22]. The size and nature of the heteroatom and introduction of benzenoid ring in the core reflects direct effect on the cavity size and the metal ion binding.

Porphodimethene is proposed to be a key intermediate for the formation of a porphyrin from a porphyrinogen in both the laboratory and the natural process [16]. This intermediate is readily oxidized to porphyrins unless protected by the alkyl or aryl group at sp^3 hybridized *meso*-carbons [23]. In comparison with that of porphyrinogen chemistry, only limited investigations about the chemistry of porphodimethene have been reported [24] - [27]. *meta*-Benziporphodimethene, firstly synthesized by Latos-Grazynski and coworkers, is a new benziporphyrin type porphyrin derivatives with two tetrahedral *meso* carbons at position 6 and 21 (Scheme 1) [28]. The coordination of zinc metal ion to the central cavity of *meta*-benziporphodimethene has been examined [28] -

[30]. Recently, we have found that the ligand can be served as a highly selective and long wavelength zinc ion sensing fluorophore [28]-[30]. Nevertheless, the synthesis and chemistry of its core-modified analog has not yet been thoroughly examined.

Computational studies on porphyrin analogs using DFT calculation can provide important information to understand how the alternations play role in amending the physical properties [9], [31]– [54].

Molecular modelling or computational chemistry is a method to analyse molecular systems virtually without performing any laboratory experiments to study different chemical properties of various molecular systems. Problems such as chemical reactivity, molecular geometry, UV, IR, and NMR spectra, physical properties of substance, interaction of substrate with enzyme can be solved using different tools of molecular modelling. Five techniques are used in computational chemistry which are density functional theory (DFT) calculations, molecular mechanics (MM), molecular dynamics, *ab-initio* calculations, and semi-empirical (SE) method. Density functional theory (DFT) method is based on density distribution across the system in consideration. In present chapter, DFT method is widely used to study porphyrin analogs to analyse how various alterations play role in altering physical properties.

In order to determine the structural features that lead to a thermodynamically stable moieties, various tautomers have been analysed, which were obtained either by shuffling N-confused pyrrole subunits, oxygenated pyrrole subunit (both O-up and O-down), position of hydrogen on inner nitrogen atom of pyrrole or replacing pyrrolic nitrogen with a heteroatom.

4.2 Density Functional Theory (DFT)

4.2.1. Basics of Density Functional Theory (DFT)

DFT is based on electron density function which is designated as $\rho(x,y,z)$ wherein, symbol ρ is a function of three spatial coordinates x,y,z and it denotes probability of finding an electron in a unit volume *dxdydz*.Density functional theory focusses on electronic charge distribution over a given space. Walter Kohn and John Pople both received the Noble Prize for their contributions to the development of density functional theory and the practical wave function-based methods, respectively.

4.2.2. Principle of DFT

In 1920s, Enrico Fermi and P. A. M. Dirac envisioned and performed calculations independently which led to establishment of molecular properties and atomic properties from electron density and this was named as Fermi-Dirac statistics. Thomas-Fermi-Dirac model stated that molecules are extremely unstable when dissociated into atoms. In 1921, Slater did modification to improvise the results for molecular systems exchange correlation was introduced in the Thomas-Dirac theorem. Later on, Kohn-Sham type DFT method replaced the Thomas-Fermi-Dirac method.

4.2.3. Theorems of DFT

Modern density function theory is based on Kohn-Sham approach which is derived from two theorems given by Kohn and Hohenberg in the year 1964. As per Kohn and Hohenberg, at ground state all the properties of molecules can be calculated using ground state electron density function $\rho_o(x,y,z)$. In other words, the ground state property of any molecular system is a functional of its electron density. This has been

named as *existence theorem*. Another theorem is the *variational theorem* which states that any trial electron density functional yields certain energy value which is always greater than or equal to the true ground state energy of that system.

4.3 Computational methods

The DFT calculation has been conducted by using DFT method of three parameter hybrid exchange correlation functional, the B3LYP[55]– [58]. 6-31g** basis set was chosen for relative energies and geometries optimization calculations. DFT methods implemented in the Gaussian 03 and Gaussian 09W suit of programs are used in this theoretical work. The choice of B3LYP/6-31g** is excellent in the modelling of this type of molecules[55]– [58]. The most stable isomers were also re-optimized by using B3LYP/6-311G** and again optimized by B3LYP/6-311+G** with added diffused function. Starting geometries were taken from the single crystal X-ray structures which were then modified by Gauss-View 5.0 software. All geometrical structures are optimized under C1 symmetry. All the minima are characterized by frequency calculations, which show all real frequencies. The optimized three-dimensional structures were examined by the Gauss View computer graphic programs.

4.4 Results and Discussion

11, 16-bis (phenyl)-6, 6, 21, 21-tetramethyl-*meta*-benzi-6, 21-porphodimethene (1) and two novel N-confused *meta*-benziporphodimethene containing *γ*–lactam ring (2, O-up and 3, O-down) (**Figure 4.1**) were synthesized and studied by ^{1}H NMR spectra by Hung

and co-workers[59]– [61]. Their solid-state structures were determined in high quality by single crystal X-ray diffraction and the geometrical parameters were used directly for total energy calculation. The phenyl rings were kept intact with *meta*-benziporphodimethene and with the isomers of γ – lactam ring containing N-confused *meta*-benziporphodimethene to get the real picture of the molecules. In this chapter, the relative energies of *meta*-benziporphodimethene system and its inverted isomers have been discussed, followed by the analysis of relative energy of N-confused *meta*-benziporphodimethenes with or without γ– lactam ring. Later, the studies of relative energy of all isomers have been added in connection with the N-H tautomerism.

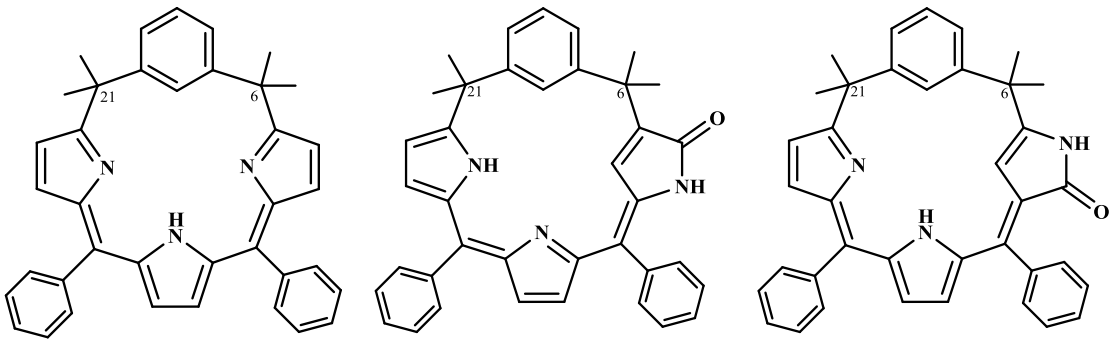

Figure 4.1. Structures of *meta*-benziporphodimethene (**1**) and N-confused *meta*-benziporphodimethene containing γ – lactam ring isomers (O-up, **2**, and O-down, **3**).

4.4.1. The Relative Energy of 1 and its Inverted Isomers

The tautomer of **1** and its inverted compounds originated from single pyrrole α,α- to α,β linkage isomerization are shown in Chart 1. To understand the relative energy between all tautomeric forms, all isomers resulted from hydrogen tautomerization are included in the calculation. The total energy of **1** and its isomers under B3LYP/6-31g** as well as 6-311g** basis level of theory are given in **Table 4.1**. The corresponding optimized

geometries of structures **1a** to **2i** have been added as **Figure 4.2**. The energy of each tautomer relative to **1a** is given in **Chart 4.1** in parenthesis beneath each molecule code. The relative energy suggests that structure **1a** is energetically more favourable than **1b**. Apparently, the inner core hydrogen bonding interaction plays an important role in stabilizing the tautomer **1a**. Though **1a** and **1b** both have the same π-electron conjugation pathway (12π-electrons), in tautomer **1a** the inner-NH can have hydrogen bonding interaction with two nitrogen atoms in the core while in **1b**, only one nitrogen atom is within hydrogen bonding distance. Similar stabilization of tautomer form by the more extended inner core hydrogen bonding interaction has been observed in the case of HCTPPH [34]. Additionally, we study the mono-confusion approach at one of the pyrrole rings as shown in Chart 2 to evaluate the potential of synthesis of this type of benziporphodimethene. In general, the changing of α,α- to α,β- linkage on a pyrrole ring causes pyrrole ring inversion and resulted in an increase of relative energy. The inverted pyrrole ring nearby the sp^3 *meso* carbon with nitrogen atom away from the sp^3 carbon (2f, N-down) is 1.17 Kcal/mol more stable than N-up (**2c**) isomer. It is also concluded that N-confused pyrrole ring adjacent to the sp^3 *meso* carbon is a more stable compound than N-confused pyrrole ring located opposite to the benzenoid ring since the inverted pyrrole ring in opposite to phenylene ring either breaks the π-electron-conjugation path (**2g)** or diminishes the strength of hydrogen bonding interaction (**2h** and **2i**) and leads to higher energy. Noticeably, the total energy increases when inner amino hydrogen atom tautomering to outer nitrogen. In the cases containing inverted pyrrole ring, the number of weak inner hydrogen interaction between inner C-H and inner pyrrolic nitrogen, and

symmetry of molecule become dominate factors in total energy which can explain the lower energy of **2g** than **2b** and **2e**. The optimized structures have shown that 17/sp^3-vector angle which defines the average deviation of atoms from the 17-tripyrin-atoms-mean-plane is higher in **2b** and **2e** relative to that in **2g**, **2h** and **2i** (Table 4.4). As expected, **1a** which is isolated as a thermodynamic stable compound is energetically more stable than all isomers shown in **Chart 4.1**. The energy difference of 3.34 kcal/mol was found between the most stable regular *meta*-benziporphodimethene (**1a**) and most stable inverted isomer (**2f**).

Table 4.1. Total Energy, Relative Energy of the Theoretically Optimized Structures of **Chart 4.1**and**4.2**.

Structures	**E_{total} (Hartree)**	**E_{rel} (kcal/mol)**	**E_{total}(Hartree) re-optimized using B3LYP/6-311g****	**E_{total}(Hartree) re-optimized using B3LYP/6-311+g****
1a	-1632.1995	0.0	-1632.5337	-1632.5482
1b	-1632.1931	4.03		
2a	-1632.1874	4.3		
2b	-1632.1741	12.6		
2c	-1632.1923	1.17		
2d	-1632.1912	1.88		
2e	-1632.1709	14.6		
2f	-1632.1942	0.0	-1631.8297	-1631.8448
2g	-1632.1793	9.34		
2h	-1632.1855	5.46		
2i	-1632.1825	7.30		
3a	-1652.0335	0.0	-1652.3721	-1652.3821
3b	-1652.0301	2.06		
3a’	-1652.2865	0.0	-1653.6276	-1653.6421
3b’	-1652.2854	0.68		
4a	-1975.0093	0.0	-1975.3454	-1975.3602
4b	-1974.9990	6.48		
4a’	-1976.2529	0.0	-1976.5900	-1976.6050
4b’	-1976.2454	4.76		

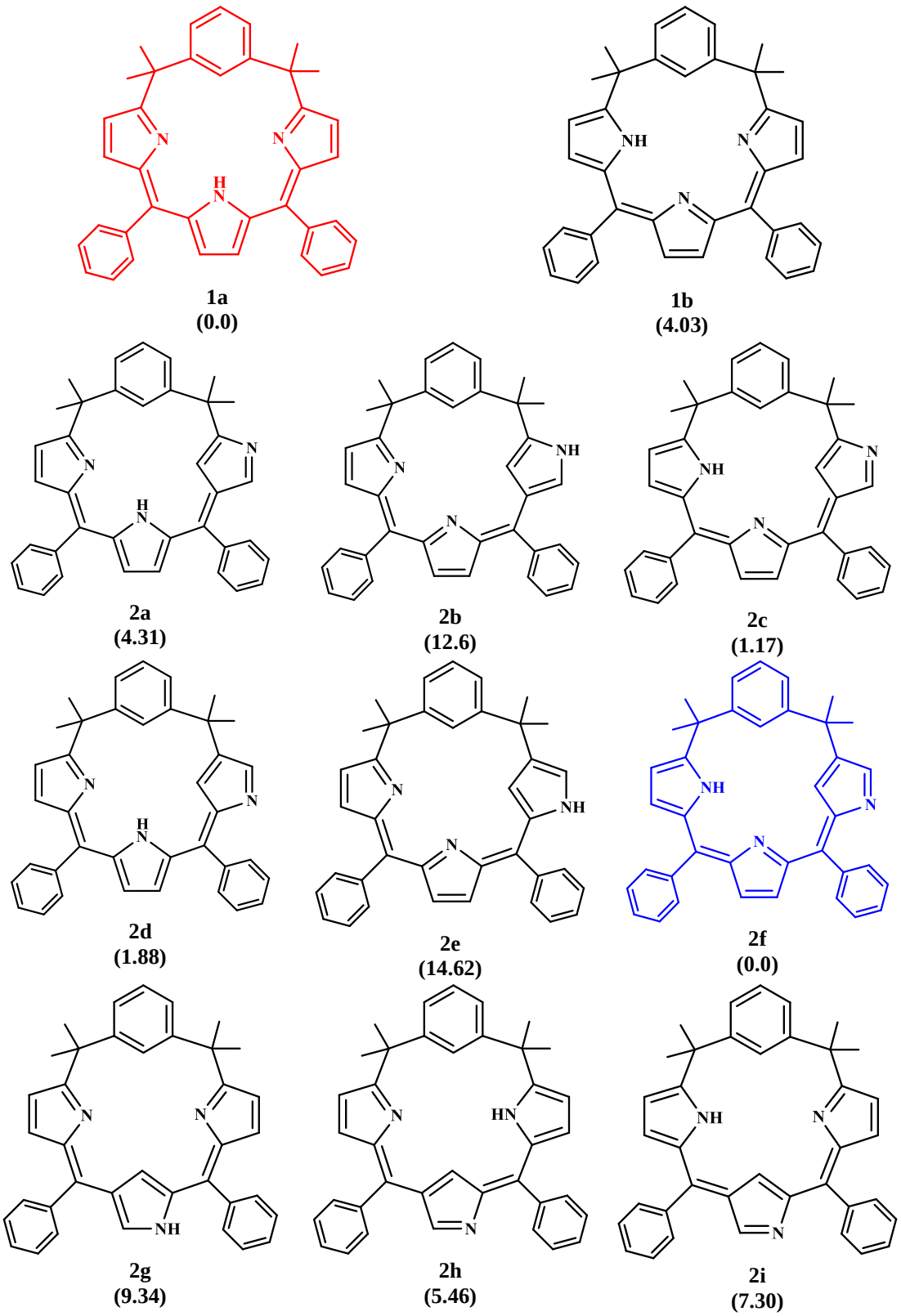

Chart 4.1. *meta*-Benziporphodimethene, **1** and its inverted tautomers, in parenthesis relative energy of **1b**, **2a** to **2i** are given with respect to **1a** and **2f**, respectively in kcal/mol.

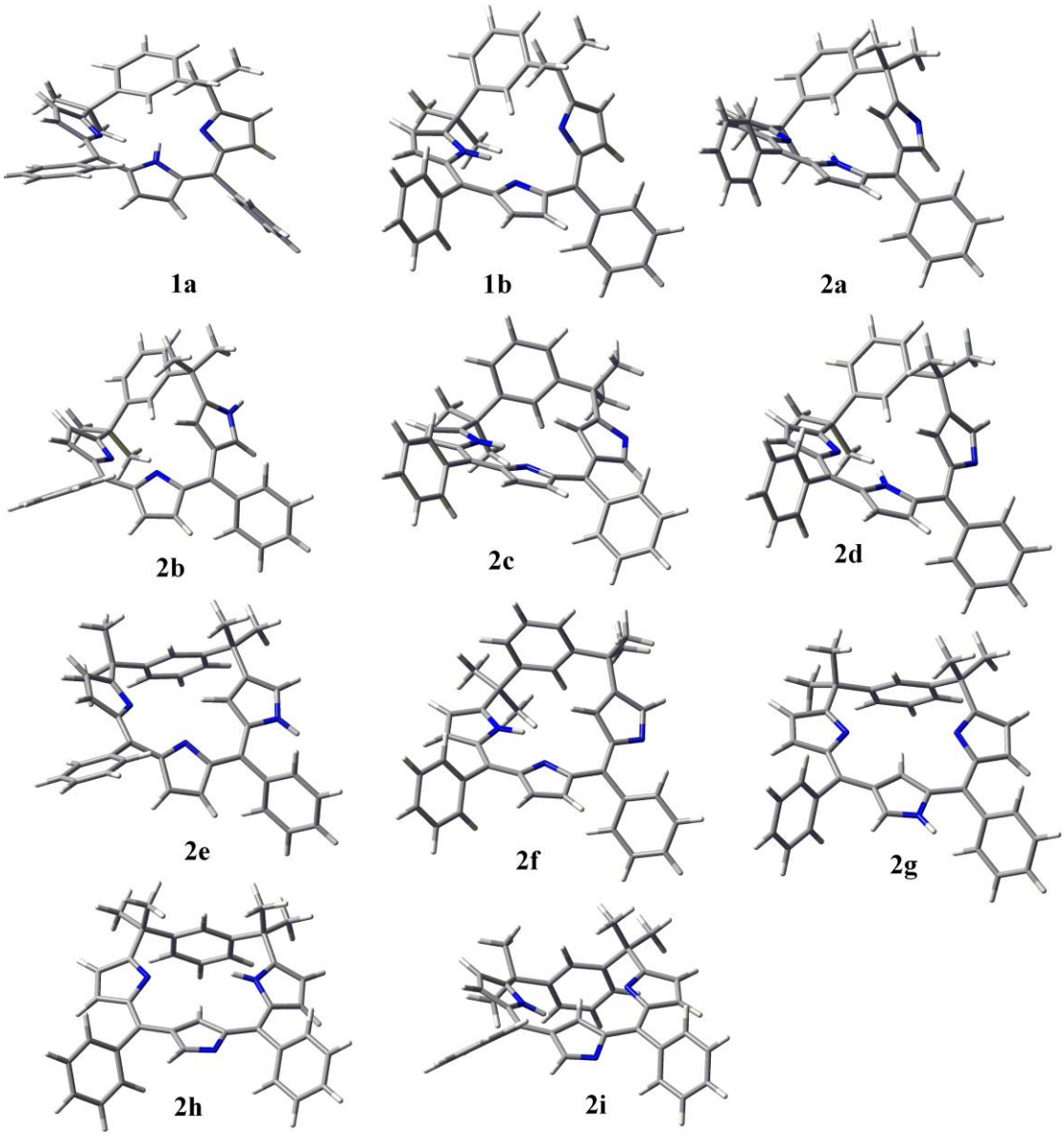

Figure 4.2. B3LYP/6-31g** optimized geometries of **1** and its inverted isomers.

4.4.2. The Relative Energy of Oxa and Thia Analogues of 1

The relative energies of oxa- and thia-analogues and their structures are shown in **Chart 4.2** and their corresponding optimized geometries are shown in **Figure 4.3**. Herein, thiophene and furan rings adjacent or away to the sp^3 *meso*-carbon atoms have been taken into account. The thiophene or furan ring opposite to the phenylene ring in structure with or without hydrogen atom on nitrogen is more stable. The presence of two

O•••H–N interaction lower the energy by a value of 0.68 kcal/mol in 3a' than 3b'. Detailed structural differences have been discussed in subsequent sections of this chapter.

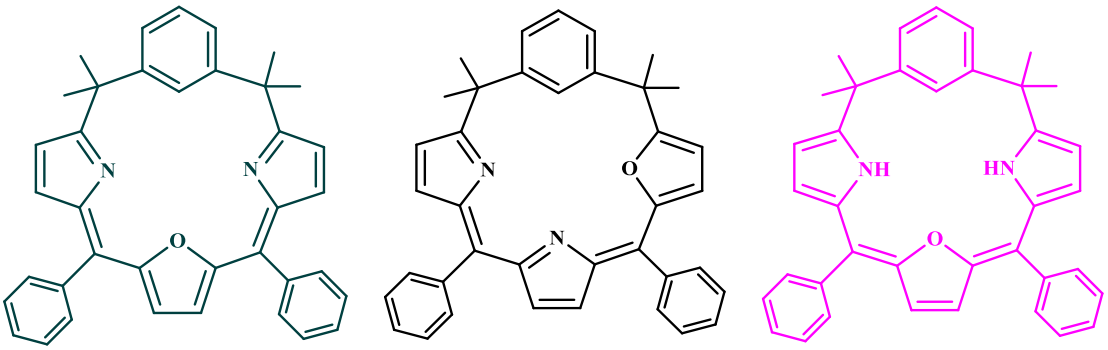

3a **(0.0)** **3b** **(2.06)** **3a′** **(0.0)**

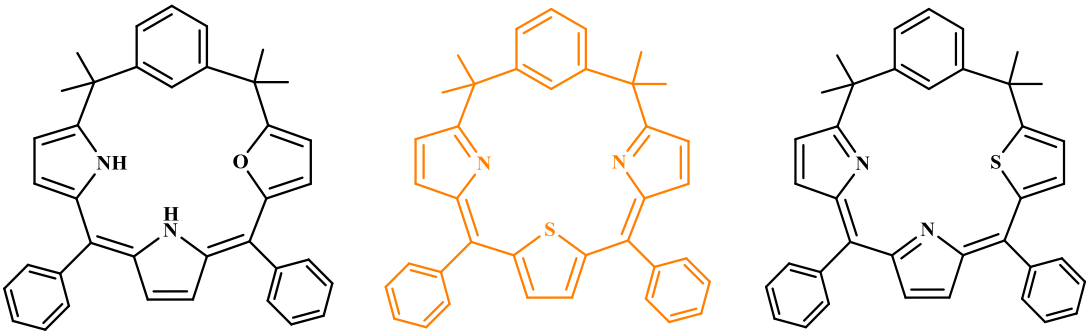

3b′ **(0.68)** **4a** **(0.0)** **4b** **(6.48)**

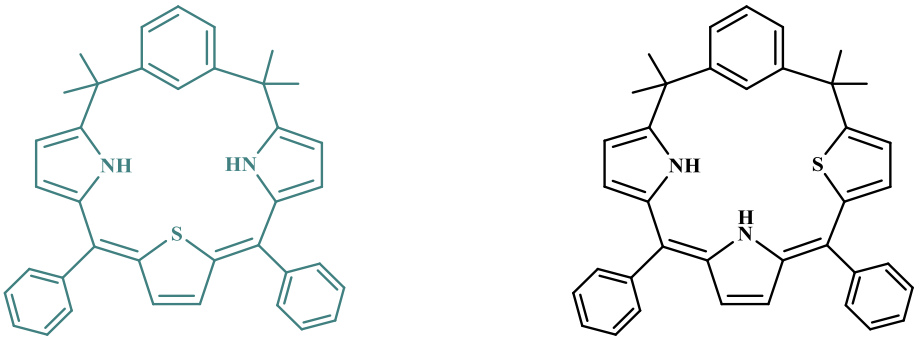

4a′ **(0.0)** **4b′** **(4.76)**

Chart 4.2. Oxa- and Thia- analogues of *meta*-benziporphodimethene, relative energy of **3b**, **3b'**, **4b** and **4b'** are given with respect to **3a**, **3a'**, **4a** and **4a'**, respectively in parenthesis in kcal/mol.

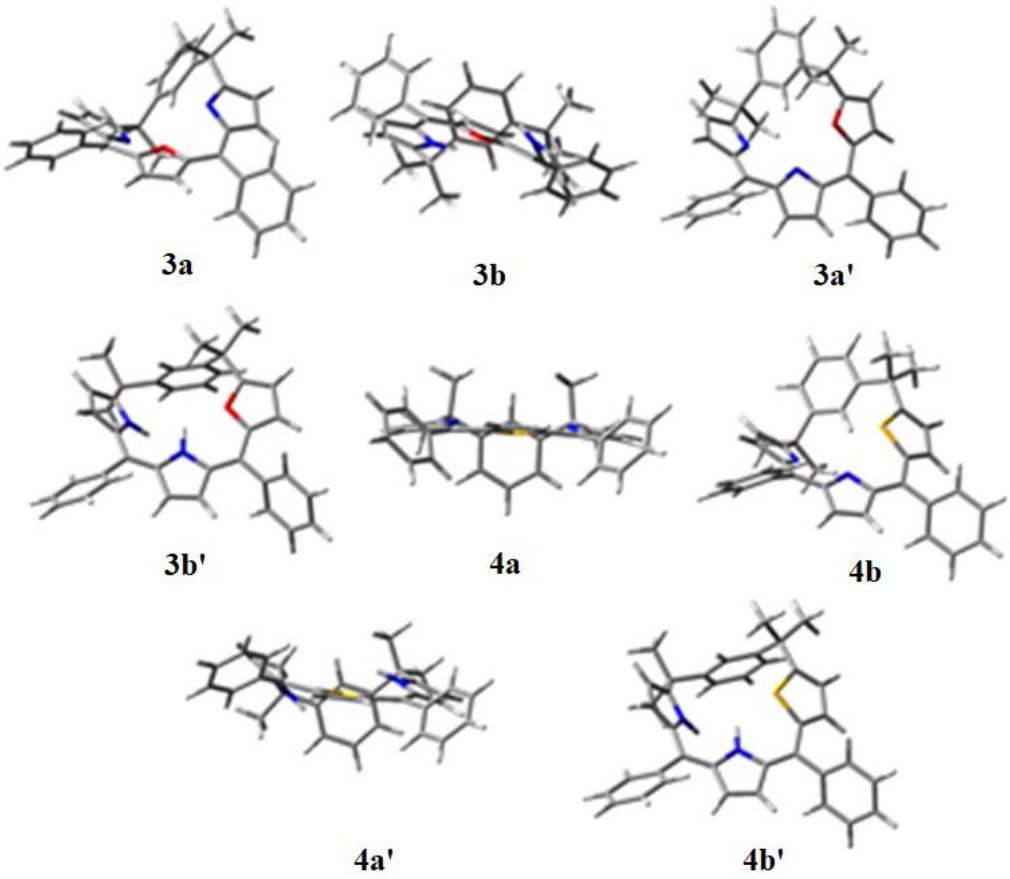

Figure 4.3. Optimized geometries of thia and oxa analogues of 1.

Table 4.2. Non-bonded distance (Å) and Angle (degrees) for structures in **Charts 4.1** to **4.8**.

	D1 (Å)[a]	D2 (Å)[b]	17/C_6 (°)[c]	C_6/N_2X (°)[d]	17/sp^3 (°)[e]	P_0[f]	P_{core}[g]	Py_1/17[h]	Py_2/17[i]	Py_3/17[j]
1a	3.99	4.38	36.13	19.23	38.33	46.20	-2.78	41.53	31.81	49.30
1b	4.11	4.34	38.64	19.75	38.50	47.92	6.42	45.40	18.04	20.71
2a	4.06	4.51	36.37	14.62	37.36	45.33	7.98	46.49	15.31	24.09
2b	4.28	4.45	36.74	12.71	38.52	45.14	1.58	42.60	12.43	41.88
2c	4.19	4.68	79.95	69.03	20.41	27.24	4.59	30.82	11.79	8.42
2d	4.03	4.50	38.72	16.18	37.95	7.19	4.62	45.54	17.25	23.15
2e	4.14	4.66	84.11	73.45	18.27	23.26	1.36	3.29	8.74	32.82
2f	4.21	4.63	81.37	68.31	23.73	31.52	4.58	35.51	14.33	8.94
2g	4.51	4.38	76.07	84.74	13.22	17.59	6.89	18.87	8.69	7.65
2h	4.58	4.59	78.76	84.08	1.29	-3.95	7.56	21.33	12.76	19.66
2i	4.53	4.40	88.33	81.48	18.57	21.56	2.03	8.53	5.78	32.82
3a	4.15	4.28	40.36	17.80	42.23	50.55	-0.01	39.33	11.99	39.32
3b	4.29	4.58	83.44	76.11	27.42	33.37	3.12	11.10	8.89	46.16
4a	4.74	4.02	86.79	81.17	0.0	-0.01	6.95	10.30	5.43	10.31
4b	4.93	4.07	89.09	86.67	18.19	18.75	6.88	16.23	4.87	37.09

	D1 (Å)[a]	D2 (Å)[b]	17/C_6 (°)[c]	C_6/N_2X (°)[d]	17/sp^3 (°)[e]	P_0[f]	P_{core}[g]	Py_1/17[h]	Py_2/17[i]	Py_3/17[j]
5a	4.36	4.49	77.27	79.54	22.11	28.55	-4.96	18.78	9.92	23.06
5b	4.29	4.63	78.97	74.42	20.70	27.10	0.71	24.50	9.22	13.93
5c	4.23	4.69	77.79	73.86	20.64	26.82	0.07	24.74	8.89	14.26
5d	4.28	4.71	87.77	76.85	13.41	19.02	2.79	33.69	12.97	17.19
5e	4.17	4.61	73.54	77.68	20.62	24.61	-9.34	16.66	6.41	33.18
5f	4.28	4.68	79.78	82.50	16.23	19.88	-8.15	17.05	5.47	21.61
6a	4.38	4.41	64.65	72.65	23.05	30.24	-6.38	15.26	10.86	32.67
6b	4.17	4.63	63.58	70.93	21.98	29.43	-3.79	12.07	10.65	31.87
6c	4.49	4.35	78.05	81.22	17.69	21.37	-5.32	20.62	5.88	17.37
6d	4.50	4.34	79.40	81.43	17.30	20.84	-4.99	20.42	3.84	16.72
6e	4.11	4.69	84.27	63.02	5.36	-13.83	5.34	35.81	15.78	34.12
6f	4.13	4.67	86.90	64.25	7.23	-17.11	5.45	16.85	18.44	35.75
7a	4.08	4.37	40.29	22.11	39.49	46.96	0.01	43.89	14.21	25.39
7b	4.56	4.63	78.99	85.39	0.96	0.58	6.36	20.78	12.54	17.64
7c	4.16	4.54	38.19	14.93	38.43	44.10	6.74	56.41	12.74	25.14
7d	4.18	4.69	74.63	66.99	34.13	29.20	2.83	39.28	8.10	11.48
7e	4.18	4.79	67.51	75.46	17.71	22.84	2.54	26.25	12.56	6.49
7f	4.24	4.79	68.46	78.43	14.36	18.05	3.13	26.77	12.99	6.19
8a	4.20	4.30	39.05	17.44	40.11	46.67	5.24	43.81	18.86	30.21
8b	4.37	4.33	69.68	81.24	20.86	29.29	9.61	26.67	14.24	13.53
8c	4.10	4.44	37.40	14.51	38.86	47.48	7.86	40.32	18.14	31.39
8d	4.15	4.70	57.07	72.78	21.21	29.89	6.94	36.73	22.87	5.37
9a	4.30	4.36	78.11	71.21	31.55	41.03	-2.94	40.71	12.88	16.53
9b	4.11	4.37	39.35	21.36	39.31	46.51	-2.48	23.66	13.66	25.82
9c	4.27	4.46	81.16	74.12	29.28	37.84	-3.82	42.01	10.35	13.32
9d	4.24	4.62	77.81	72.31	22.84	29.76	0.70	29.17	9.37	14.21
9e	4.20	4.67	76.28	71.41	22.71	28.79	0.19	29.23	8.31	14.44
9f	4.30	4.74	87.97	76.81	15.71	20.27	4.01	45.68	7.36	17.53
9g	4.63	4.35	84.41	87.02	24.00	28.52	-7.34	34.42	8.68	19.29
9h	4.65	4.37	83.51	86.58	23.55	27.50	-7.28	31.53	6.06	22.74
9i	4.55	4.37	87.22	83.45	18.13	22.85	-3.03	25.24	5.25	10.77
9j	4.54	4.37	88.03	82.36	19.77	24.90	-2.93	29.38	6.45	10.40
9k	4.24	4.63	79.71	71.71	22.70	28.54	-2.35	13.62	8.22	32.51
9l	4.28	4.61	77.45	71.62	24.11	30.23	-2.43	13.01	8.78	37.39

[h, i, j] *angle between each pyrrole ring plane and 17 tripyrin atom mean plane.*
[a] *N (25)-X (23), X = C, N, O, S.*
[b] *C (22)-X (24), X = N, O, S.*
[c] *Angle between the 17 tripyrin atom mean plane and phenylene ring plane.*
[d] *Angle between the phenylene ring plane and inner tri atom core.*
[e] *Angle between the 17 tripyrin atom mean plane and the vector along the two sp^3meso carbons.*
[f] *dihedral angle between the four meso carbons C (6)-C (11)-C (16)-C (21).*
[g] *dihedral angle between the inner core atoms C (22)-X (23)-X (24)-N (25), X = C, N, O, S.*

Table 4.3. Total Energy, Relative Energy the Theoretically Optimized Structures of Chart 4.3 to 4.6[a]

Structure	E_{total} (Hartree)	E_{rel} (Kcal/mol)	E_{total}(Hartree) re-optimized using B3LYP/6-311g**	E_{total}(Hartree) re-optimized using B3LYP/6-311+g**
5a	-1707.4177	25.21		
5b	-1707.4579	0.00	-1707.1167	-1707.8252
5c	-1707.4558	1.32		
5d	-1707.4196	24.03		
5e	-1707.4091	30.62		
5f	-1707.4124	28.55		
6a	-1707.1318	14.18		
6b	-1707.1544	0.00	-1705.8884	-1706.5264
6c	-1707.1490	3.38		
6d	-1707.1431	7.09		
6e	-1707.1385	9.97		
6f	-1707.1418	7.90		
7a	-1707.4198	8.15		
7b	-1707.4328	0.00	-1707.7853	-1707.8031
7c	-1707.4137	11.98		
7d	-1707.4187	8.85		
7e	-1707.4036	18.32		
7f	-1707.4036	18.32		
8a	-1707.1357	11.73		
8b	-1707.1544	0.00	-1707.1544	-1706.5273
8c	-1707.1316	14.31		
8d	-1707.1384	10.04		

[a] Relative energy for structures **5a** to **5f, 6a** to **6f, 7a** to **7f** and **8a** to **8d** were calculated with respect to the structure **5b**,**6b, 7b** and **8b,** respectively**.**

4.4.3. The Relative Energy of O-Up Isomers of 2

The isomers with or without inverted pyrrole ring in the presence of an O-up oxygenated pyrrole ring have been used for DFT investigation. The O-up isomers have been classified into two categories, *viz.* the reduced form of O-up isomers (**Chart 4.3**) and oxidized form of O-up isomers (**Chart 4.4**). Refer to **Figure 4.4** and **4.5** for visual depiction of these geometries. The relative energies demonstrate that **5b** is the most stable compound among the structures described in **Chart 4.3**. Interestingly, **5b** is also the only one that has been experimentally isolated and structurally characterized. The structure **5a** with regular pyrrolic α,α-linkage and oxygenated in the β-pyrrolic position gives higher energy comparing with **5b**. The relative energy difference between **5b** and **5c** which has different tautomer form on dipyrromethene moiety is relatively small in value. Although both **5b** and **5c** possess inner core hydrogen bonding interactions, bifurcated hydrogen bond (H-bond) interactions between N−H•••N (2.02 Å) and C−H•••N (2.52 Å) makes **5b** more stable compound in comparison with **5c** where only single hydrogen bonding of N−H•••N (2.00 Å) is possible. Because of comparable H-bond network, energy differences between **5e** and **5f** are relatively small and, similar to relative energy of N-confused *meta*-benziporphodimethenes, as described above. N-down isomer, **5f**, again exhibits a lower energy than the N-up isomer. The presence of inverted pyrrole ring opposite to the oxidized pyrrole ring in **5e** and **5f** gives higher energy relative to **5b** likely because of a shorter conjugation pathway.

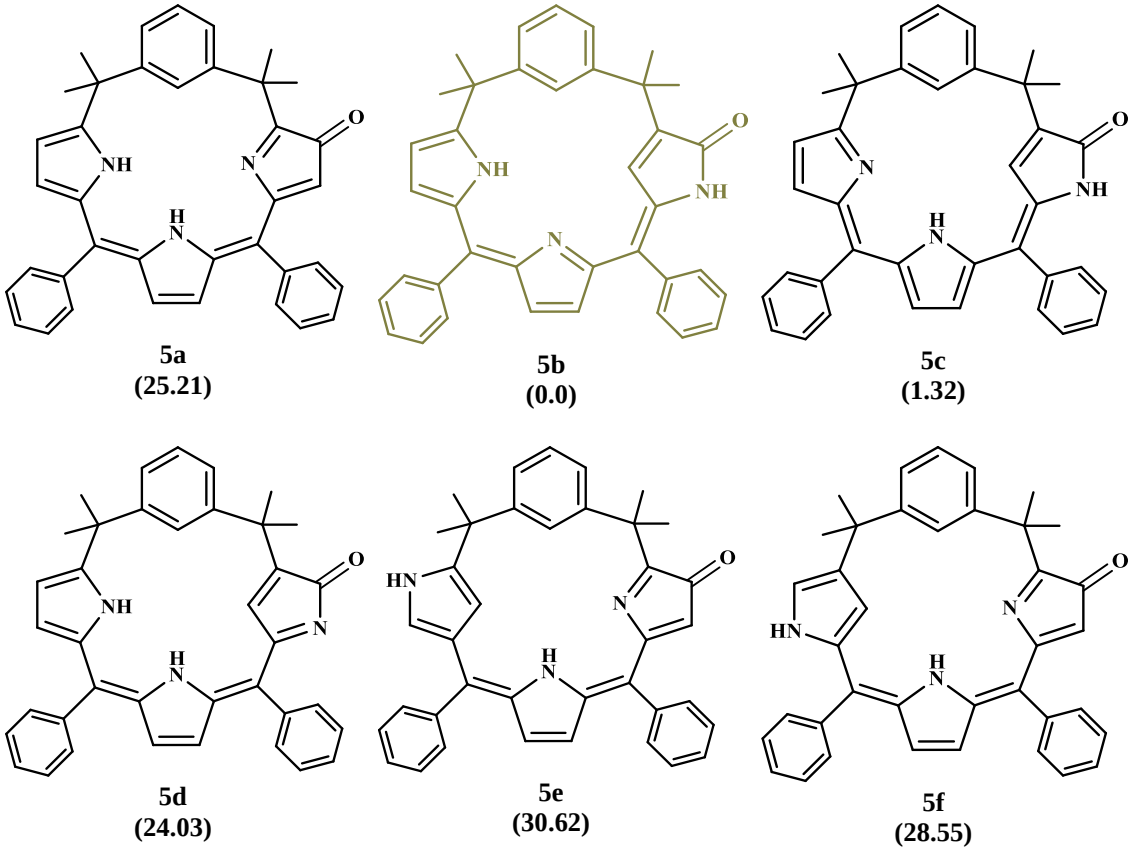

Chart 4.3. Reduced form of O-up, **2** isomers; their relative energy are given in parentheses with respect to **5b** in kcal/mol.

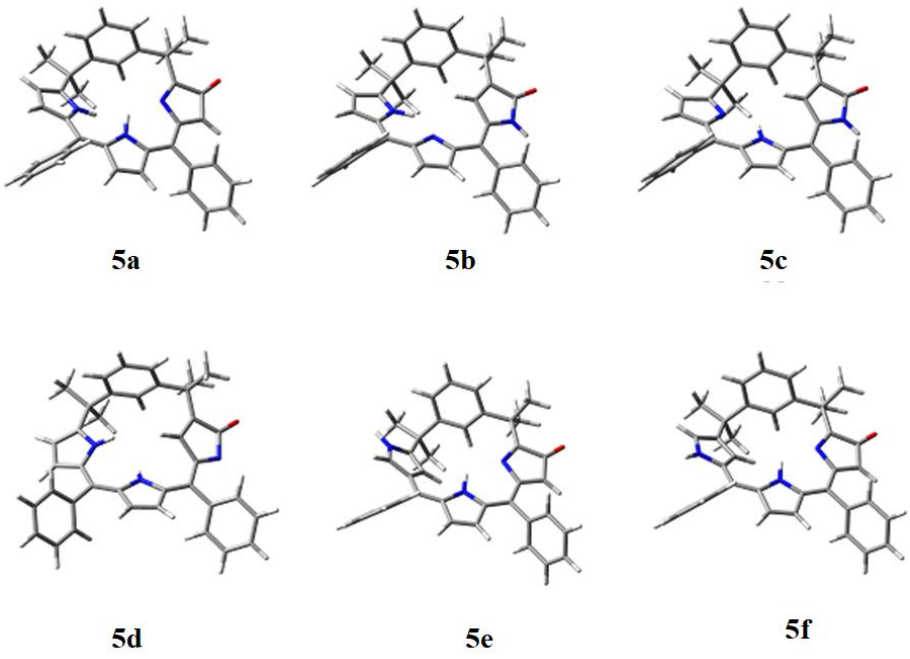

Figure 4.4. Optimized geometries of O-up isomers with hydrogen on nitrogen.

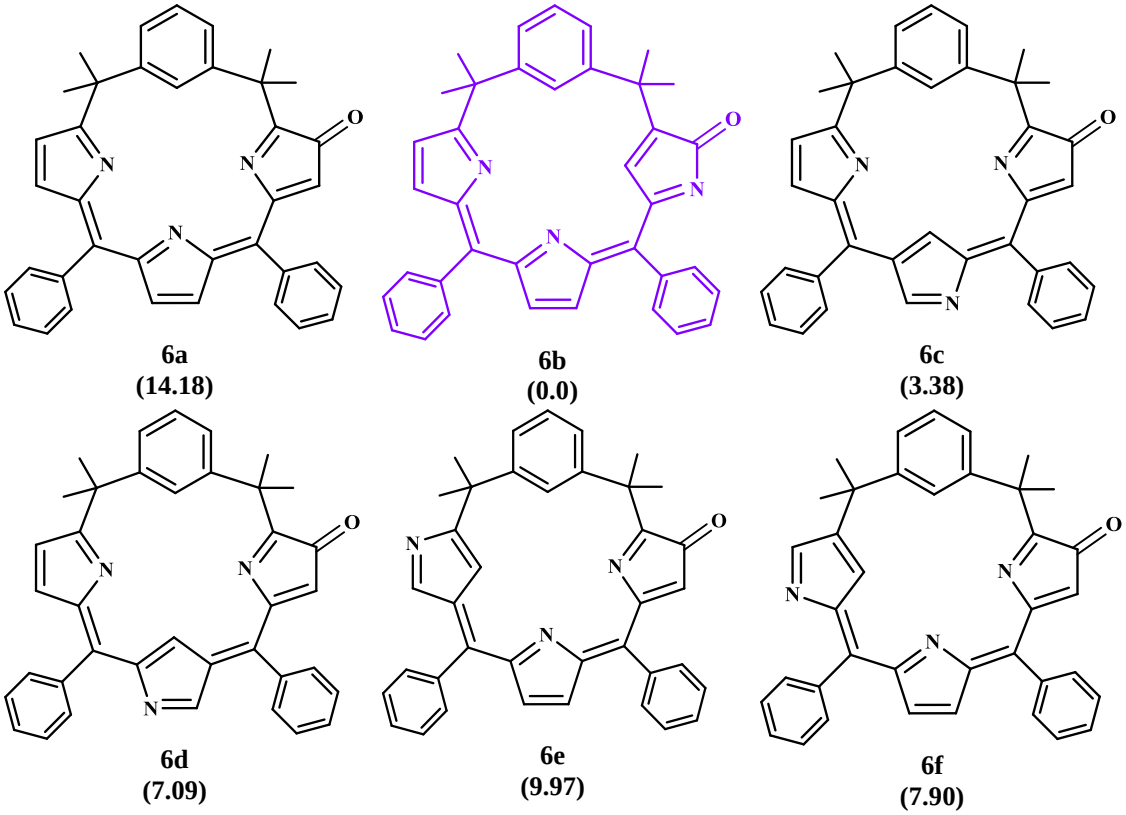

Chart 4.4. Oxidized form of O-up, **2** isomers; their relative energy are given in parentheses with respect to **6b** in kcal/mol.

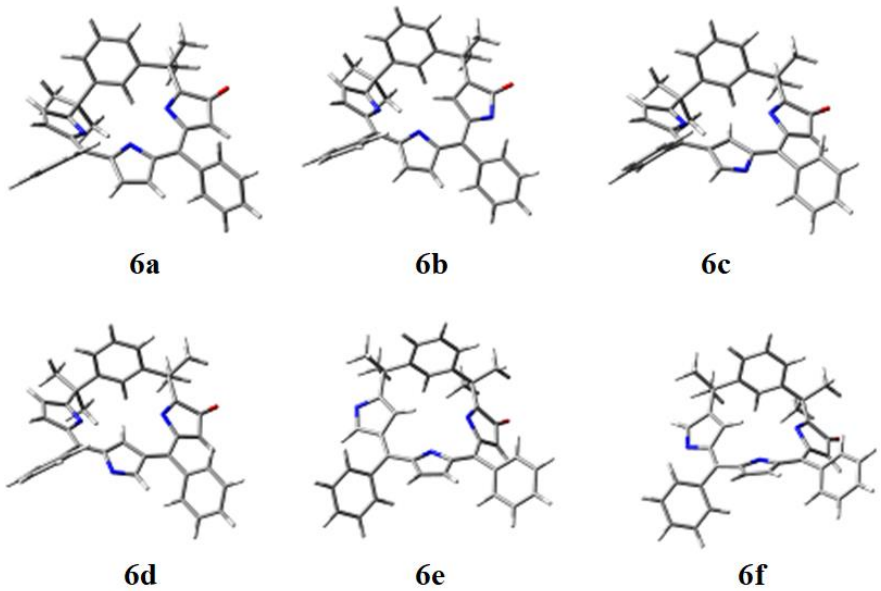

Figure 4.5. Optimized geometries of O-up isomers without hydrogen on nitrogen.

The oxidized structures without hydrogen atom on the nitrogen atom followed the same trend in **6b**, which is oxidized form of **5b**, as the most stable structure. The structures from **6a** to **6f** have same π-conjugated systems but the structure with an inverted pyrrole ring opposite to the phenylene ring (**6c** and **6d**) were bearing lower relative energy compared to structures with an inverted pyrrole ring opposite to the oxidized pyrrole ring (**6e** and **6f**).

4.4.4. The Relative Energy of Lactam Ring Containing Isomers Presented in Chart 4.5 and Chart 4.6

In **Charts 4.5** and **4.6**, isomers containing oxygenated pyrrole ring opposite to the phenylene ring either with or without the presence of an additional inverted pyrrole ring have been considered. Two types of linkage for oxygenated pyrrole ring are proposed *viz.* with either an α,α-pyrrolic linkage and oxygenation on β-pyrrolic position to give a regular benziporphyrin type conformation or an α,β-pyrrolic linkage with oxygenation on α-pyrrolic position to generate a N-confused porphyrin type atom arrangement. Among the studied compounds, compound **7b** is the most stable one in **Chart 4.5** while compound **8b** is the most stable one in oxidized isomers in **Chart 4.6**. This result is not surprising since **7b** and **8b** are the only compounds that exhibit both extended π-conjugate system (12 π-electrons) and inner core hydrogen bonding network. Obviously, the presence of a regular α,α-linkage pyrrole ring with an oxygenated on the β-pyrrolic carbon ruptures the π-conjugate system and raises the energy. However, the large energy distribution with relative energy ranging from 8.17 to 18.32 kcal/mol separated into two distinctive groups in line with the degree of H-bond interactions. Among those oxidized isomers without hydrogen atom on nitrogen, **8b** is the most stable because of doubly C−H•••N interactions in comparison to **8a**,**8c** and **8d** where only one C−H•••N interaction is found.

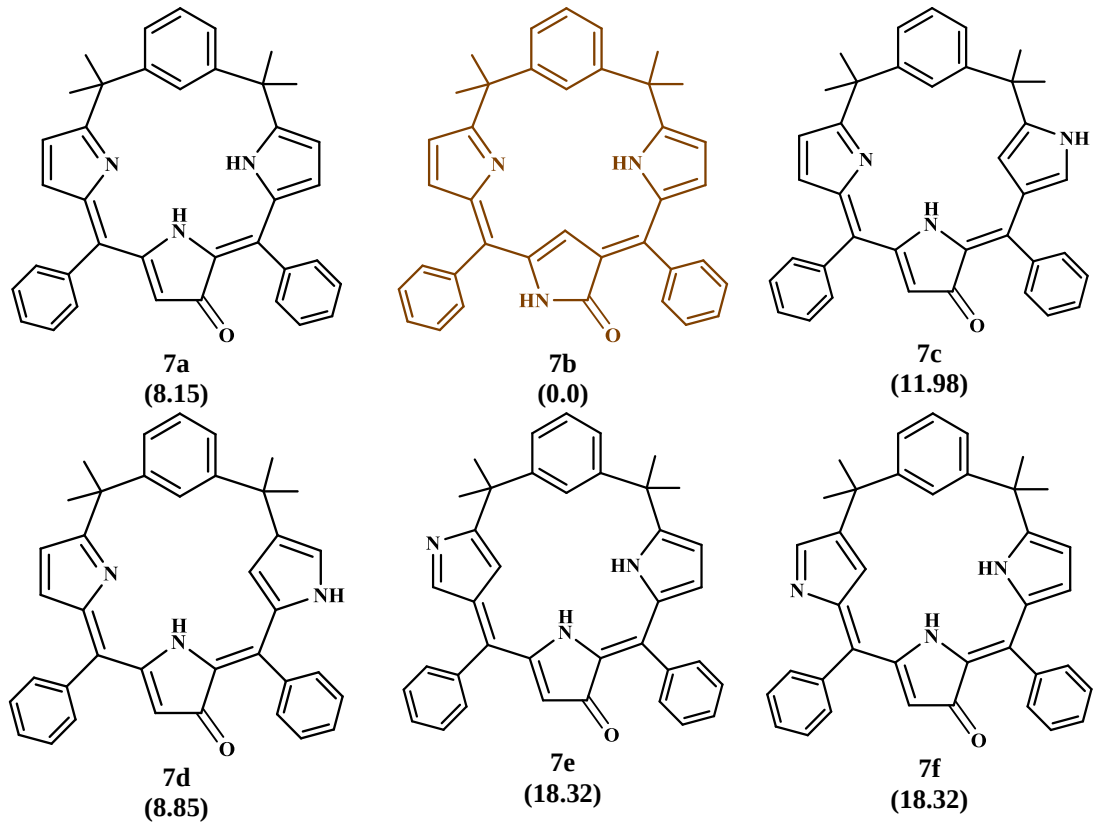

Chart 4.5. Reduced form of isomers having oxidized pyrrole ring opposite to the phenylene ring; their relative energies are given in parentheses with respect to **7b** in kcal/mol.

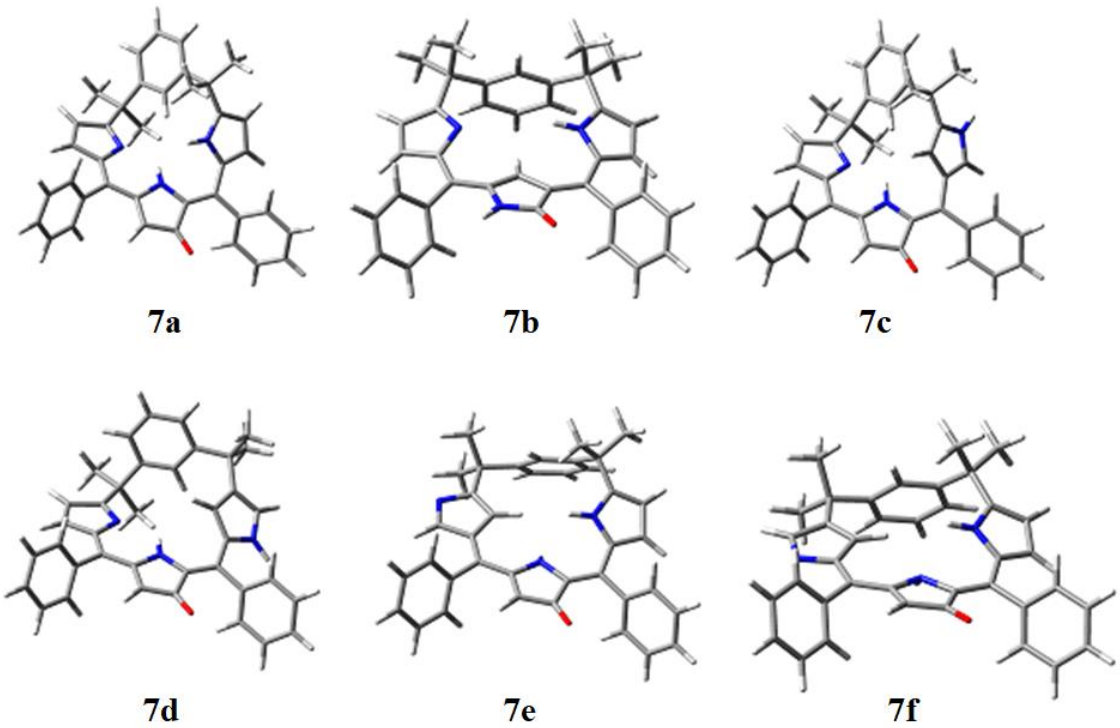

Figure 4.6. Optimized geometries of isomers presented in Chart 4.5 oxidized at pyrrole ring opposite to the phenylene ring with hydrogen atom.

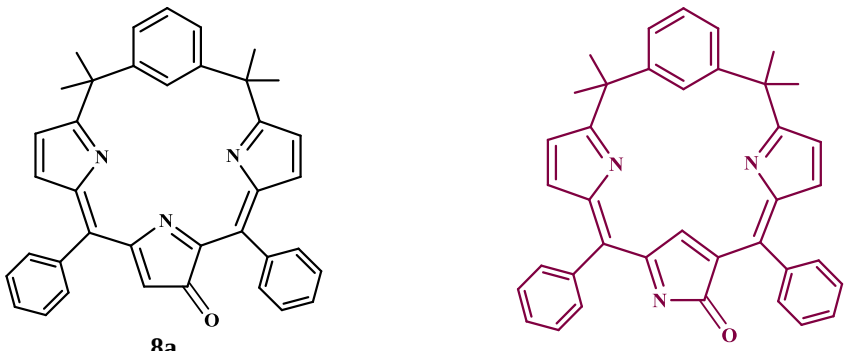

8a **(11.73)** **8b** **(0.0)**

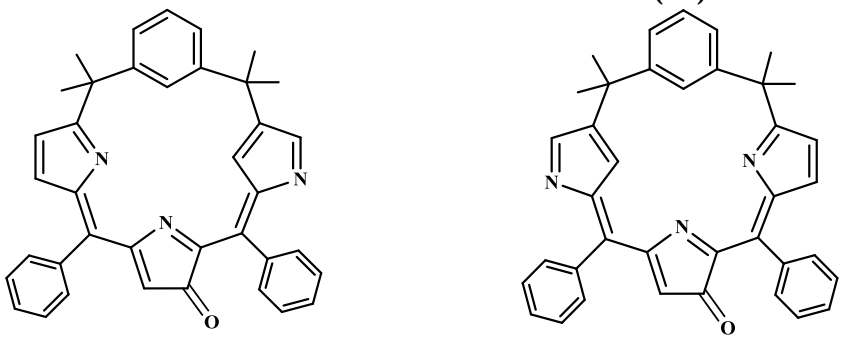

8c **(14.31)** **8d** **(10.04)**

Chart 4.6. Oxidized form of isomers having oxidized pyrrole ring opposite to the phenylene ring; their relative energies are given in parentheses with respect to **8b** in kcal/mol.

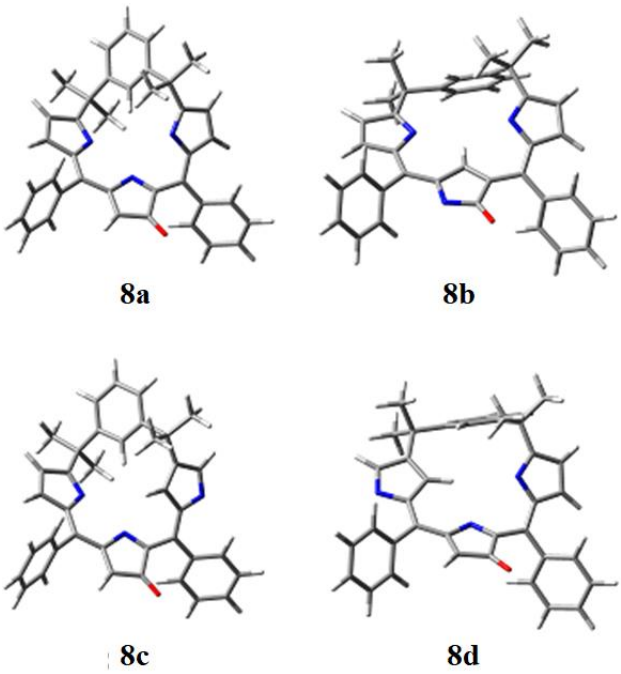

8a **8b** **8c** **8d**

Figure 4.7. Optimized geometries of isomers presented in Chart 4.6 oxidized at pyrrole ring opposite to the phenylene ring without hydrogen atom.

4.4.5. The Relative Energy of O-Down Isomers of 3 Presented in Chart 4.7 and 4.8

In this section, all the possibilities of O-down isomers with or without inversion in the oxygenated pyrrole ring have been taken into account. While keeping the oxygenation at the same pyrrole ring, both α,α- to α,β-pyrrolic linkage for un-oxygenated pyrrole rings were examined. DFT calculation suggested that O-down isomers like **9d** and **9e** are the most stable isomer. Although **9d** is 0.42 kcal/mol higher in energy than **9e**. The single crystal X-ray structural determination confirmed that **9d** is the synthetic product at ambient temperature. The discrepancy might reflect the difference of total energies in theoretical calculations under gas phase and in synthetic procedures under solution phase. With the same trend (*vide supra*), the isomers having elaborated inner C−H•••N and N−H•••N interactions and longer π-conjugation are energetically more favourable. The isomers without inverted pyrrole ring (**9a**) are more stable than those having inverted pyrrole ring opposite to the phenylene ring (**9g** to **9p**). The isomers containing outer N−H (**9d**, **9e**, **9i**, **9j,9k**, **9n**, **9p**) are more stable than those without outer N−H (**9g**, **9h**, **9m**, **9o**).

Table 4.4. Total Energy, Relative Energy of the Theoretically Optimized Structures of Chart 4.7 and 4.8[a]

Structure	E_{total} (Hartree)	E_{rel} (Kcal/mol)	E_{total}(Hartree) re-optimized using B3LYP/6-311g**	E_{total}(Hartree) re-optimized using B3LYP/6-311+g**
9a	-1707.4353	5.71		
9b	-1707.4211	14.62		
9c	-1707.4316	8.03		
9d	-1707.4437	0.43		
9e	-1707.4444	0.00	-1707.7863	-1707.8157
9f	-1707.4156	18.07		
9g	-1707.4068	23.59		
9h	-1707.4111	20.89		
9i	-1707.4173	17.00		
9j	-1707.4151	18.38		
9k	-1707.4256	11.79		
9l	-1707.4285	9.97		
9m	-1707.4097	21.77		
9n	-1707.4145	18.76		
9o	-1707.4114	20.70		
9p	-1707.4214	14.43		
10a	-1707.1377	11.73		
10b	-1707.1564	0.00	-1707.8463	-1707.5283
10c	-1707.1485	4.95		
10d	-1707.1402	10.16		
10e	-1707.1417	9.22		
10f	-1707.1436	8.03		

[a] Relative energy for structures **9a** to **9p** and **10a** to **10f**were calculated with respect to the structures **9e** and **10b,** respectively**.**

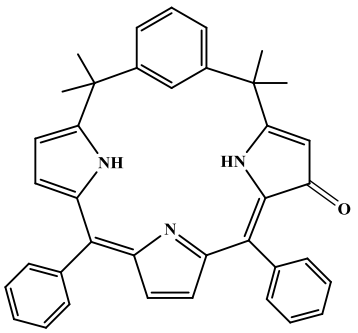

9a
(5.71)

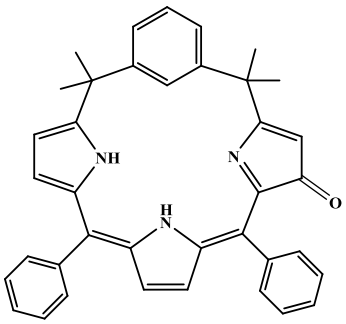

9b
(14.62)

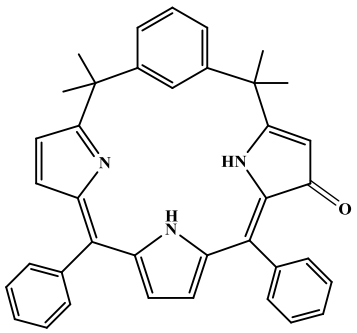

9c
(8.03)

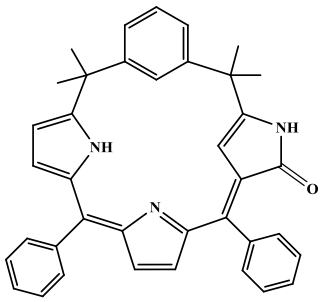

9d
(0.43)

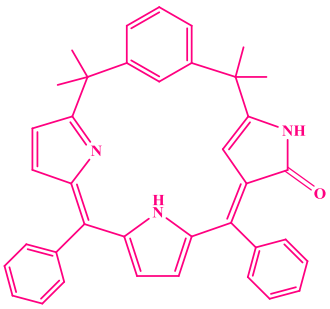

9e
(0.0)

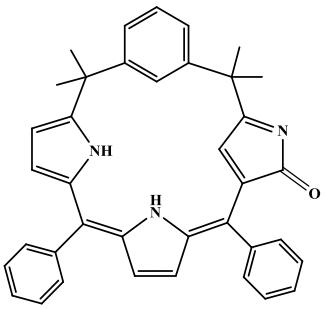

9f
(18.07)

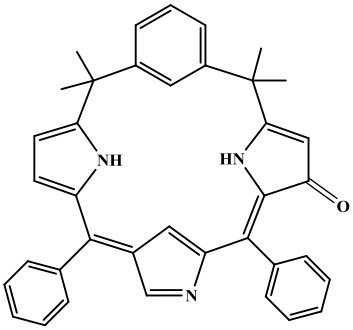

9g
(23.59)

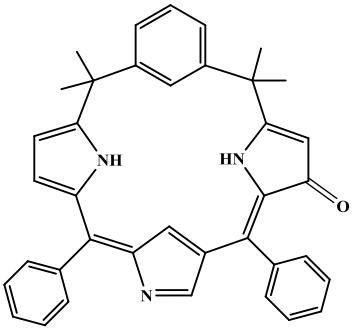

9h
(20.89)

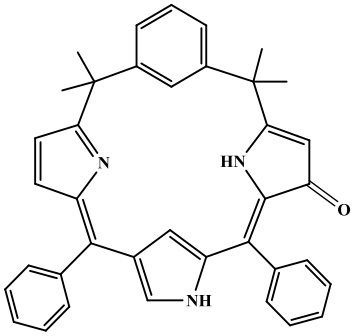

9i
(17.0)

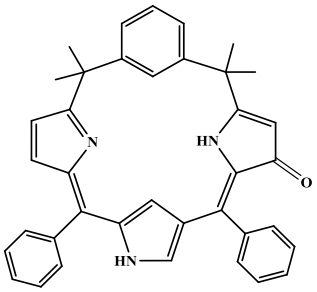

9j
(18.38)

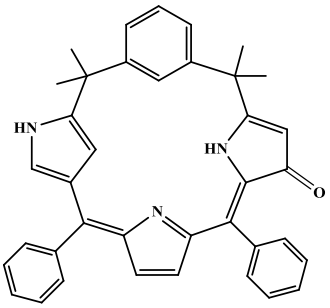

9k
(11.79)

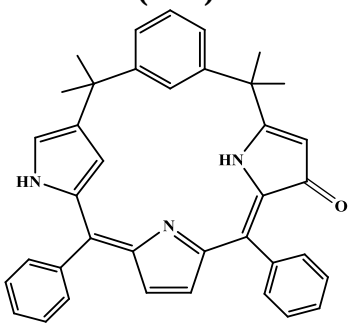

9l
(9.97)

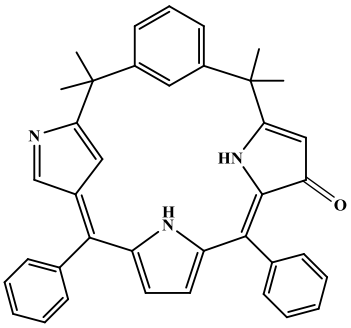

9m
(21.77)

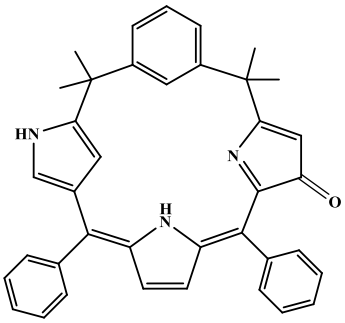

9n
(18.76)

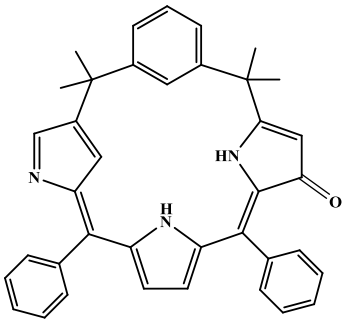

9o
(20.70)

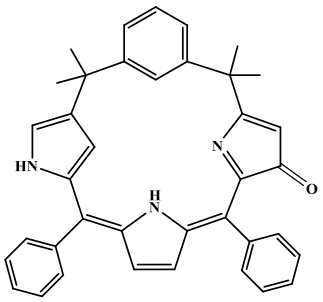

9p
(14.43)

Chart 4.7. Reduced form of O-down, **3** isomers, and their relative energy are given in parentheses with respect to **9e** in kcal/mol.

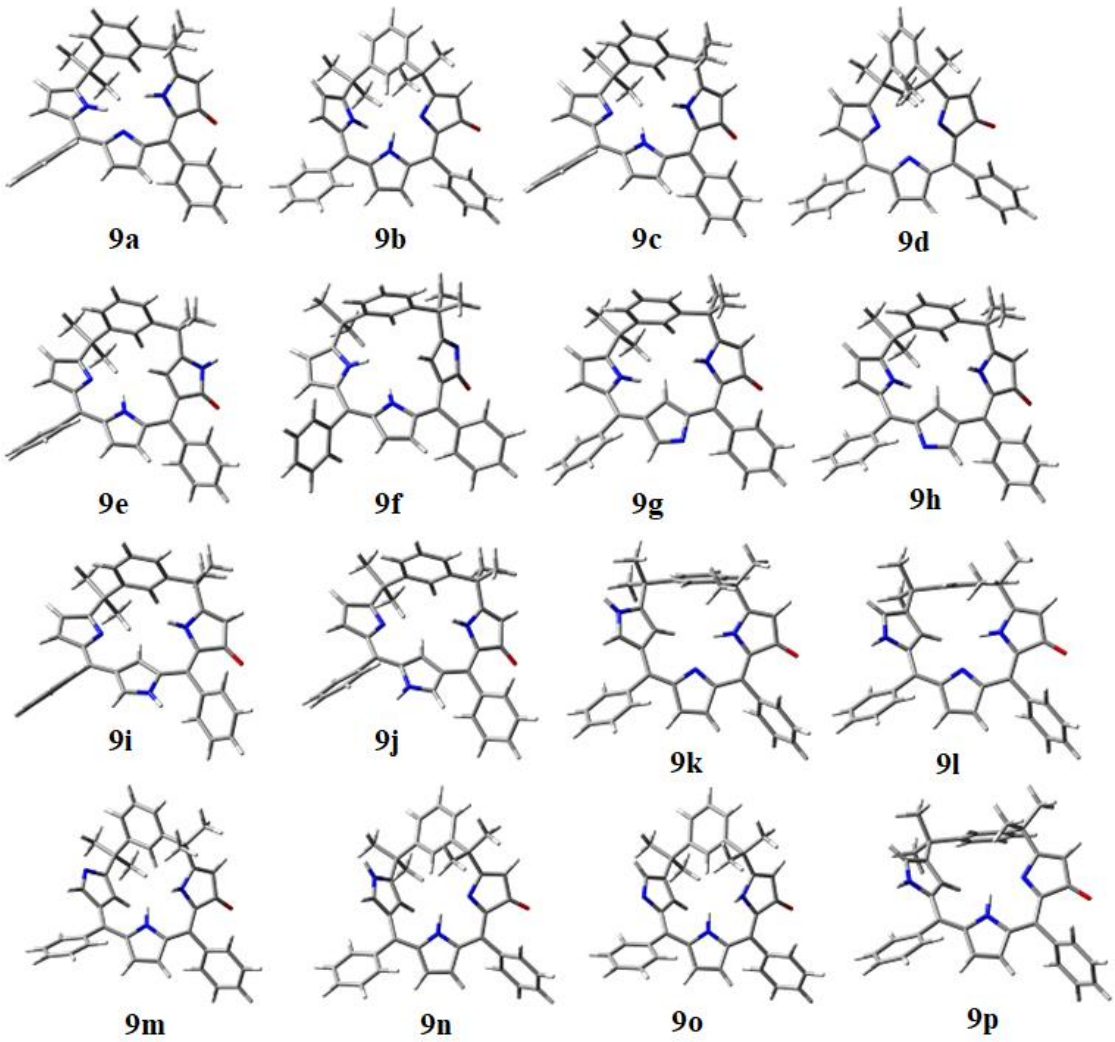

Figure 4.8. Optimized geometries of o-down isomers presented in Chart 4.7 oxidized at pyrrole ring adjacent to the phenylene ring with hydrogen atom.

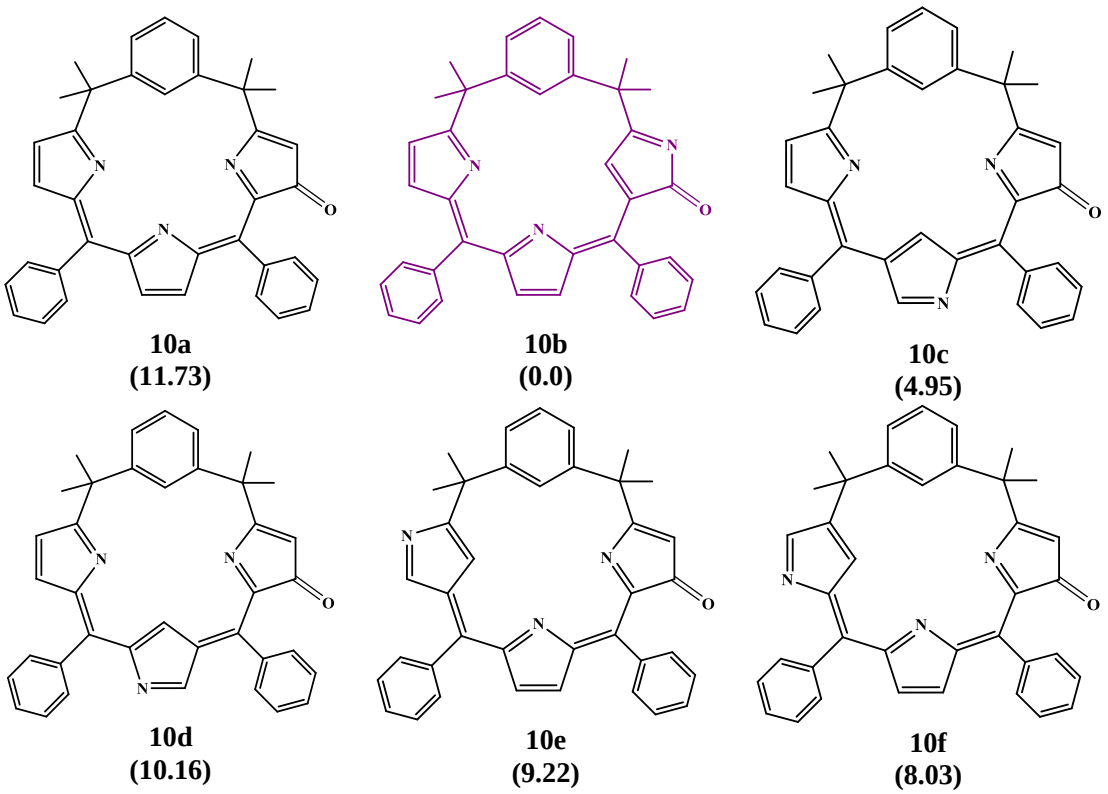

Chart 4.8. Oxidized form of O-down, **3** isomers, their relative energy are given in parentheses with respect to **10b** in kcal/mol.

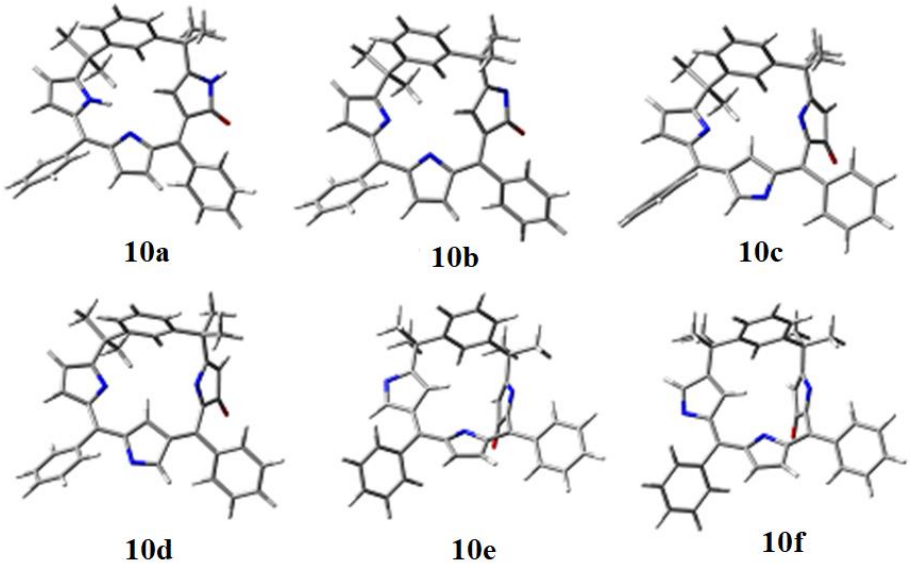

Figure 4.9. Optimized geometries of O-down isomers presented in Chart 4.8 oxidized at pyrrole ring adjacent to the phenylene ring without hydrogen atom.

4.4.6. The Structural Features of the Isomers

The stabilization of isomers discussed above is mainly dependent on the inner N−H H-bond interactions, oxidation at the pyrrole ring, π-conjugation. The other factor which also influences the stabilization of isomers discussed herein (*vide infra*) is the structural differences.

The actual shapes of the optimized structures of **1** and its inverted isomers are shown in **Figure 4.2**. The structures of oxa and thia analogues are shown in **Figure 4.3**. The geometries of O-up isomers and O-down are shown in **Figures 4.4** and **4.5**, **4.8** and **4.9**, respectively. The comparisons of isomers with an oxygenation at pyrrole ring opposite to the phenylene ring are shown in **Figures 4.6** and **4.7**. The top view of the optimized structures of aza, oxa, and thia containing benziporphodimethenes with bond angles and bond distances labelled have been shown in **Figure 4.1**. For comparison the geometrical parameters of thiophene and furan are also shown in Figure 2. For more quantitative analysis on the structures, the non - bonded distances, angles for optimized structures for 1 and its inverted isomers along with oxa, thia analog are given in Table1. Currently, the X-ray crystal structures of 1, 2 and 3 are reported in the literature. The comparison between X-ray structures and results from theoretical calculations reveals that the deviations in bond lengths and angles are within 0.01 Å and 0.3^{o}, respectively. Similar accuracy has been reported in the literature[59]–[61].

The plane containing four *meso* positions is used as a reference plane to define the deformation of *meta*-benziporphodimethene. The planarity of the reference plane is given by dihedral angle, P_0. Another dihedral angle, P_{core}, is also calculated to reveal the planarity of four inner core and potential ligation atoms. The puckeredness of two sp^3 *meso* carbons is given by the angle between the vector along the *meso* sp^3 carbon atoms and mean plane of the 17 triphyrin atom, $17/sp^3$.The deviation in the phenylene ring, C_6/N_2X (X= N, S, O or C), is given by the angle between the mean plane of phenylene ring and mean plane of three inner core atoms on the five member rings. The deformation of three pyrrole rings from the mean plane of 17 triphyrin atom are defined by, $Py_n/17$ (n= 1-3), the angle between a specific pyrrole ring and mean plane of the tripyrin.

First of all, we will discuss the DFT optimized geometries for **1** and its inverted isomers shown in Figure 4.2. The front view of the DFT optimized geometries as well as the values of P0 and P_{core}, reflect the deviation of molecules from planarity. As discussed above, **1a** is energetically more stable than **1b**. The major structural difference is that the $Py_1/17$ in **1a** is less than in the case of **1b** while **1b** has smaller $Py_2/17$ and $Py_3/17$ than **1a**. These deviations are majorly dependent on geometries of molecules. The P0 in **1b** is 1.727º higher than **1a** while the values of $17/sp^3$, C_6/N_3 angles are almost identical for **1a** and **1b**. The lower values of inner NH•••N distance is 1.8566 Å in the case of **1a** makes it more stable than those **1b** where inner NH•••N distance are 2.0257 and 2.433 Å. While in the case of inverted isomers, **2a** to **2i**, P0 angles differ from each other and mainly depend on the location of inverted pyrrole

ring. The lowest values were found for the structures **2d** and **2h** while the P_{core} values are lower for **2b** and **2e**. The isomer **2f** is energetically more stable structure. However, it's inner NH•••N interaction are not strong enough than isomers. This may be attributed to some other structural difference which makes its more favourable (**Figure 4.2** and **Table 4.1**).

The optimized structure reveals that the O-up isomers, **5a** to **5f** and **6a** to **6f**shown in **Chart 4.3**, **4.4** and **Figure 4.5**, **4.6**, are less puckered than **1a**, **1b** and **2a** to **2i**, shown in **Figure 4.2**. The structural features are given in **Table 4.2**. The most stable **5b** is having shortest inner NH•••N interactions, 2.072 Å. The $Py_n/17(n\pm1\text{-}2)$ angles are in good agreement with other isomers discussed above. The most stable O-down isomers **9e** is having one inner NH•••N interaction, 2.027 Å while least stable structure **9g** do not have any inner NH•••N interaction The $17/C_6$angle in **9e** is 2.679º higher than **5b** and $17/sp^3$-vectorangle is lesser, 2.006ºthan **5b** which suggest lesser deviation in structure **5b**. However, both P_{core} and P_0 are little bit higher than **9g** but other factors dominate to make it energetically more favourable. The other structural features also support the O-up and O-down isomers of **5b** than O-up and O-down isomers of **9e** in terms of stability. For other isomers, **7a** to **7f** and **8a** to **8d,** the details structural features are given in **Table 4.2**. The most stable isomer, **7b** does not have strong inner NH...N interaction but other structural feature favours this geometry.

The bond distance between the pyrrole carbon which is directly linked to *meso* carbon and sp^3 *meso* carbons does not change much and varies from 1.5027 to 1.5295 Å in

the structures shown in **Figures 4.2** to **Figure 4.9** but longer distance was measured for the **3a**, 1.5499 Å (**Figure 4.1**). The other bond distance also does not change much, C=O bond distance lies in the order of double bond distance. The N-H and C-H (inverted pyrrole) bond distance remains unchanged but some time it increases due to strong inner NH•••N interactions. Due to repulsions in the inner core hydrogen atoms, the structures with 3-H inside the core hydrogen atoms are more deviated from the mean plane than other structures.

To predict the binding character of the core ligands towards the incoming transitions metal, the size of the core cavity is estimated by the diagonal distances D1 and D2, where D1 is the distance between the atoms along x-axis and D2 is the distance between the atoms along the y-axis. The distance variations are small and form square shape and little difference were found by the replacement of nitrogen atom in **1** by Sulphur atom, **4b**. The different shapes of the core cavity deserve to be noted in anticipating the coordinating properties of *meta*-benziporphodimethene systems.

4.4.7. The Structural Features of oxa- and thia- Analogues.

To understand the effect of replacement of either nitrogen N (23) or N (24) by oxygen and sulfur atoms. We carried out DFT calculations on oxa (**3a, 3a', 3b** and **3b'**) and thia (**4a, 4a', 4b** and **4b'**) analogues of **1**. The DFT optimized geometries are shown in **Figure 4.3**. Detailed structural features are given in **Table 4.2**. To understand the conjugation effects on the bond distance and angles, the furan and thiophene moiety inside the structures of **3a**, **3a**, **3b**, **3b'**, **4a, 4a', 4b** and **4b'** was compared with DFT optimized geometries of thiophene (**11**) and furan (**12**). The DFT optimized bond lengths and bond angles of thiophene and furan are in satisfactory agreement with

previous reported X-ray crystallographic values. From the X-ray crystallographic studies, the bond distances of pyrrole molecules follow the order C_α-C_{meso}> C_α-C_β> C_β -C_β in the case of **1** while in case of regular porphyrins the order follows C_α-C_β> C_α-C_{meso}> C_α-N >C_β-C_β. Interestingly, in **3a', 4a',** and **3b'**and **4b'** the order follows like C_α-C_{meso}> C_β -C_β>C_α-C_β> C_α-O and C_α-C_β> C_α-C_{meso}> C_α-N> C_β -C_β, respectively. The molecule **3b'** and **4b'** reproduce the pattern of regular pyrrole as in porphyrins macrocycle. The C_α-C_β and C_α-X distances are longer and C_β -C_β distances are shorter than in free thiophene and furan molecule (**Figure 4.3**). Thus, the pattern of C_α-C_β and C_β -C_β thiophene and furan distances follows the regular pyrrole rings and reflects the inclusion of the thiophene and furan moiety in the π-delocalization pathway of the macrocycle. The inclusion of thiophene and furan molecule in the macrocycle markedly effects the C_α-C_{meso} bond adjacent to thiophene but C_α-C_{meso} distances are shorter than without thiophene and furan containing macrocycle. The marked differences in bond distances have been found between the C_α-N bond for protonated and unprotonated pyrrole rings.

4.4.8. The intramolecular hydrogen bond energy

We calculated the intramolecular hydrogen bond energy in *meta* -Benziporphodimethenes and other analogues with the help of molecular tailoring-based approach (MTA)[62]–[65]. A general fragmentation procedure for estimation of N-H---N hydrogen bond (HB1) in parent molecule 2f is shown in **Scheme 4.1**.

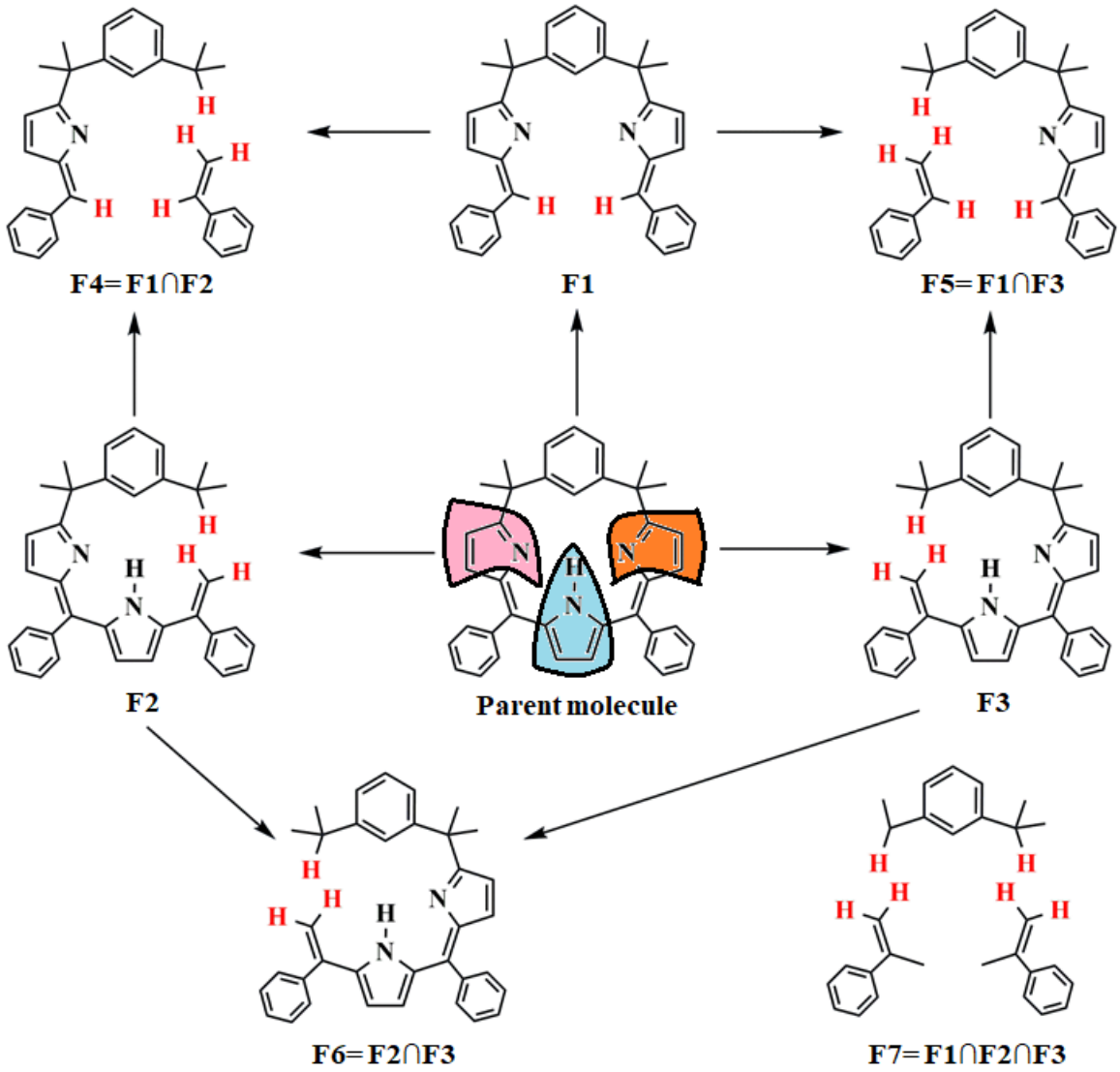

Scheme 4.1. Molecular tailoring based approach for estimation of intramolecular H-bond energies.

As seen in **Scheme 4.1**, the parent molecule (**1a**) is cut into two primary fragments F1 and F2. These cut regions are shown by dotted regions on the parent molecule. To satisfy the valences of cut regions, dummy hydrogen atoms were added at an appropriate C-H distance and directions. Fragment F3 is obtained by taking the intersection of these primary fragments, i.e., (F1∩F2). A single point energy evaluation has been carried out on all fragments at B3LYP/6- 311 + G** level of theory. The fragments are not optimized so that conformational changes in them are avoided. The intramolecular hydrogen bond

energy E_{HB1} in (2f) (parent molecule in **Scheme 4.1**) is calculated as (E_{F1} + E_{F2} - E_{F3}) - E_{2c} = -1631.820005 - (-1631.844845) = 15.59 kcal mol^{-1}. In a similar fashion, the hydrogen bond energies were estimated for all the other most stable conformers; see **Table 4.5**. For the geometries of hydrogen bonds in these molecules, see Fig. 3. It is clear from **Table 4.5** that the estimated hydrogen bond energies fall in a range expected from chemical intuition and is able to distinguish the strong and weak hydrogen bonds. The hydrogen bond energies vary between 0.08 and 15.59 kcal mol^{-1}. Particularly noteworthy is the strongest hydrogen bond (15.59 kcal mol^{-1}) is found in 2f which has smallest H-bond distance of 1.965 Å (see **Table 4.5**). On the other hand, the longest distance of 2.679 Å was found in 4a corresponding to the C-H-N interaction. The C-H-N interaction energy calculated in 4a was found to be 0.08 kcal mol^{-1}. Also, the calculated H-bond energies are in general agreement with the fact that the N-H/N hydrogen bond energy is stronger than N-H/S and N-H/O hydrogen bonds and the C-H/N is weakest H-bond; see **Table 4.5**.

Table 4.5. Intramolecular hydrogen bond (H-Bond) distances (Angstrom) and energy (kcalmol^{-1}). See **Figure 4.1** for corresponding geometries of the molecules.

Molecule	H-bond Distance		H-bond Energy	
	HB1	HB2	HB1	HB2
1a	2.220	2.220	6.31	6.31
2f	1.965	–	15.59	–
3a	2.273	2.274	10.07	10.03
4a	2.679	2.679	0.08	0.08
4a'	2.541	2.540	11.18	11.17
5b	1.969	–	13.48	–
6b	2.471	–	0.57	–
7b	2.24	–	4.44	–
8b	2.159	2.629	0.72	0.72
9e	1.970	–	10.99	–
10b	2.639	–	2.11	–

4.5. DFT of metalated *meta*-benziporphodimethene complexes

The computational calculations were performed for metalated (Cd and Hg) *meta*-benziporphodimethene complexes, employing density functional theory method. The Los-Almos Laboratory double zeta (LANL2DZ) basis set was used in combination with Becke-three parameter exchange correlation function by Lee, Yang and Parr (B3LYP). The geometrical structures were optimized under C1 symmetry using Gaussian 09W suits of program. The optimized structures then subjected to frequency calculations to ensure that the global minima were obtained for both the metal complexes. Furthermore, the optimized structures were utilized to visualize the frontier molecular orbitals for Cd(II) and Hg(II) *meta*-benziporphodimethene complexes. **Figure 4.10** depicts the optimized structures of metalated *m*-BPDM complexes. GaussView 5.0 software has been used for the visualization of these frontier molecular orbitals. In addition to this, the HOMO-LUMO gaps were calculated for these geometries and individual energies of the frontier molecular orbitals have been added in **Figure 4.11 and Table 4.6, respectively**.

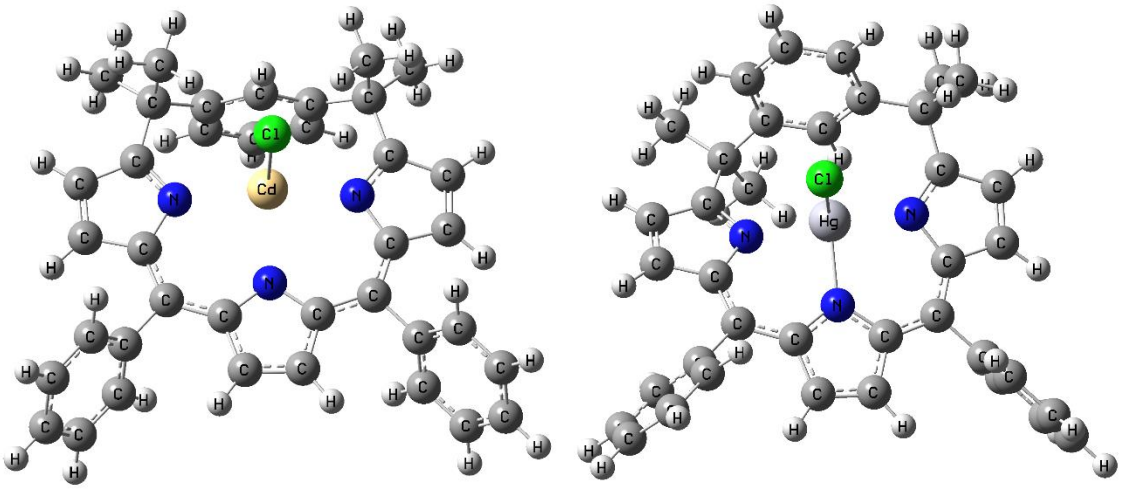

(a) **(b)**

Figure 4.10. Optimized geometries of (a) CdCl-BPDM and (b) HgCl-BPDM.

Table 4.6. Energies of frontier molecular orbitals in eV.

Complex	Energy (eV)			
	HOMO-1	**HOMO**	**LUMO**	**LUMO+1**
CdCl-BPDM	-7.11	-6.79	-6.51	-5.62
HgCl-BPDM	-8.30	-8.14	-6.59	-5.61

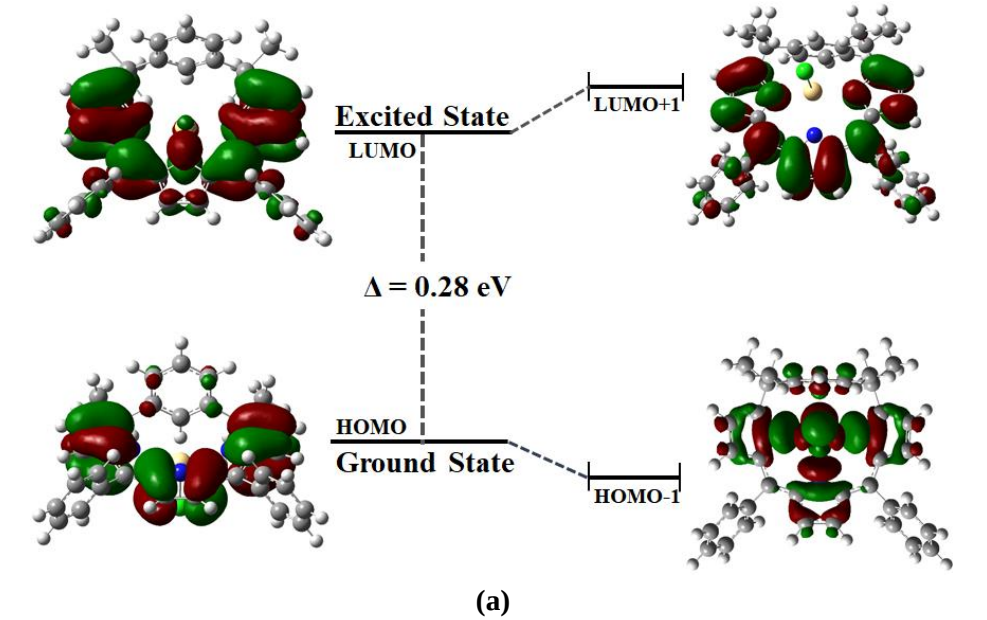

(a)

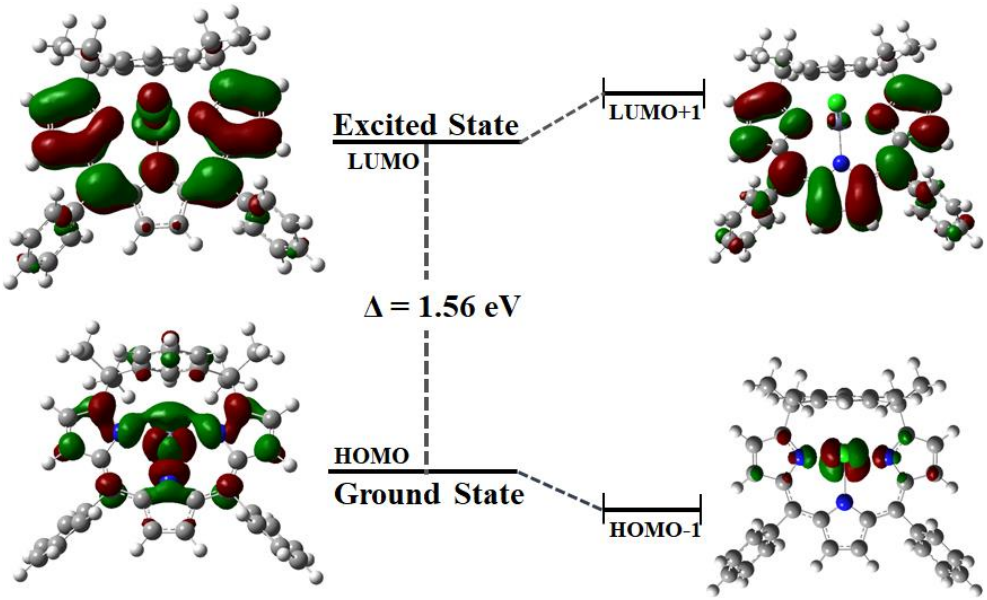

(b)

Figure 4.11. Frontier molecular orbital of (a) **CdCl-BPDM** and (b) **HgCl-BPDM** (Isosurface value= 0.02)

References

[1] R. Bonnett, "Photosensitizers of the porphyrin and phthalocyanine series for photodynamic therapy," *Chemical Society Reviews*, vol. 24, no. 1. pp. 19–33, 1995.

[2] Y. Joo *et al.*, "Theoretical study on the structure, stability, and tautomerism of 2-aza-21-carba-23-X(thia or oxa)-porphyrin isomers," *Journal of Physical Chemistry A*, vol. 106, no. 6, pp. 1035–1045, 2002.

[3] A. Gebauer *et al*., "Synthesis, characterization and properties of a lithium 21-thiaporphyrin complex," *J. Inorg. Chem.*, vol. 39, no. 15, pp. 3424–3427, 2000.

[4] A. Ulman *et al.*, "Synthesis of New Tetraphenylporphyrin Molecules Containing Heteroatoms Other than Nitrogen. I. Tetraphenyl-21, 23-dithiaporphyrin," *Journal of the American Chemical Society*, pp. 6540-5644, 1975.

[5] A. Ulman *et al.,* Synthesis and properties of tetraphenylporphyrin molecules containing heteroatoms other than nitrogen.6. Electro chemical studies, *Inorg. Chem.* vol. 20, pp. 1987-1990, 1981.

[6] R. L. Hill *et al*., "Tetraphenylporphyrin Molecules Containing Heteroatoms Other Than Nitrogen. 7.[1] Emission and Electronic Structure of Rings Containing Sulfur and Selenium," *Inorganic Chem.*, vol. 21, pp. 1450-1455, 1982.

[7] G. D. Munno *et al*., "21, 23-Dithiaporphycene: The First Aromatic Sulfur-containing System with Porphycene Structure," *Tetrahedron*, vol. 49, no. 31, pp. 6863-6872, 1993.

[8] T. Nußbaumer *et al.*, "21, 23-Dithia-3, 13-diazaporphycenes - Novel Aromatic Porphycene Analogues Incorporating Thiazole," *Eur. J. Org. Chem., pp*. 2449-2457, 2000.

[9] L. L. Grazynski *et al.*, "Geometry and tautomerism of 26,28-dioxasapphyrin and 26,28-dithiasapphyrin: DFT studies," *Journal of Physical Chemistry A*, vol. 103, no. 17, pp. 3302–3309, 1999.

[10] M. J. Brodhurst *et al.*, "Sulphur Extrusion Reactions Applied to the Synthesis of Corroles and Related Systems," pp. 1124-1135, 1972.

[11] J. L. Sessler *et al.*, "Sapphyrins and Heterosapphyrins," *Tetrahedron*, vol. 48, no. 44, pp. 9661-9672, 1992.

[12] A. Srinivasan *et al.*,"Tetrathia- and tetraoxarubyrins: aromatic,core-modified,expandedporphyrins,*AngewChem.Int.Ed.Engl.*, vol. 36, pp. 2598-2601, 1997.

[13] W. M. Dai *et al.*, "First synthesis of dioxadithiaporphycene with a benzene ring fused onto the double bond," *Tetrahedron Letters*, vol. 41, pp. 10277-10280, 2000.

[14] E. Pacholska *et al.*, "Pyrrole-inverted isomer of 5,10,15,20-tetraaryl-21-selenaporphyrin," *Journal of Organic Chemistry*, vol. 65, no. 24, pp. 8188–8196, 2000.

[15] E. Vogel *et* al., Novel porphyrinoidmacrocycles and their *meta*l complexes, *J. Heterocycl. Chem.*, vol.33, pp. 1461-1487, 1996.

[16] I. Bischoff *et al.*, "One-pot synthesis of functionalized, highly substituted porphodimethenes," *Tetrahedron*, vol. 57, pp. 5573-5583, 2001.

[17] B. Krattinger *et al.*, "Addition of sterically hindered Organolithium Compounds to *meso*-tetraphenylporphyrin," *Tetrahedron Letters*, vo. 39, pp. 1165-1168, 1998.

[18] C.-H. Lee *et al.*, "Synthesis of meso-tetraaryl-21-oxa-22-thiaporphyrin from 2+2 condensation," *Tetrahedron Letters*, vol. 40, pp. 8879-8882, 1999.

[19] D. Kumaresan *et al.*, "Photophysical properties of boron-dipyrrin appended porphyrins with heteroatom cores," *Chem Phys Lett*, vol. 395, no. 1–3, pp. 87–91, 2004.

[20] V. G. Anand *et al.*, "30π aromatic *meso*-substituted heptaphyrin isomers: Syntheses, characterization, and spectroscopic studies," *Journal of Organic Chemistry*, vol. 67, no. 18, pp. 6309–6319, 2002.

[21] S. K. Pushpan *et al.*, "Aromatic core-modified expanded porphyrinoids with *meso*-aryl substituents," vol. 74, no. 11, pp. 2045-2055, 2002.

[22] N. Sprutta *et al*., "25,27-dithiasapphyrin and pyrrole-inverted isomer of 21,23-dithiaporphyrin from condensation of pyrrole and 2,5-bis(*p*-tolylhydroxymethyl) thiophene," *Org Lett*, vol. 3, no. 12, pp. 1933–1936, 2001.

[23] M. Stępień *et al*., "Cadmium (II) and Nickel (II) Complexes of Benziporphyrins. A Study of Weak Intramolecular Metal-Arene Interactions," *J Am Chem Soc*, vol. 126, no. 14, pp. 4566–4580, 2004.

[24] D. Bhattacharya *et al*., "Direct incorporation of a ferric ion in the porphyrinogen core: Tetrakis (cyclohexyl)iron porphyrinogen anion with different conformers and its reaction with iodine," *Inorg Chem*, vol. 44, no. 22, pp. 7699–7701, 2005.

[25] J. P. Hill *et al.*, "Highly nonplanar, electron deficient, N-substituted tetra-oxocyclohexadienylidene porphyrinogens: Structural, computational, and electrochemical investigations," *Journal of Organic Chemistry*, vol. 69, no. 18, pp. 5861–5869, 2004.

[26] P. Belanzoni *et al*., "A theoretical analysis of the fundamental stepwise six-electron oxidation of porphyrinogen to porphyrins: The energetics of porphodimethene and artificial porphyrin intermediates," *Journal of the Chemical Society, Dalton Transactions*, no. 9, pp. 1492–1497, 2001.

[27] T. D. Lash *et al.*, "Normal and abnormal heme biosynthesis. 6. Synthesis and metabolism of a series of monovinylporphyrinogens related to harderoporphyrinogen. Further insights into the oxidative decarboxylation of porphyrinogen substrates by coproporphyrinogen oxidase," *Journal of Organic Chemistry*, vol. 75, no. 10, pp. 3183–3192, 2010.

[28] C. H. Hung *et al.*, "*m*-Benziporphodimethene: A new porphyrin analogue fluorescence zinc (II) sensor," *Chemical Communications*, no. 8, pp. 978–980, 2008.

[29] R. K. Sharma *et al.*, "Synthesis, characterization and fluorescence turn-on behavior of new porphyrin analogue: *meta*-benziporphodimethenes," *Spectrochimica Acta Part A: Molecular and Biomolecular Spectroscopy*, vol. 169, pp. 58–65, 2016.

[30] R. K. Sharma *et al.*, "*meta*-Benziporphodimethenes: New Cell-Imaging Porphyrin Analogue Molecules," *Chemistry Select*, vol. 1, no. 13, pp. 3502–3509, 2016.

[31] Y. D. Wu *et al.*, "Porphyrin Isomers: Geometry, Tautomerism, Geometrical Isomerism, and Stability," *J. Org. Chem.*, vol. 62, pp. 9240-9250, 1997.

[32] Y. D. Wu *et al*., "Geometrical and electronic properties of dibenzoporphycenes," *J. of Mol. Str. (Theochem)*, pp. 325-332, 1997.

[33] A. Ghosh *et al.*, "Molecular structures, tautomerism, and carbon nucleophilcity of free-base inverted porphyrim and carbaporphyrins: A density functional theoretical study," *Journal of Physical Chemistry B*, vol. 102, no. 50, pp. 10459–10467, 1998.

[34] A. Ghosh *et al*., "*Cis-Trans* Isomerism in Porphyrin Isomers," *J. Phys. Chem. B*, vo. 101, pp. 5459-5462, 1997.

[35] A. Ghosh, "First-Principles Quantum Chemical Studies of Porphyrins," *Acc. Chem. Res.*, vol. 31, pp. 189-198,1998.

[36] L. Latos-Grazynski *et al*., "Geometry and tautomerism of 26,28-dioxasapphyrin and 26,28-dithiasapphyrin: DFT studies," *Journal of Physical Chemistry A,* vol. 103, no. 17, pp. 3302–3309, 1999.

[37] A. Ghosh *et al*., "The ultraviolet photoelectron spectrum of free-base porphyrin revisited. The performance of local density functional theory," *Chemical Physics Letters,* vol. 213, pp. 519-521, 1993.

[38] A. Ghosh *et al.*, "Structure and Stability of *cis*-Porphyrin," *J. Phys. Chem.,* vol. 99, pp. 1073-1075, 1995.

[39] J. R. Reimers *et al*., "The Mechanism of Inner-Hydrogen Migration in Free Base Porphyrin: *Ab Initio* MP2 Calculations," *J. Am. Chem. Soc.,* vol. 117, pp. 2855-2861, 1995.

[40] K. M. Kadish *et al.*, "The Porphyrin Handbook Editors," *Academic Press,* vol 1.

[41] M. Punnagai *et al*., "Theoretical study on the structure and stability of ring inverted porphyrin isomers," *Journal of Molecular Structure: Theochem,* vol. 684, no. 1–3, pp. 21–28, 2004.

[42] M. Punnagai *et al*, "A density functional theory study on the porphyrin isomers: effect of *meso*-bridge length, relative stabilities, *cis-trans* isomerism," *Arkivoc,* pp. 258-283, 2005.

[43] J. L. Sessler *et al.*, "Expanded Porphyrins," *Topics in Current Chemistry,* vol. 161, 177-273, 1991.

[44] D. K. Maity *et al*., "Mechanism and quantum mechanical tunneling effects on inner hydrogen atom transfer in free base porphyrin: A direct *ab initio* dynamics study," *J Am Chem Soc*, vol. 122, no. 5, pp. 897–906, 2000.

[45] J. Braun *et al*., "Observation of kinetic tritium isotope effects by dynamic NMR. The tautomerism of porphyrin, *J. Am. Chem. Soc.*, vol. 118, pp. 7231-7232, 1996.

[46] W. J. Hehre *et al.*, "Self-consistent molecular orbital methods. XII. Further extensions of Gaussian-type basis sets for use in molecular orbital studies of organic molecules," *J. Chem. Phys.*, vol. 56, no. 5, pp. 2257–2261, 1972.

[47] J. Almlof *et al*., "Electron Correlation in Tetrapyrroles. *Ab Initio* Calculations on Porphyrin and the Tautomers of Chlorin," *J. Phys. Chem.*, vol. 97, pp. 10964-10970, 1993.

[48] K. Malsch *et al.*, "The importance of electron correlation for the ground state structure of porphycene and tetraoxaporphyrin-dication," *Chemical Physics*, pp. 331-348, 1998.

[49] J. Helaja *et al.*, "NH tautomerism in the dimethyl ester of Bonellin, a natural chlorin," *Journal of Organic Chemistry*, vol. 64, no. 2, pp. 432–437, 1999.

[50] L. Szterenberg *et al.*, "Structure and Stability of 2-Aza-21-carbaporphyrin Tautomers Prearranged for Coordination," *Inorg. Chem.*, vol. 36, pp. 6287-6291, 1997.

[51] T. S. Rush *et al*., "Computational Modeling of Metalloporphyrin Structure and Vibrational Spectra: Porphyrin Ruffling in NiTPP," *Journal of Physical Chemistry B*, vol. 104, no. 20, pp. 5020–5034, 2000.

[52] K. A. Nguyen *et al.*, "Triplet excited states of free-base porphin and its β-octahalogenated derivatives," *Journal of Physical Chemistry A*, vol. 104, no. 20, pp. 4748–4754, 2000.

[53] K. A. Nguyen *et al*., "Photoinduced Hydrogen Atom Transfer of Free-Base Porphin," *Journal of Physical Chemistry A*, vol. 104, no. 19, pp. 4549–4552, 2000.

[54] H. Furuta *et al*., "Stability and structure of doubly N-confused porphyrins," *Journal of Organic Chemistry*, vol. 65, no. 13. pp. 4222–4226, 2000.

[55] A. Ghosh, "Electronic Structure of Corrole Derivatives: Insights from Molecular Structures, Spectroscopy, Electrochemistry, and Quantum Chemical Calculations," *Chemical Reviews, American Chemical Society Publications,* vol. 117, no. 4, pp. 3798–3881, 2017.

[56] A. D. Becke, "Density-functional exchange-energy approximation with correct asymptotic behavior," *Physical Review A*, vol. 38, no. 6, pp. 3098-3100, 1988.

[57] A. D. Becke, "Density-functional thermochemistry III The role of exact exchange," *J. Chem. Phys.*, vol. 98, no. 7, pp. 5648–5652, 1993.

[58] C. Lee *et al*., "Development of the Colle-Salvetti correlation-energy formula into a functional of the electron density," *Physical Review B,* vol. 37, no. 2, 1987.

[59] G. F. Chang *et al.*, "Tetramethyl-*m*-benziporphodimethene and isomeric α,β-unsaturated γ-lactam embedded N-confused tetramethyl-*m*-benziporphodimethenes," *Chem Asian J*, vol. 4, no. 1, pp. 164–173, 2009.

[60] G. F. Chang *et al.*, "Factors that regulate the conformation of *m*-benziporpho-dimethene complexes: Agostic metal-arene interaction, hydrogen bonding, and η^2,π coordination," *Chemistry - A European Journal*, vol. 17, no. 40, pp. 11332–11343, 2011.

[61] Y. C. Chao *et al.*, "An organic hydrogel film with micron-sized pillar array for real-time and indicator-free detection of Zn^{2+}," *Org. Electronics*, vol. 12, no. 11, pp. 1899–1902, 2011.

[62] M. M. Deshmukh *et al*., "Estimation of N-H•••O=C Intramolecular hydrogen bond energy in polypeptides," *Journal of Physical Chemistry A*, vol. 113, no. 27, pp. 7927–7932, 2009.

[63] M. M. Deshmukh *et al.*, "Intramolecular hydrogen bonding and cooperative interactions in carbohydrates via the molecular tailoring approach," *Journal of Physical Chemistry A*, vol. 112, no. 2, pp. 312–321, 2008.

[64] M. M. Deshmukh *et al.*, "Estimation of intramolecular hydrogen bond energy via molecular tailoring approach," *Journal of Physical Chemistry A*, vol. 110, no. 45, pp. 12519–12523, 2006.

[65] M. M. Deshmukh *et al.*, "Intramolecular hydrogen bond energy in polyhydroxy systems: A critical comparison of molecular tailoring and isodesmic approaches," *Journal of Physical Chemistry A*, vol. 111, no. 28, pp. 6472–6480, 2007.

Chapter 5

Conclusion and Future Prospects

CHAPTER 5

CONCLUSION AND FUTURE PROSPECTS

5.1. Conclusion

In Chapter 1, starting with a concise overview about porphyrin, we have presented a brief study about the carbaporphyrinoids reported by far by various research groups. The review the focused on detailed study of the new benziporphyrin analogue: *meta*-benziporphodimethenes. The synthetic pathways reported for both free-base *meta*-benziporphodimethenes and its metal complexes, the UV-Vis spectra studies, NMR studies, crystal structure analysis, agostic interactions, fluorescent studies and other applications has been discussed in detailed. The electronic structure studies that have been recently reported have also been inculcated in this article. This molecule can play a crucial role in biological systems owing to its tendency to detect of toxic metal ions, its biological applications in cancer cell detection etc. However, the researchers have struggled with the low product yield, which has prevented them from exploring these compounds as thoroughly. In Chapter 3, we have discussed synthetic pathways of a sterically hindered analogues of *meta*-benziporphodimethene and its cadmium and mercury complexs. UV-Vis, ^{1}H-NMR and mass spectrometry was used to confirm the synthesis of different analogues. The present study aims to draw the attention of the chemists towards *meta*-benziporphodimethene analogues, providing various factors that may enhance the product yield, as concluded from their computational analysis, as reported in Chapter 4. The complication of this study was further enhanced by comparing the *syn*- and *anti*-conformers not only with each other but also with their reported X-ray crystal structure data.

5.2. Future Prospects

We think that the researchers will be able to further synthesize, characterize, and investigate a wide range of applications for this class of carbaporphyrinoid systems with the execution of our findings. Furthermore, we are confident that the most stable structures established through the research documented in Chapter 4 of this thesis will be energetically more stable. Additionally, we think that combining the most promising findings from Chapters 3 and 4 will result in the development of a novel *meta*-benziporphodimethene molecule, which could aid in overcoming the poor yield and speedy oxidation drawbacks of this moiety. We were successful in identifying a sizable research gap while carefully examining the compound's previously documented work. For instance, electronic structural studies and synthesis of *para*-benziporphodimethenes have not yet been attempted. Additionally, the development of a water soluble *meta*-benziporphodimethene system could pose a challenge to the research groups engaged in this field. We are confident that if research groups address these challenges, *meta*-benziporphodimethene systems having such distinctive features, would progress significantly.

On this note, I would like to sum up my doctoral thesis.

List of Publications and Conferences

LIST OF PUBLICATIONS AND CONFERENCES

1. Anil Kumar, Chen-Hsiung Hung, Shikha Rana, Milind M. Deshmukh, Study on the Structure, Stability, and Tautomerisms of *meta*-Benziporphodimethene and N-Confused Isomers Containing γ–Lactam Ring, *Journal of Molecular Structure*, 2019, 1187, 138–150, https://doi.org/10.1016/j.molstruc.2019.03.064

2. Structural characterization and bioimaging of Zn^{2+} using *meta*-benziporphodimethene analogue; Shikha Rana, Ravi Kumar Sharma, Natalia Fridman, Anil Kumar, Luminescence, 2022, https://doi.org/10.1002/ bio.4382

CONFERENCES

1. Poster Presentation: Shikha Rana and Anil Kumar *"meta*-Benziporphodimethene: A new macrocyclic molecule*",* International conference on advances in analytical sciences (ICAAS -2018), 15-17 March 2018, CSIR – Indian Institute of petroleum, Dehradun, India.

2. Attended International Conference on Researches in Science and Technology (ICRST-19).

3. Oral Presentation: 3rd International Conference on "Recent Advances in Materials, Manufacturing and Thermal Engineering (RAMMTE-2022)" organized by DTU.

ABOUT THE AUTHOR

Name : **Shikha Rana**

Father's Name : Rajesh Kumar Rana

Mother's Name : Nigam

Nationality : Indian

The author completed her schooling from St. Xavier's Public School, Delhi. She then pursued her Bachelor's and Master's degree in Chemistry from University of Delhi. She has also completed her Bachelor of Education (B. Ed). She joined DTU in the year 2017 as full-time research scholar. She started her Ph.D. journey in July 2017 under the supervision of Prof. (Dr.) Anil Kumar at the Department of Applied Chemistry, DTU. Her research work revolves around the synthesis, structural characterization and DFT calculations of *meta*-benziporphodimethenes and their metal complexes. During her Ph.D. she has received Commendable Research Excellence Award, from Delhi Technological University. In 2019, she joined Indian Patent Office as Examiner of Patents and Designs (Group-A, Gazetted) in the Office of Controller General of Patents, Designs and Trade Marks under Ministry of Commerce and Industry (Department for Promotion of Industry and Internal Trade).